ISSN 1590-8844
Vol. 07 No 02
2006

International Journal of Mechanics and Control

Honorary Editor: Guido Belforte

Editor: Andrea Manuello Bertetto

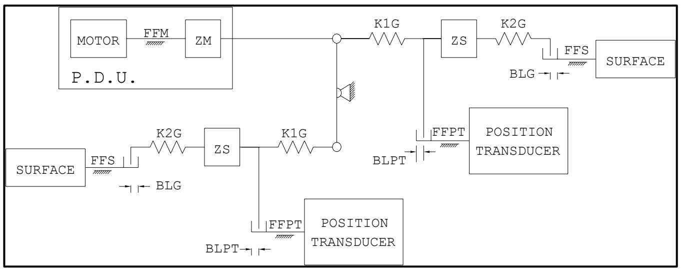

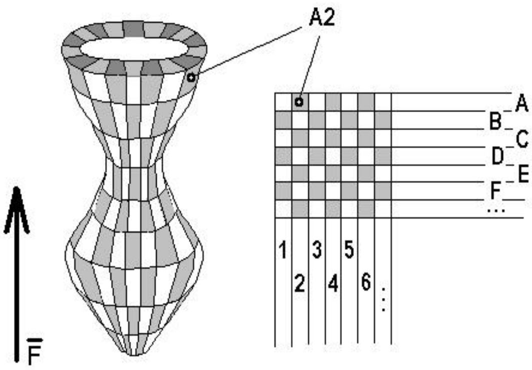

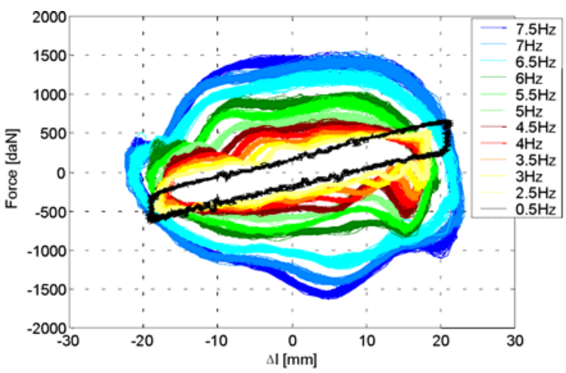

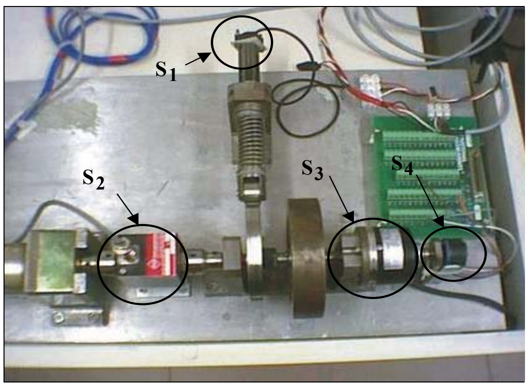

LIBRERIA EDITRICE UNIVERSITARIA
LEVROTTO & BELLA
TORINO

Editorial Board of the

International Journal of Mechanics and Control

Published by Levrotto&Bella – Torino – Italy E.C.

Official Torino Italy Court Registration
n.5390, 5th May 2000

Deposito presso il Tribunale di Torino
numero 5390 del 5 maggio 2000
Direttore responsabile:
Andrea Manuello Bertetto

International Journal of Mechanics and Control

The Journal is addressed to scientists and engineers who work in the fields of mechanics (mechanics, machines, systems, control, structures). It is edited in Turin (Northern Italy) by Levrotto&Bella Co., with an international board of editors. It will have not advertising.

Turin has a great and long tradition in mechanics and automation of mechanical systems. The journal would will to satisfy the needs of young research workers of having their work published on a qualified paper in a short time, and of the public need to read the results of researches as fast as possible.

Interested parties will be University Departments, Private or Public Research Centres, Innovative Industries.

Aims and scope

The *International Journal of Mechanics and Control* publishes as rapidly as possible manuscripts of high standards. It aims at providing a fast means of exchange of ideas among workers in Mechanics, at offering an effective method of bringing new results quickly to the public and at establishing an informal vehicle for the discussion of ideas that may still in the formative stages.

Language: English

International Journal of Mechanics and Control will publish both scientific and applied contributions. The scope of the journal includes theoretical and computational methods, their applications and experimental procedures used to validate the theoretical foundations. The research reported in the journal will address the issues of new formulations, solution, algorithms, computational efficiency, analytical and computational kinematics synthesis, system dynamics, structures, flexibility effects, control, optimisation, real-time simulation, reliability and durability. Fields such as vehicle dynamics, aerospace technology, robotics and mechatronics, machine dynamics, crashworthiness, biomechanics, computer graphics, or system identification are also covered by the journal.

Please address contributions to

Prof. Guido Belforte
Prof. Andrea Manuello Bertetto
PhD Eng. Elvio Bonisoli

Dept. of Mechanics
Technical University - Politecnico di Torino
C.so Duca degli Abruzzi, 24.
10129 - Torino - Italy - E.C.

e_mail: jomac@polito.it

Subscription information

Subscription order must be sent to
the publisher:

Libreria Editrice Universitaria
Levrotto&Bella
2/E via Pigafetta – 10129 Torino – Italy

www.levrotto-bella.net
e_mail: info@levrotto-bella.net
tel. +39.011.5097367
+39.011.5083690
fax +39.011.504025

ISSN 1590-8844
International Journal of Mechanics and Control, Vol. 07, No. 02, 2006

ON THE PIEZOELECTRIC MECHANICAL MICROELEMENTS

Lubomír Uher Danica Janglová

Institute of Informatics, Slovak Academy of Sciences, Bratislava, Slovak republic

ABSTRACT

Modern microchirurgy applications require some new parts capable of precise micro motions and "around the corner" operation. Here we suggest a construction of the proper effectors for operation with the microinstruments, which is based on a set of chessboard-structured field of piezoelectric elements. The same structures may be also applied as sensors with great local spatial resolution.

Keywords: Microelements, Piezoelectric elements

1 INTRODUCTION

Modern microchirurgy applications require some new parts capable of precise micro motions and "around the corner" operation. This kind of instruments we suggest as a construction based on a set of chessboard-structured field of piezoelectric elements. The same structures may be also applied as sensors with great local spatial resolution.
Also the modern chemical microreactors are required manipulating with extremely small amounts of fluids.
One application of piezoelectric micropumps is well known in jet-printers, where the piezoelectric pumps produce the separate drops of the picoliter mass order in pulse mode. Here we introduce an idea of construction of the pump capable of operation with very small amounts of fluids but operating in continuous mode.

2 THE PROPOSED MICROSTRUCTURES

Let us figure a whisker made of a great number of elementary piezoelectric cells separated by insulator layers. In [1] it is possible to find any information from history of piezoelectricity experienced by brothers Pierre and Jacques Curie's, elementary definitions up to the exact theoretical chapters and special applications.

Contact author: Danica Janglová

Institute of Informatics Slovak Academy of Science,
Dúbravská cesta 9, 842 37 Bratislava, Slovakia
E-mail: utrrjang@savba.sk

The function of the piezoelectric elementary cell is illustrated in Fig. 1. When the electric field E is applied across the cell, as a result mechanical deformation appears. The type of deformation depends on orientation of electric field relative to crystal axes of the piezoelectric medium used. It may be of the strain, stress, torque or shear type. The simultaneous action of all cells results in integral motion of the end of the whole fibre.

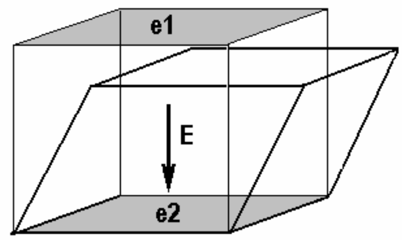

Figure 1 Mechanical deformation of elementary piezoelectric cell subdued to electrostatic field E generated between electrodes e1, e2.

Fibres may be glued together, forming more complicated structures of separately controlled cells, enabling thus complicated deformations of the body as a whole. On the right hand side of the Fig. 3 a principal scheme of control of separate cells is depicted in expanded form. Alphabetical and numeric labelled lines form two different and independent sets of insulated conductors, enabling two-dimensional addressing of each of the cells.

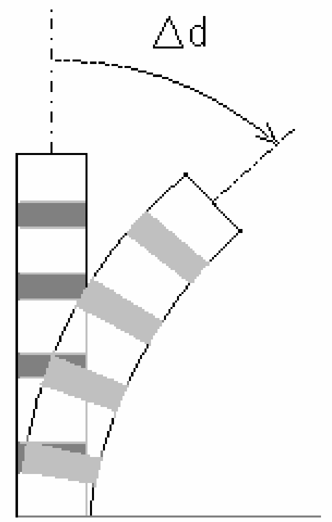

Figure 2 A battery of ***n*** cells.

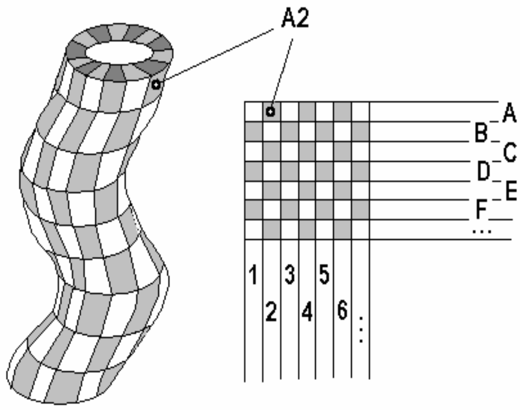

Figure 3 Alphabetical and numeric labelled enable two-dimensional addressing of all cells.

Principal structure of the single piezoelectric cell is depicted on Fig. 4. CE1, CE2 are control electrodes, Scr is a grounded screening electrode, NI is non - piezoelectric dielectric material, P is the active piezoelectric core of the cell. Relative dimensions are exaggerated.

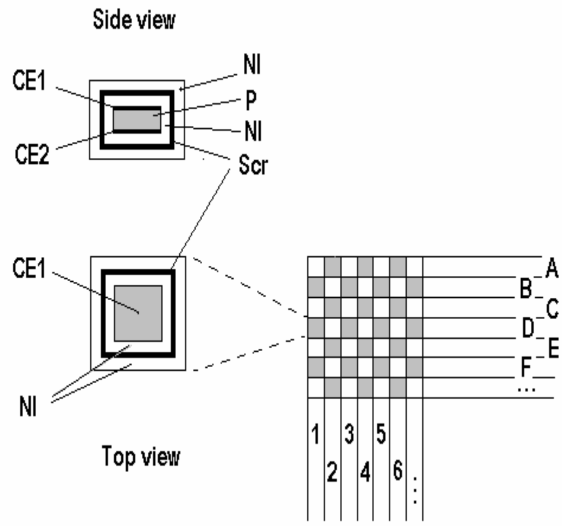

Figure 4 Principal structure of the single piezoelectric cell.

3 THE BASIC EQATIONS

Any of the piezoelectric elements may be used for sensor, giving information of the instant strain or stress situation at its position.
Micromechanismes (mms) are arranged in series as batteries of ***n*** cells. When its lower end is fixed, the free end deflects. Its motion $\Delta\vec{d}$ is described by the equations (3) to (7). Each mms is steered by its own electric signal, controlling its mechanical expansion. The length increment Δl per mms may be expressed as

$$\Delta l = \frac{\alpha \cdot x}{n} \tag{1}$$

where x means the voltage per element. For a series of n mms

$$l = l_0 \cdot (1 + \frac{\alpha \cdot x}{n})^{\mathrm{n}} \tag{2}$$

If a number of mms were increased to infinity, we obtain for the resulting length of the system

$$l = l_0 \cdot \exp(\alpha \cdot x) \tag{3}$$

In a similar way a series of torque elements may be described using φ for the angular variable and v for the applied voltage:

$$\Delta\varphi = \frac{\beta \cdot v}{n} \tag{4}$$

$$\varphi = \varphi_0 \cdot (1 + \frac{\beta \cdot v}{n})^n \tag{5}$$

$$\varphi = \varphi_0 \cdot \exp(\beta \cdot v) \tag{6}$$

If both increments $\Delta l, \Delta\varphi$ acting simultaneously and they were kept small enough, we can write with arbitrary exactness the total deformation vector $\Delta\vec{d}$ in a form of single matrix equation

$$\Delta\vec{d} = \begin{bmatrix} \cos\Delta\varphi & \sin\Delta\varphi & \Delta x \\ -\sin\Delta\varphi & \cos\Delta\varphi & \Delta y \\ 0 & 0 & 1 \end{bmatrix} * \begin{bmatrix} x_0 \\ y_0 \\ t \end{bmatrix} \tag{7}$$

in homogeneous coordinate system in (x y) - plane with homogenous coordinate $t = 1$. x_0, y_0 are "endpoint" coordinates of the n-cell set before the deformation and

$$\vec{d} = \vec{d}_0 \cdot \left(1 + \Delta\vec{d}\right) \tag{8}$$

In synthetic polycrystalline materials and many organic piezoelectric materials isotropy takes place, and as a consequence of their low stiffness greater deformations are expected compared with inorganic crystals.
As a whole, the whole system may be ended with instruments of desired purpose as needles, syringes or scalpels for medical application, see for instance [2].

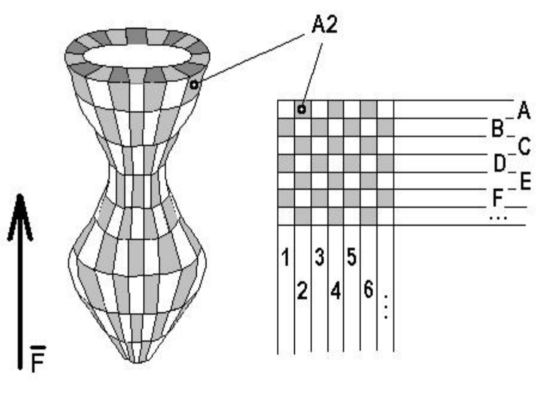

Figure 5 The micropump operating in peristaltic mode.

4 EXAMPLE

One application of piezoelectric micropumps is well known in jet-printers [3], where the piezoelectric pumps produce separate drops of the picoliter mass order operating in pulse mode. Here we introduce an idea of construction of the pump capable of operation with very small amounts of fluids which can operate in continuous mode.
The pumping application of tube is possible according to the Fig. 5, where F means the peristaltic force acting onto the fluid moved inside the tube. The tube may be enforced into the peristaltic motion so that the tube functions as a simple micropump. When internal side of the tube were protected against chemical reactivity of the operation fluids by a coating, the pump may control chemical processes in microscopic chemical reactors.

5 CONCLUSIONS

The present letter gives a suggestion of chessboard structured fields of piezoelectric elements, capable of micromanipulation with small instruments and of the control of very small fluid flows of the order of several nanoliters per second. The piezoelectric pumps can operate in continuous mode, differing thus from the jet pumps, used in microdrops creation in jet printers .

ACKNOWLEDGEMENTS

The work has been supported by the grant agency VEGA MŠ SR a SAV grant No. 2/4147/04.

REFERENCES

[1] Wikipedia: *Piezoelectricity,* en.wikipedia.org/wiki/ piezoelectricity, 2006

[2] Fukuda T., Menz W., *Micro Mechanical Systems, principles and technology.* Handbook of Sensors and Actuators 6. ELSEVIER, Amsterdam, 1998

[3] EPSON jet printers, firmware, 2000 to 2006.

ISSN 1590-8844
International Journal of Mechanics and Control, Vol. 07, No. 02, 2006

MECHANICAL FAILURES OF FLAP CONTROL SYSTEMS AND RELATED POSITION ERRORS: PROPOSAL OF INNOVATIVE CONFIGURATION EQUIPPED WITH CENTRIFUGAL BRAKES

Lorenzo Borello Matteo D. L. Dalla Vedova

Department of Aerospace Engineering, Politecnico di Torino
Corso Duca degli Abruzzi 24 – 10129 TORINO

ABSTRACT

This work analyses two different reversible actuator (with wingtip brakes) architectures for flap actuation systems in order to compare their dynamic behaviour in case of torque transmission mechanical failure. The mathematical models and the related simulation computer programs of the above mentioned flap actuation systems have been prepared (a typical system architecture in the first case and an innovative layout, with the adoption of centrifugal brakes, in the second). This computer simulation program further analyses the flight control dynamic behaviour and the airplane lateral-directional behaviour under the action of the primary and secondary flight controls and of the autopilot. The purpose of this paper is to evaluate the effects of innovative system architecture, equipped with centrifugal brakes, in case of failure conditions. Some simulations of the control system and airplane behaviour in the event of the above mentioned failures have been performed. The results of the present work show the high sensitivity of the aircraft controllability to the flap control system architecture adopted to detect flaps asymmetries and demonstrate like the adoption of the proposed centrifugal brakes, without having to modify considerably the system's constructive complexity, remarkably increases its performances in case of critical failure and avoids the verifying of potentially catastrophic situations.

Keywords: flap, failure, centrifugal, brake

1 INTRODUCTION

The flap actuation systems of most commercial and military aircraft consist of a centrally located Power Drive Unit (PDU), a shaft system and a certain number of actuators (normally two for each flap surface). Depending on the performance requirements and on the specified interface with the other aircraft systems and structure, several different configurations have been used in the design of such actuation systems. PDU's can be either hydromechanical or electromechanical and be either of a single or dual motor type. In the last case the outputs of the two motors can be either torque summed or speed summed. The shaft system generally consists of torque tubes connecting the PDU output with the right and the left wing actuators; however, the flap actuation systems of small commercial aircrafts often use flexible drive shafts rotating at high speed in place of the low speed rigid shafts. The actuators are normally linear and are based on ballscrews (usually of reversible type), though some flap actuators use an ACME screw (irreversible); some flap actuators are of a rotary type (usually reversible). Whichever the actual configuration of the flap actuation system is, the limitation of the asymmetry between the left and the right wing flaps is one of the major requirements for the design of the actuation and control system. Under normal operating conditions the actual asymmetry between the right and the left flaps (or slats) is generally very small because the backlash and the deflection of the mechanical transmission (actuators and shaft system) under asymmetrical loads are generally a small fraction (much less than 1% total) of the full travel. However, if a fracture occurs in the mechanical transmission, an increasing asymmetry builds up between the flaps surfaces, which may become excessive and turn to be flight safety critical if appropriate corrective actions are not taken. It

Contact author: Matteo D. L. Dalla Vedova

E-mail matteo.dallavedova@polito.it

must be noted that a mechanical failure can occur in any component of the actuation system (shafts, PDU, actuators).
The failure of the PDU or of an actuator results in the inability to operate the affected flap system. Such a failure condition, though being regarded as a major type of failure, is not critical for the flight safety, as it is the case of large asymmetries between left and right surfaces resulting from uncontrolled shaft failures. If a shaft failure occurs the following events take place. The part of the actuation system upstream of the fracture point keeps rotating with the PDU in the commanded direction until a shutoff command is not given to the PDU. The portion of the shaft system downstream of the fracture point exhibits a behaviour that depends on its design characteristics.

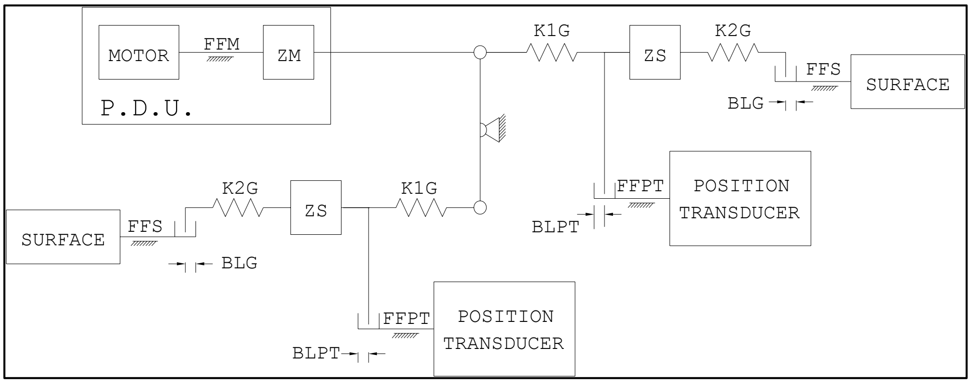

Figure 1 Actuation system mechanical model

If the actuators are non reversible (Fig. 2), this part of the system decelerates rapidly to a stop because the aerodynamic loads cannot backdrive the actuators and the small kinetic energy of the shaft system is soon dissipated by the tare losses of the rotating shafts. If the actuators are reversible, the aerodynamic loads are capable of backdriving the failed part of the actuation system, which can accelerate fast when subjected to large loads because of its low inertia. In this case, in order to stop the uncontrolled surfaces, the actuation system must be equipped either with wingtip brakes (Fig. 3) or irreversibility brakes (Fig. 4). These two alternate configurations are based on:

- controlled wingtip brakes (one for each wing) located at the end of the transmission line, close to the position transducers (Fig. 3), that become engaged and brake the system after a failure has been positively recognized;
- self-acting irreversibility brakes within each actuator, which self engage when the actuator output overruns the input shaft (Fig. 4).

The relative merits of the three solutions (non reversible actuators, reversible actuators with wingtip brakes, reversible actuators with irreversibility brakes) and which of the three is better is a long debated matter: the maximum asymmetry in failure conditions is greater with the wingtip brake solution, the solution with non reversible actuators requires higher hydraulic power owing to its lower efficiency and the irreversibility brake solution, that overcomes the shortcomings of the two previous solutions, is more expensive. Therefore, the most commonly used architecture for high-medium performance aircrafts employs the reversible actuators with wingtip brakes and centrally located PDU (of a dual motor type for operational reliability) because it is cheaper and more efficient, nevertheless the associated high asymmetries in case of failure; whereas for low-medium performance aircrafts the most commonly used architecture employ the irreversible actuators, nevertheless the associated lower efficiencies. Whichever design solution is taken, an asymmetry between the surfaces upstream and downstream of the failure develops as long as the PDU is running and the wingtip brakes, if present, are not engaged.
This developing asymmetry must be detected and a corrective action taken in order to keep its maximum value within a safe limit by means of appropriate monitoring devices equipped with suitable software whose selection is dealt in [5]. Further, when a failure occurs in the wingtip brakes (reversible actuators architecture), consisting of the inability to apply the proper brake torque to the transmission, a flight safety critical condition can arise, particularly following a previous shaft failure; a similar condition can occur when the irreversible actuators turn to be reversible because of structural vibrations and/or temperature troubles. Another possible trouble can occur when the supply pressure of the hydraulic system drops under a defined value, not allowing position servomechanism proper operations.
The monitoring system must be able to detect and properly correct the above mentioned failures. According to the different failure modes above mentioned, different monitoring techniques are considered. In the event of the inability of the wingtip brakes (reversible actuators architecture) to

apply brake torques or in the event of an irreversible actuator turning to be reversible (irreversible actuators architecture) the following monitoring technique is employed: if a position error greater than a defined value is produced by a surface position variation without any command variation, then wingtip or irreversibility brake failure is recognized and the hydraulic system is permanently pressurized. In case of a supply pressure drop in the hydraulic system the monitoring device is able to shutoff the control system until the correct pressure is restored.

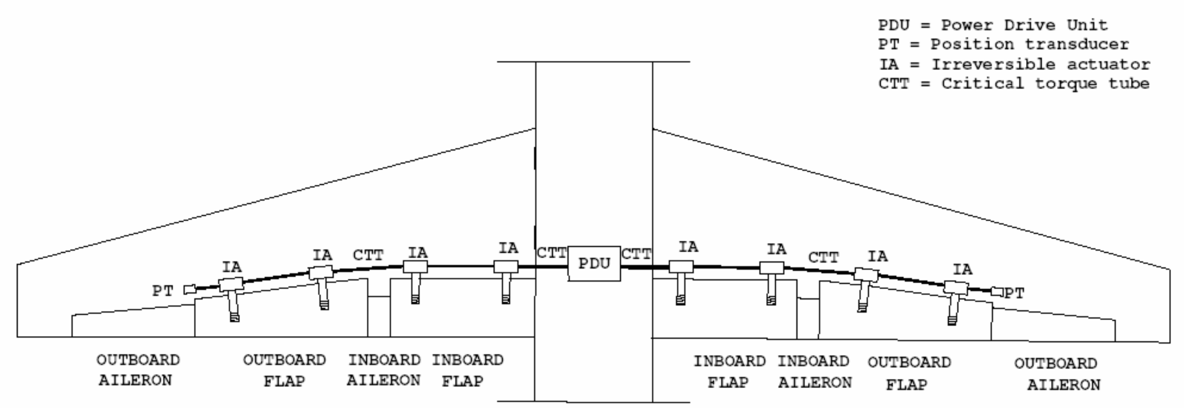

Fig. 2 - Irreversible actuator architecture

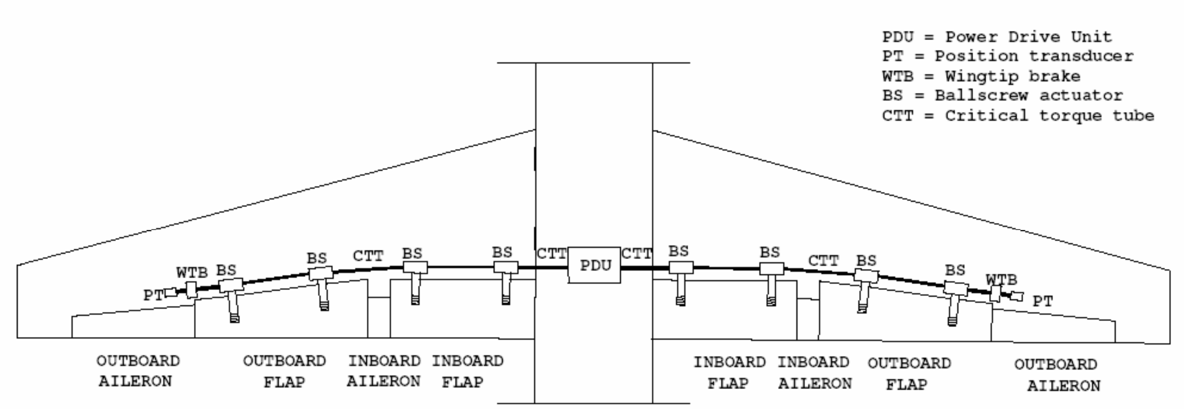

Fig. 3 - Wingtip brakes architecture

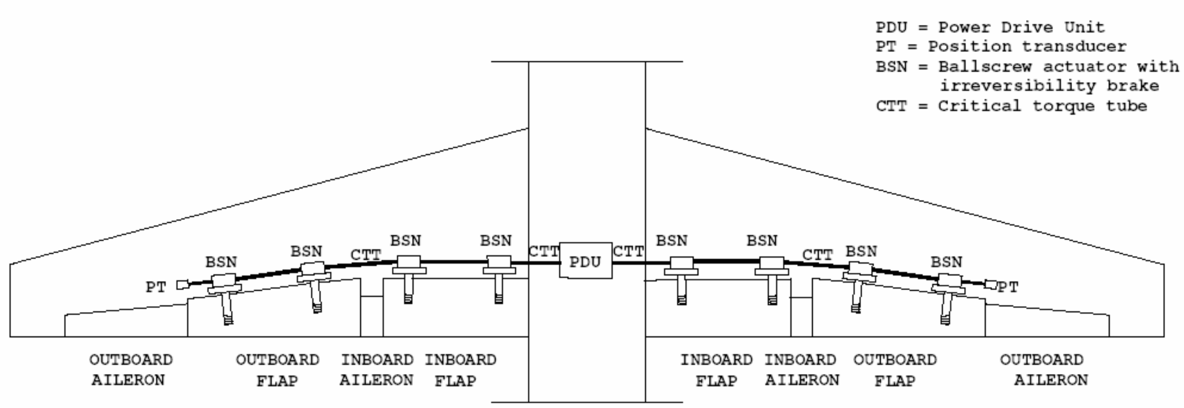

Fig. 4 - Irreversibility brakes architecture

2 MONITORING SYSTEM

The model adopted in this work represents the flap actuation system of a high-medium performance commercial aircraft equipped with single motor PDU (located in fuselage), shaft system realized by means of torque tubes, reversible actuators and controlled wingtip brakes (one for each wing, located at the end of the transmission line, close to the position transducers); this flap layout, almost common in aeronautical applications, joins good efficiency and contained costs but needs an appropriate monitoring system able to detect failure timely and engage adequate corrective actions. In literature we can found many different monitoring techniques, characterized by increasing complexity and performances; in this work is employed the differential position control, a monitoring technique commonly used in aeronautical applications.

3 DIFFERENTIAL POSITION CONTROL

The asymmetry detection is obtained by comparing the electrical signals of position transducers that are placed at the ends of the right and left shaft systems. If a difference greater than an established limit is measured, and it persists for more than a given time, an asymmetry is recognized and shutoff commands are provided to the PDU and to the wingtip brakes. The affected flap or slat system is thus brought to a standstill with a limited asymmetry and it remains inoperative in that condition for the remainder of the flight; this asymmetry control technique is used in the large majority of flap and slat actuation systems.
In this case the maximum resulting asymmetry in a failure condition is a value that, obviously, depends on several factors and in some cases may become large unless appropriate asymmetry control techniques are taken. The maximum asymmetry after a shaft failure mainly depends on the following factors:

- value of the established threshold beyond which the position difference between left and right position sensors signals is considered an asymmetry; this threshold in turn depends on the position sensors accuracy, backlash and stiffness of the shaft system, accuracy errors of the associated electronics;
- asymmetry confirmation time; if an asymmetry is signalled, it must persist for a certain amount of time to be positively confirmed to avoid nuisance system shutdown;
- delay travel of the system over the period of time between asymmetry confirmation and beginning of system deceleration as a result of brakes engagement and power removal;
- shutdown travel from power removal to a standstill.

In order to limit the maximum asymmetry following a shaft failure each of the above factors should be minimized. However, not much can be done on the delay and shutdown travels since they depend on physical factors such as system components inertia and time response of the electrical and hydraulic components, which are generally at the minimum attainable with today technology. Moreover, the delay and shutdown travels make up a low portion of the total asymmetry. The asymmetry threshold is a parameter that provides a large contribution to the final asymmetry. It is generally in the range of 2 to 3% of the full travel to avoid nuisance disconnection of the actuation system resulting from an adverse combination of all the components errors in normal operating conditions.
However, since the developing asymmetry, in case of a shaft failure, can be in a direction opposite to that of the components errors, the actual asymmetry between right and left surfaces before an asymmetry is detected is equal, in the worst case, to the sum of the threshold plus all the components errors and could end up in being 4 to 5% of full travel neglecting the other above mentioned effects. In order to reduce this contribution to the final asymmetry, position sensors and associated electronics with lower errors should be used. Accuracy improvements are possible, but they are practical only up to a given limit, beyond which the cost effectiveness of the improvement is negative. If the final asymmetry after a failure must be maintained within tight limits, a differential position and speed control technique should be used.

4 DIFFERENTIAL POSITION AND SPEED CONTROL

This asymmetry control technique is based on detecting the differences of both position and speed of the two ends of the transmission shafts. If either the position or the speed differential exceeds an established threshold for more than a given amount of time, than an asymmetry is recognized and a system shutdown is performed in the same way as for the differential position control technique described in the former paragraph. This control technique is faster in detecting rapid developing asymmetries since it recognizes an asymmetry as soon as large speed differences come up between the right and the left ends of the transmission shafts. Thus, the system shutdown procedure can be started well before the differential position threshold is reached, with a resulting lower final asymmetry. The measurement of the speed at the end of the transmission shaft can be obtained either from dedicated speed sensors (tachometer dynamo) or as a result of an algorithm that computes the speed as the time derivative of the position measured by the position sensor. It must in fact be noted that the positions of the two ends of the transmission shafts must always be measured and compared with each other to detect asymmetries which could develop at a slow rate and thus not be picked up by the differential speed control. Each of the two solutions (additional speed sensors or time derivation of the position measurements) has its own advantages and drawbacks. Therefore, this type of control technique supplies a forecast of the future differential position, allowing to the monitor ing system faster corrective actions and more contained asymmetries. A partially analogous effect can also be obtained by means of a differential position monitoring system equipped whit a phase anticipator filter (typically a lead-lag filter, able to supply an esteem of the evaluation of future differential position).If the final asymmetry, produced after a failure of flap control system, had to be contained within tightest limits, literature suggest adopting alternative, but more complicated, monitoring techniques, able to detect the failure and operate opportune corrective actions aimed to minimize such asymmetry. An example of "active" monitoring technique is the active differential position and speed control technique [5], which is intended to minimize the final asymmetry between right and left flap surfaces following a failure by driving the part of the actuation system which is still connected to the power drive unit to a standstill in a controlled position. This control technique provides the advantage of yielding a minimum final asymmetry. It can be pursued, however, only if the asymmetry control is performed by means of a digital controller; moreover it creates an additional burden to the computer.

5 AIMS OF WORK

Aim of the work is the proposal of modified flap actuation system architecture with respect to the typical layout having reversible actuators and commanded wing-tip brakes: the employment of wing-tip brakes having both electrical or hydraulic command and automatic centrifugal engagement. So the present work shows the comparison between the dynamic behaviours of a traditional flap actuation system, equipped with a typical reversible actuators (with wingtip brakes) architecture, and an analogous flap actuation system, further equipped with the proposed centrifugal brakes (one for each wing, assembled between wingtip brake and outboard flap or directly integrated into the same wingtip brake). Our goal is to show the interesting behaviours of the proposed system and suggest a possible alternative solution able to integrate a differential position control system (robust and cheap) increasing its performances (reduced final asymmetries).

6 ACTUATION SYSTEM MODELLING

In order to compare the behaviour of a typical flap actuation system (reversible actuators with wingtip brakes) with an equivalent system further equipped with the proposed centrifugal brakes, an actuation system was considered, typical of those currently used for flaps actuation (Fig. 3). The schematic of such actuation system is shown in Fig. 1. The system consists of a Power Control and Drive Unit (PDU), a shaft system and ballscrew actuators (BS) driving the flaps (or slats). Each ballscrew actuator is an assembly containing a gear reducer (ZS) and a ballscrew. The two torsion bars (CTB) between the PDU and the inboard actuators are considered to be the weak link in the power drive system. At the two outer ends of the shaft system are located the wingtip brakes (WTB), the position transducers (PT) and the speed sensors, if present. The system control is performed by an Electronic Control Unit (ECU), not shown in Fig. 2, 3 and 4, which closes the position control loop. The position information provided by the transducers is also used by appropriate monitoring routines to detect possible asymmetries between right and left flap (or slat) surfaces. The PDU contains the hydraulic motors, the gear reducer (ZM) and solenoid, shutoff and control valves. The hydromechanical system considered for this work is assumed to also contain tachometers for a continuous actuation speed control. Fig. 1 shows the mechanical model of the actuation system. The model takes into account the hydraulic and mechanical characteristics of all system components, including their friction, stiffness and backlash. In particular, the model takes into account the following:

- Coulomb friction in the PDU (FFM), in the actuators (FFS) and in the position transducers (FFPT),
- stiffness (K1G) and backlash of the torsion bar of the right and left shaft systems,
- errors and temperature effects in the position transducers and backlash (BLPT) within the position transducers drive,
- errors in the position transducers electronics and in the A/D conversion,
- stiffness (K2G), backlash (BLG) and lead errors of the ballscrew actuators,
- third order electromechanical dynamic model of the servovalve with position and speed limitations and complete fluid-dynamic model [6],
- dynamic and fluid-dynamic hydraulic motor and high speed gear reducer model taking into account, beside the above mentioned Coulomb friction, viscous friction and internal leakage.

It must be pointed out that the stiffness K1G and the backlash BLPT are within the system servoloop; the stiffness K2G and the backlash BLG are parameters of a system branch off the servoloop. The mathematical model takes also into account an activation / deactivation logic of the flaps hydraulic actuation system. According to this logic, when the system is depressurized and an actuation command is given, exceeding a defined value and persisting for more than a defined time, first of all a pressurization command is performed by means of a solenoid valve - shutoff valve assembly, then, following the monitoring of the correct supply pressure level, the true actuation command is given by means of the control valve to the hydraulic motor. When the commanded position is reached with an error lower than a defined value for more than a defined time a shutoff command is given in order to depressurize the hydraulic system, so avoiding the continuous oil leakage from the supply to the return pressure which affects the pressurized system.

7 AIRCRAFT AND AUTOPILOT MODELLING

In order to assess the amount of perturbations induced on the aircraft attitude by the failures of the flap actuation system, the lateral-directional dynamics of the aircraft and of its autopilot have been simulated. The autopilot control laws have been assumed to be of a PID type, which is adequate to approximate the actual autopilot control for the purpose of the present work. By measuring the aircraft roll angle the autopilot PID controller generates the commands to the ailerons and to the rudder. These flight controls have in turn been simulated as second order systems with a saturation on their maximum speed and position. The aircraft data taken for the simulations are typical of a business jet of the Gulfstream IV class.

8 SIMULATION RESULTS

The above described models of the actuation system, of the aircraft and of the autopilot have been used to build a mathematical model of the whole system and a dedicated computer code written in Digital Visual Fortran 6.0 has been prepared. The computer code contains the models of:

- the differential position asymmetry monitoring techniques,
- the wingtip brakes failures monitoring technique,
- the supply pressure drop monitoring technique.

Several simulations have been run for the case of a mechanical failure of the transmission shaft with a resulting asymmetry between right and left surfaces. In the following figures $D\theta_M$ is the motor speed, θ_{SL} and θ_{SR} are the left and right flaps positions, θ_A is the deflection angle of the ailerons and RoA is the aircraft roll angle. Figures 5, 6, 7 and 8 show the simulations results for the cases of deploying flaps with reversible actuators in the final part of their stroke to the landing position under high values of aerodynamic loads, that act as opposing to the flap deployment. The simulation results shown in Fig. 5 and 7 refer to the cases of "traditional" flaps actuation architecture, while in Fig. 6 and 8 are illustrated the analogous cases of "improved" flap actuation system equipped with the proposed centrifugal brakes. For all these simulations, the transmission shaft failure occurs at time = 3 [s], while the actuation system is running from the initial position XJ0 of 23 [°] to the final commanded position Com of 40 [°]. In case of opposing loads the part of flap system downstream of the failure decelerates under the action of the load and then accelerates backward until the asymmetry is recognized and the wingtip brake engages providing its braking torque to arrest the system. Meanwhile, the other part of the system is driven by the PDU until the asymmetry monitoring provides the shutdown command. The deployment command don't produce an instantaneous response, because all the flaps actuation system, initially, is in stand-by condition (hydraulic system depressurized with wingtip locked and aerodynamic surfaces blocked), so a starting delay is necessary to pressurize again the hydraulic lines and verify all the items and procedures; this process, typical of the employed system's architecture, is clearly found in the phase of start of flaps system in all the cases examined from Fig. 5 to Fig. 13. In Fig. 5 is possible to state immediately as, at time ≈ 0.25 [s] when the flaps actuation system is activated and ready, begins the flap's actuation (their positions evolve form the initial position XJ0 to the commanded final position Com). At time t = 3 [s] the failure of right critical torque tube interrupts the mechanical connection between PDU and right flap, so this aerodynamic surface and the part of transmission downstream the damage, under the single action of the opposing aerodynamic forces, decelerates very fast and then accelerates backward until the asymmetry is recognized and the wingtip brake engages providing its braking torque to arrest the system. The control system, by means of dedicated position sensors located to the tip of the transmission lines (see Fig. 1), computes the relative position error θ_{SL} - θ_{SR} and, when it exceeds a tolerance limit, declares damage and assets the opportune emergency procedures. The curves θ_A and RoA show the effects of the asymmetry monitoring techniques on the aircraft attitude. It can be seen that the roll angle RoA increases as the asymmetry develops; at the same time the autopilot generates a command to the ailerons to realign the aircraft; this take place through a dynamic response which includes a dutch roll component. In the case examined in Fig. 5, in which the aerodynamic load (only depending on the flap's deflection because, in this case, have assumed null the term of constant load TRLC and TRRC) plays a limited role in total dynamic of the system, the control system equipped with differential position monitoring is able to detects failure and stops timely the surfaces intrinsically assuring the airplane's roll control. Fig. 6 shows the system response in the same loading and failure conditions and employing the same type of monitoring technique but, differently from the previous case, the now examined flap actuation architecture is equipped with the proposed centrifugal brakes (concrete proposal since these items could easily be integrated in the wingtip brakes without meant system problems or huge structural modifications). At the start the dynamic behaviour is the same one above examined, but the effects of the failure are visibly different; the final value of the relative position error Err = θ_{SL} - θ_{SR} is lower (in this case the error Err is worth 3,2 [°] while the corresponding system unequipped with centrifugal brakes produces instead an error of approximately 8,9 [°]) and, consequently, the roll oscillations as well as the ailerons deflection angle are reduced (if compared with the corresponding values of Fig.5). The reduction of the asymmetry error is a consequence of the dynamic behaviour of the proposal flap actuation architecture equipped with centrifugal brakes; in fact, for values of speed greater than a prefixed limit, this brakes supply a breaking couples strongly increasing with its angular speed. Therefore this system limits the maximum speed rate developed by the mechanical system downstream a failure and, consequently, slows down the asymmetry rate and increases the performance of the proposed architecture. Regarding the previous case (Fig.5), we notice as the final position of both the flap, in the simulation of Fig. 6, turns out increasing; also this aspect can be explained with the role played to the centrifugal brakes; in fact, in case of damage, the flaps actuation system, under the action of the high aerodynamic loads, would stretch to accelerate quickly developing high angular rate; limiting the maximum angular rate of the mechanical system, the position asymmetry develops in a longer time and so, when the warning limit is exceeded, the flap position error is smaller and the final position of aerodynamic surfaces is increased. Figures 7 and 8 show the simulation performed for the case of deploying flaps in the final part of their stroke to the landing position under the maximum opposing loads; too the failure of the transmission shaft occurs at time = 4 [s], while the actuation system is running in a steady condition, following the system's activation time. This kind of operational conditions, characterized by higher aerodynamic loads, are extremely severe for the mechanical flaps actuation devices (in consequence of the high structural stress) especially because typical of the high incidence configuration (like take-off and landing); in fact, in these flight attitude conditions, a torque tube failure may represent a critical event with possible catastrophic consequences. In this case the downstream failure transmission's section asymmetry error, aided from the elevated loads, grows so quickly that, when the monitoring system stops all the aerodynamic surfaces, the autopilot is no longer able to balance (with an opportune antisymmetric ailerons deflection) the roll moment caused by the flap's asymmetry. Fig. 7 shows as an asymmetry error Err = θ_{SL} - θ_{SR} of approximately 16 [°] saturates the autopilot's roll control (in fact the ailerons reach their ends of travel) generating an uncontrolled airplane's roll rate DRoA clearly put in evidence by the response of the aircraft roll angle RoA (with an Err ≈ 16 [°] we find a DRoA ≈ 2 [°/s]). Although the differential position asymmetry monitoring technique is generally used and considered sufficient to maintain the aircraft control after a failure, the results of Fig. 7 clearly indicate that a careful analysis should be conducted to verify whether the margins of safety are not becoming too small under a combination of adverse conditions. In such case adoption of the "improved" flap actuation system, equipped with the proposed centrifugal brakes, should strongly be considered for improving the aircraft handling after a flap transmission shaft failure.

Fig. 8 shows the system response in the same command, loading and failure conditions considered in Fig. 7, but, differently from the previous case, it is referred to the flap actuation architecture equipped with the proposed centrifugal brakes; this system overcomes the limitations related to the previous one, in fact the connected smaller asymmetries avoid ailerons deflection saturation and, as a consequence, autopilot and ailerons are able to perform an efficient atti

tude control. The reasons of the merits of the centrifugal brake solution concern the reduced angular rate of the failed portion of the system under high aerodynamic loads, thus reducing the final flap asymmetry, so preventing safety critical flight conditions. Figures 9,10, 11 12 and 13 show the simulations performed for the case of retracting flaps with different aiding loads; in these simulations too the failure of the transmission shaft occurs at time = 0.4 s, while the actuation system is running in a steady condition, following the system's activation time. Since these simulations have been run for large aiding loads cases, the portion of the shaft system downstream of the failure accelerates rapidly under the action of the loads with a resulting asymmetry until the system shutdown occurs. As for the case of large opposing loads of Figures 5, 6, 7 and 8 the employment of the proposed architecture equipped with centrifugal brakes provides a lower angular rate of the failed subsystem and a following smaller final asymmetry with a resulting lower attitude misalignment of the aircraft. Particularly the cases shown in Figures 11, 12 and 13, all characterized by high aerodynamic loads, put in evidence that the centrifugal brakes architecture (Fig. 12 and 13) improves the system response, so producing smaller asymmetries and maintaining the autopilot/ailerons ability to control the aircraft attitude. Fig. 9 shows the response of the conventional flap actuation system (without centrifugal brakes) in small angle of attack flight conditions (aerodynamic loads proportional to the flap deflection). The time history of the flap angular position θ_{SR}, since the failure onset till to the complete system stop, puts in evidence the sudden slope growth of the curve, representing the high angular rate of the failed mechanical transmission.

The comparison between the system responses reported in Fig. 9 and 10 shows the effect of the proposed centrifugal brakes (Fig. 10), improving the system behaviour in terms of final asymmetry reduction (in this case the asymmetry Err = θ_{SL} - θ_{SR} is close to 2 [°] instead of 8 [°] of the conventional architecture) although allowing a greater flaps travel (in retraction mode) since the failure time till to the complete stop (the reduced asymmetry growth rate delays the failure confirmation and the following start of the shutdown procedure. Figures 11 and 12 analyse the flap retraction in the event of high angle of attack involving higher aiding aerodynamic loads. Fig. 11 shows the behaviour of the conventional architecture: large asymmetries are the consequence of an uncontrolled high rate of the system portion downstream the failure point (especially if compared with the corresponding values shown in Figures 12 or 13): it results in the inability of the autopilot and aileron system to prevent uncontrolled roll rates and related flight safety critical conditions. Fig. 12 analyse the response of the proposed unconventional architecture, equipped with centrifugal brakes: it overcomes all the problems of asymmetries eventually exceeding a safety limit, assuring the effective and fast autopilot/aileron ability to prevent uncontrolled aircraft roll rates (limited and quickly damped roll/yaw oscillations). Fig. 13 shows the system response characteristics as a function of the centrifugal brakes performance; in fact, increasing the braking torque developed by this device in the same angular rate conditions, a reduced asymmetry following the transmission failure is performed.

Moreover, the employment of centrifugal brakes characterized by greater braking torque growth as a function of the shaft angular rate, enhances the flap travel (and the consequent average retraction), since the failure occurs till to the complete standstill condition is reached. This may be considered as a shortcoming: so, an appropriate design of the system requires the selection of the correct type of centrifugal brake, aiming at the prevention of both critical asymmetries and unacceptable growth of the system stop-travel in retracting conditions.

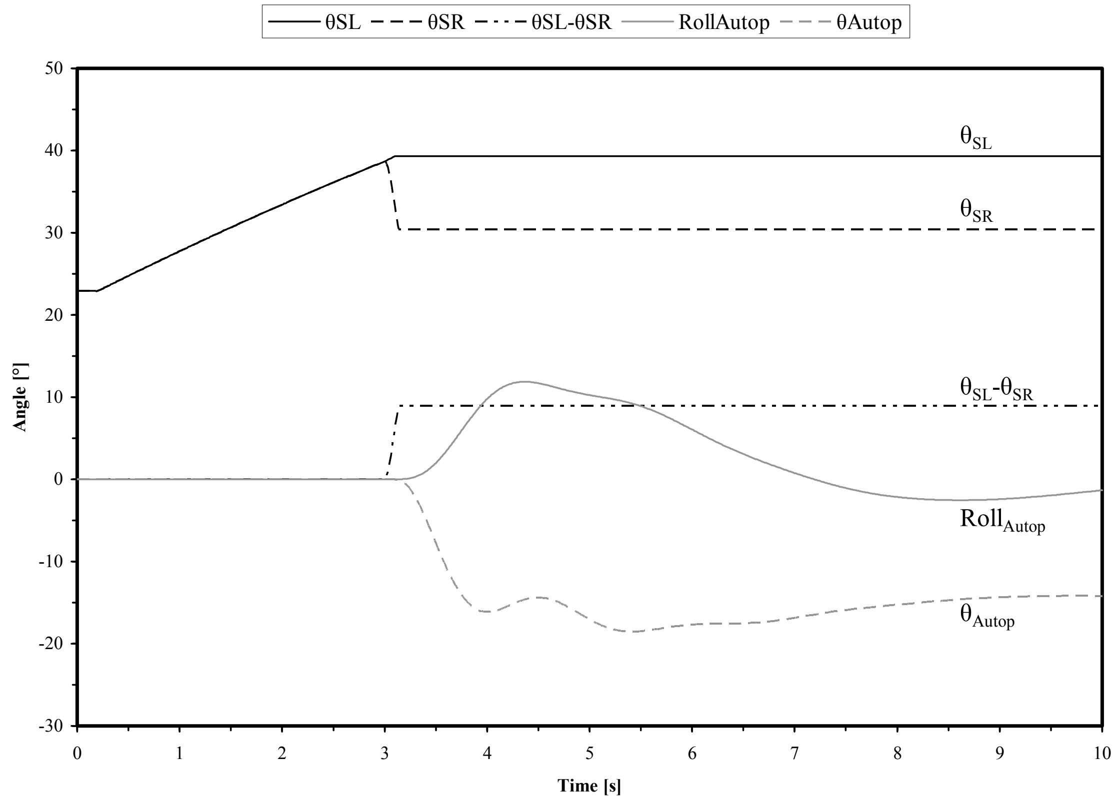

Figure 5

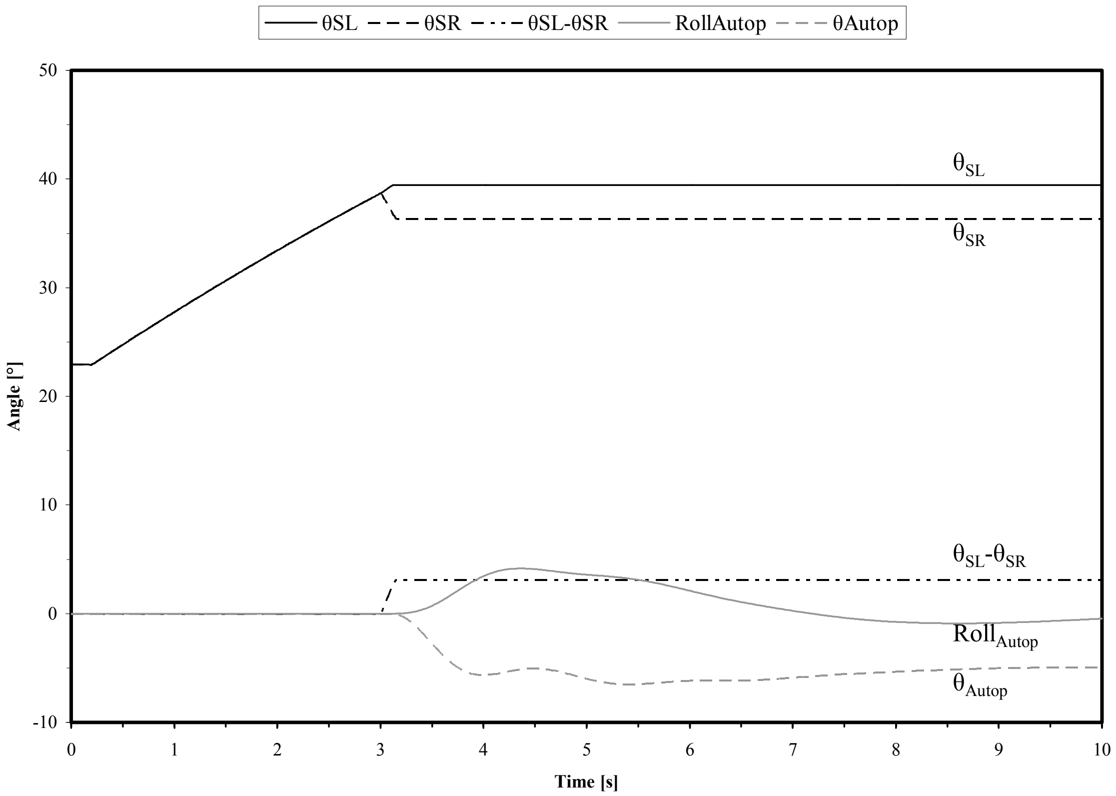

Figure 6

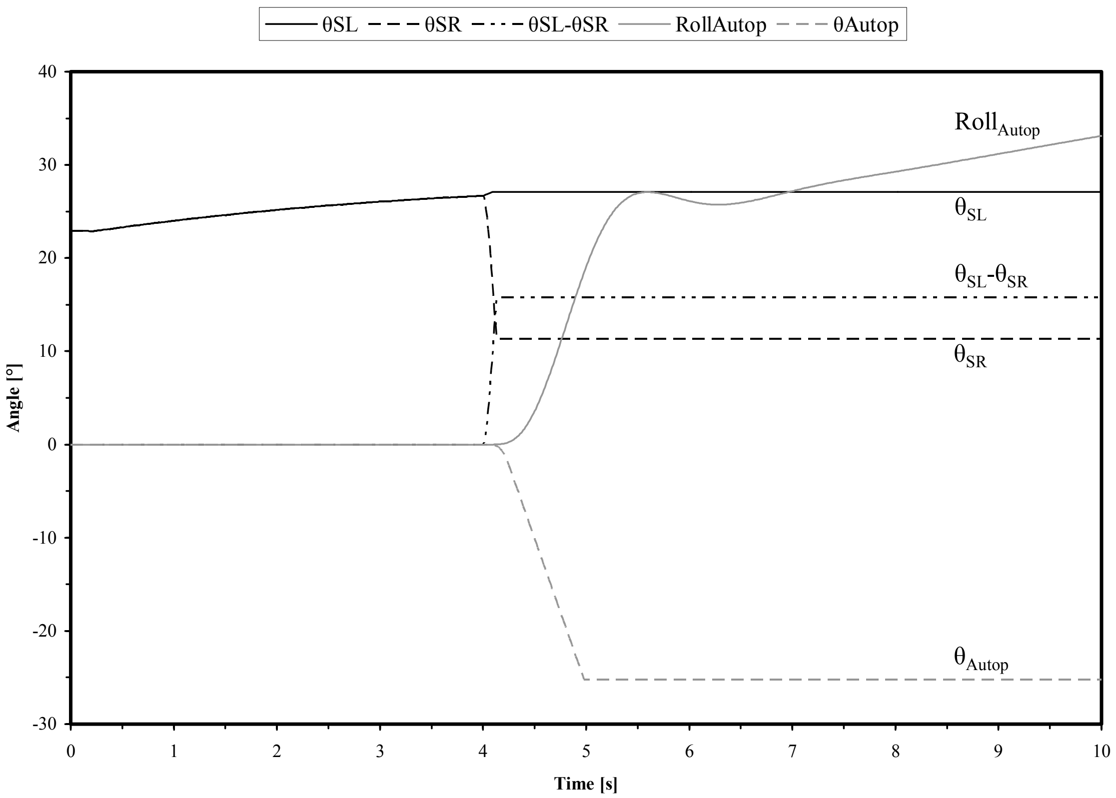

Figure 7

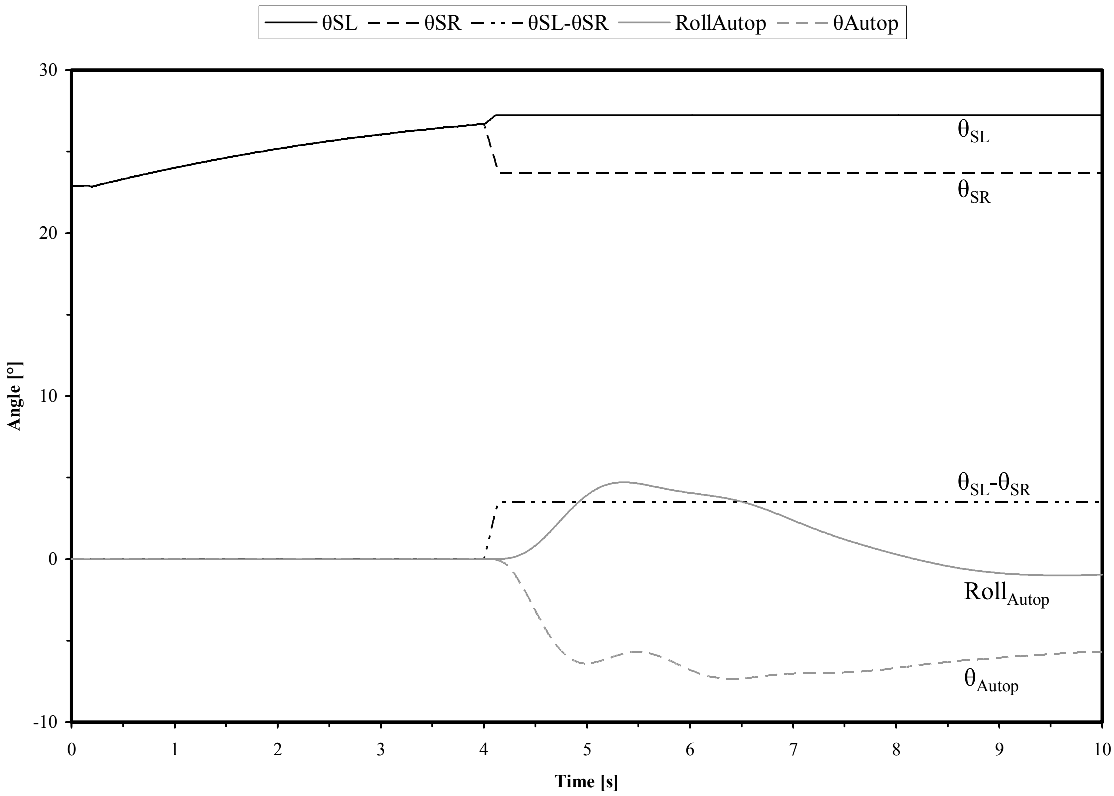

Figure 8

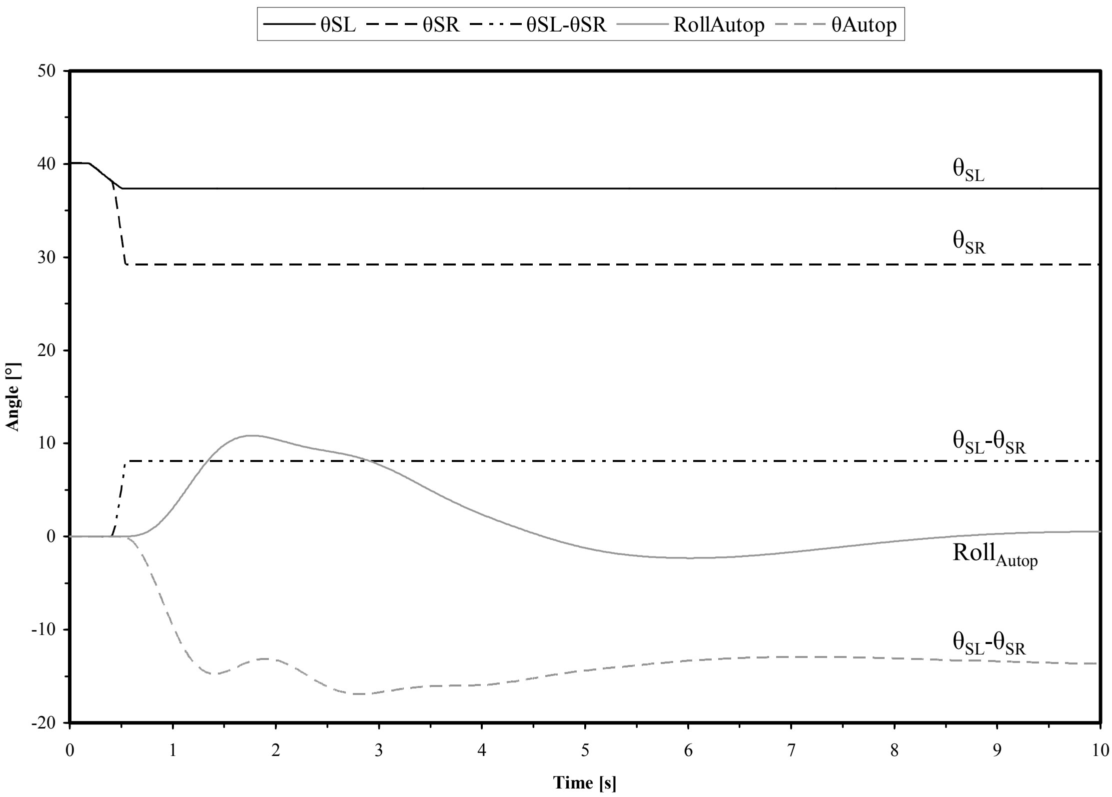

Figure 9

ISSN 1590-8844
International Journal of Mechanics and Control, Vol. 07, No. 02, 2006

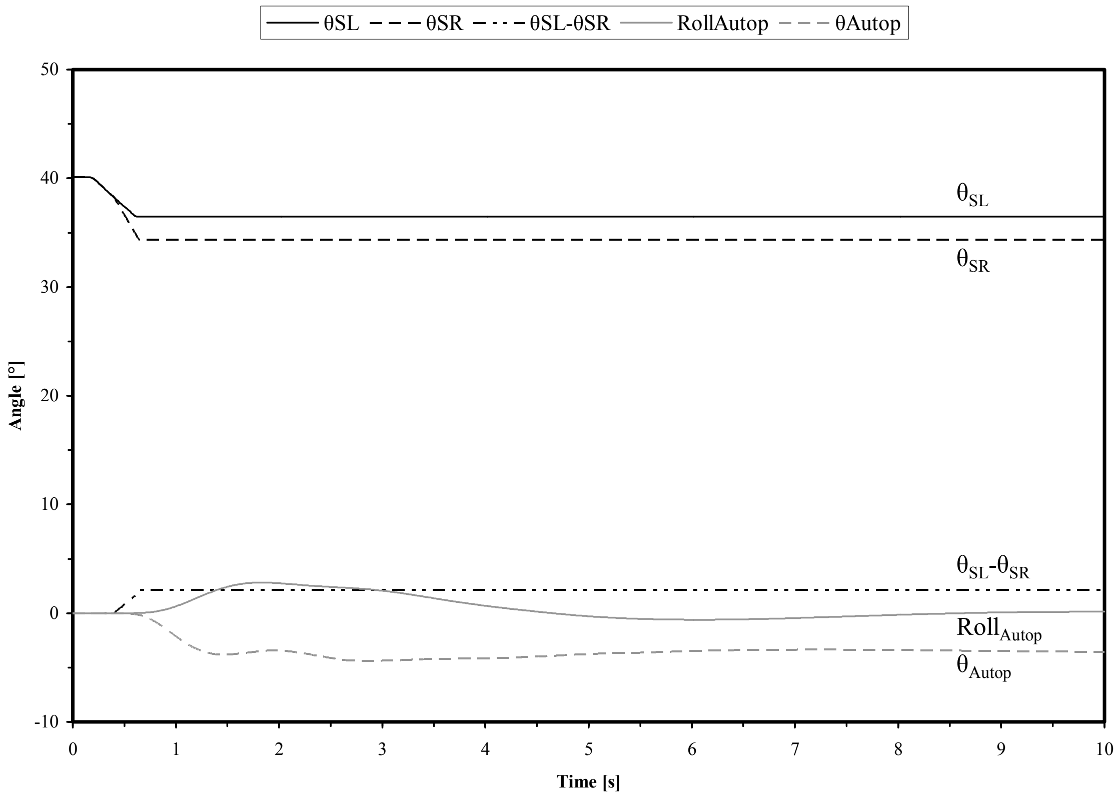

Figure 10

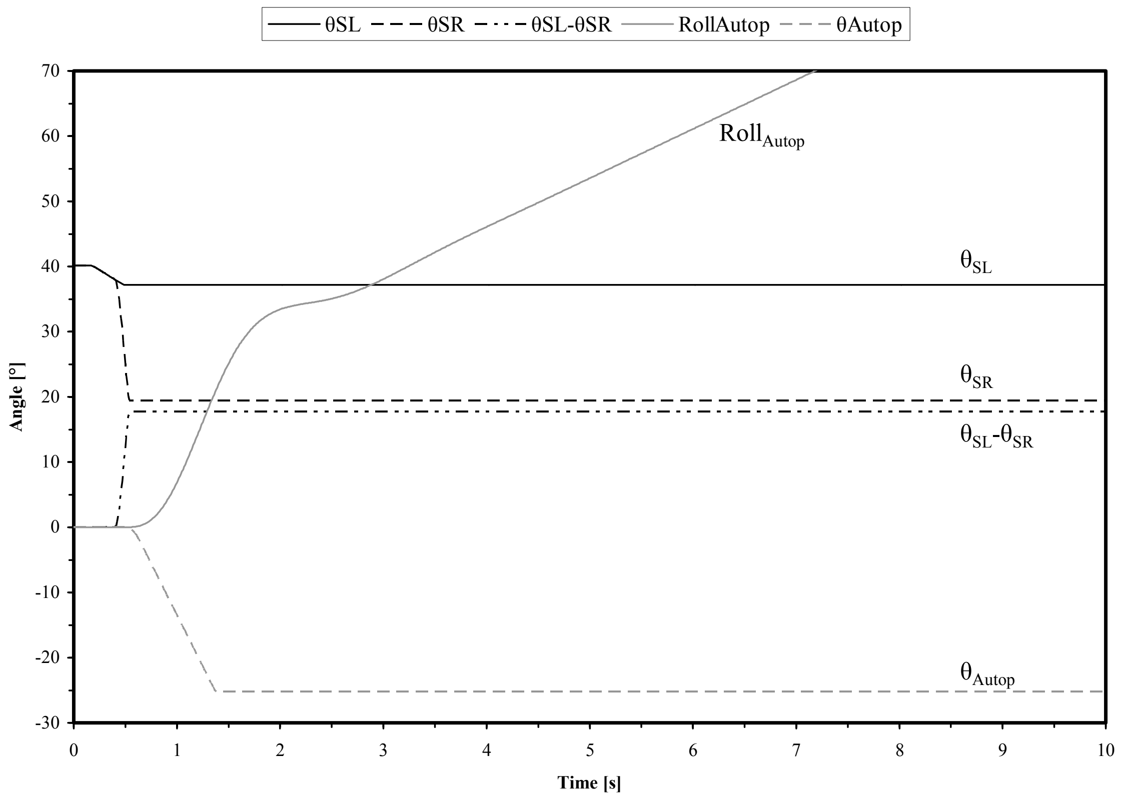

Figure 11

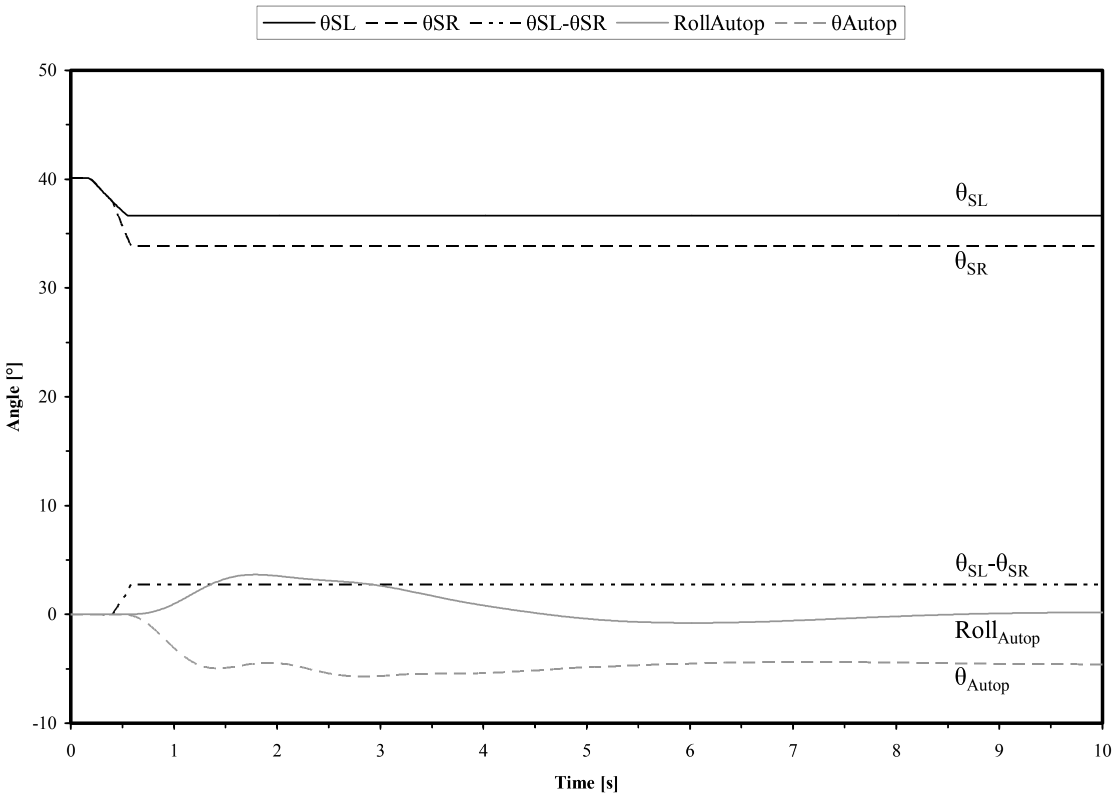

Figure 12

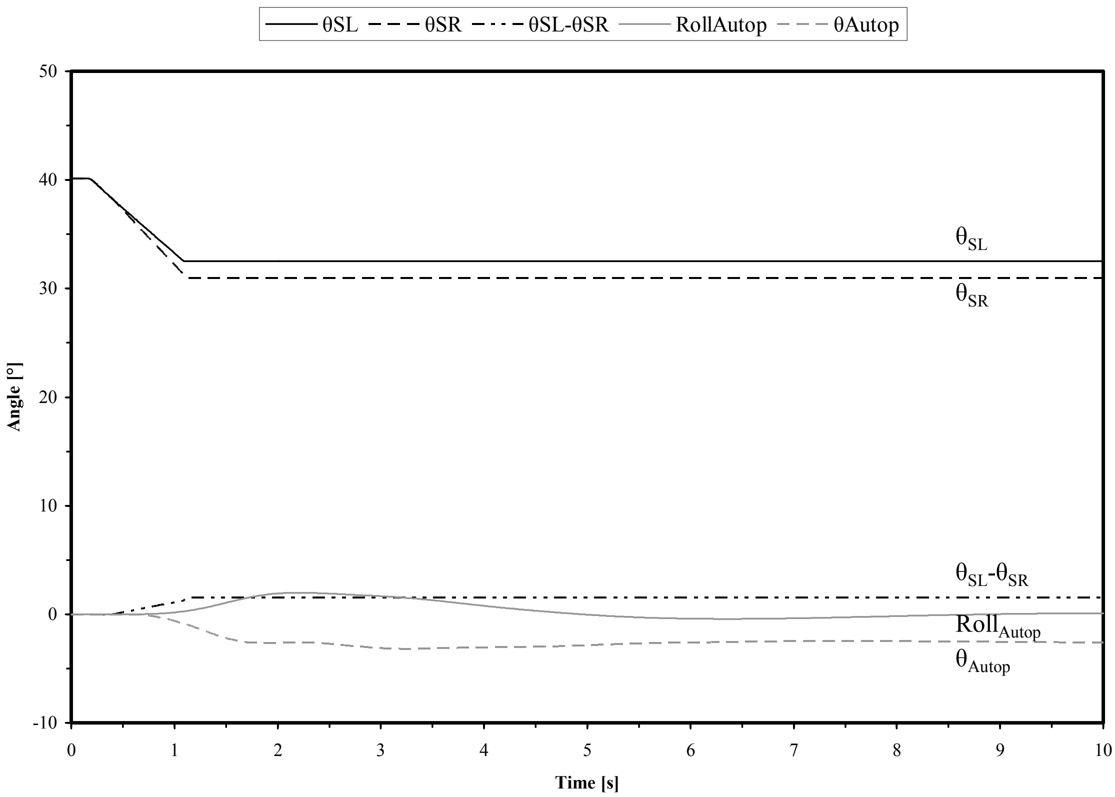

Figure 13

9 CONCLUSIONS

The results of the present work show the high sensitivity of the aircraft controllability to the flap system behaviour following a shaft failure involving asymmetries.
The simulations reported in figures 5 to 13 refer to the case of asymmetries of the flaps because they are more critical than the asymmetries of the slats; however similar results, thought less critical, can be obtained if a mechanical failure of the slat transmission shaft system is considered.
It has been shown that the aircraft control during the transient of the developing flaps asymmetry and in the following asymmetric flaps condition can be greatly improved if the actuation system is equipped by the proposed centrifugal brakes.
This type of architecture significantly reduces the flap asymmetries following a shaft failure, particularly in high load conditions (without undesirable marked growth of constructive complexity), increasing the aircraft controllability and preventing safety critical flight conditions.

LIST OF SYMBOLS

BLG	Ballscrew actuator backlash
BLPT	Position transducer backlash
BS	Ballscrew actuator
BSN	Ballscrew actuator with built-in irreversibility brake
CTT	Critical torsion tube
DThSL	Left flap angular rate
DThM	Motor angular rate
FFM	Motor Coulomb friction torque
FFPT	Position transducer Coulomb friction torque
FFS	Surface-actuator Coulomb friction torque
K1G	Torsion bar stiffness
K2G	Ballscrew actuator stiffness
PDU	Power Drive Unit
PSV	Servovalve supply pressure
PT	Position transducer
RoA	Aircraft roll angle
ThA	Angle of command for the ailerons
ThSL	Left flap position
ThSR	Right flap position
WTB	Wingtip brake
ZM	Motor gear reducer
ZS	Actuator gear reducer

REFERENCES

[1] Jacazio G., Borello L., A non-linear model of an electrohydraulic servo system with axial piston hydraulic motor, *7th International Fluid Power Symposium*, Bath, England, 16-18 September 1986.

[2] Borello L., Villero G., Modelli di attrito coulombiano nella simulazione di servomeccanismi, *NT Tecnica & Tecnologia N.3/89 (A.M.M.A.)*, Turin, Italy, pp. 11-17, May-June 1989.

[3] Jacazio G., Borello L., Villero G., Secondary flight controls: mechanical failures of transmission lines and related asymmetry problems, *19th ICAS Congress*, Anaheim, CA, U.S.A., 18-23 September 1994.

[4] Borello L., Villero G., An innovative architecture for flap control system of medium/large aircrafts, *1st AIAA Aircraft Engineering, Technology, and Operations Congress*, Los Angeles, CA, U.S.A., 19-21 September 1995.

[5] Borello L., Villero G., Mechanical failures of flap control systems and related monitoring techniques, *21st ICAS Congress*, Melbourne, Australia, 13-18 September 1998.

[6] Borello L., Villero G., Flap control system actuators: mathematical and computational model for dynamic simulation, *European Congress on Computational Methods in Applied Sciences and Engineering ECCOMAS 2000*, Barcellona, Spain, 11-14 September 2000.

[7] Jacazio G., Variable Displacement Hydraulic Motor Driven Actuation Systems for Efficient Secondary Flight Controls, *International Journal of Mechanics and Control (JoMaC)*, Turin, Italy, pp. 47-57, Vol. 01, Nr. 02, 2000.

[8] Borello L., Villero G., Mechanical Failures of Flap Control Systems: Proposal of Advanced Monitoring Techniques, *International Journal of Mechanics and Control (JoMaC)*, Turin, Italy, pp. 9-18, Vol. 05, Nr. 02, 2004.

[9] Viersma T.J., *Analysis Synthesis and Design of Hydraulic Servo-systems and Pipelines*, Elsevier, Delft, 1980.

[10] Dransfield P., *Hydraulic Control Systems. Design and Analysis of their Dynamics*, Springer Verlag, Berlin, 1981.

ISSN 1590-8844
International Journal of Mechanics and Control, Vol. 07, No. 02, 2006

PHYSIOLOGICAL PARAMETERS VARIATION DURING DRIVING SIMULATIONS

C. Zocchi* A. Rovetta* F. Fanfulla**

* Politecnico of Milano, Mechanical Department, Robotics Laboratory

** Sleep Centre, Rehabilitation Institute of Montescano, IRCCS, S. Maugeri Foundation, Pavia

ABSTRACT

This paper deals with the methodology of using biorobotics principles for creating a new intelligent system, to improve safety in an automobile transportation. Many projects in European Union programs are devoted to the increase of safety in automotive, in order to reduce deaths and accidents down to 50% in the next few years. The project here presented, named PSYCAR (feasibility analysis on a car control system by psychic-physical parameters), aims at a new driving system, where the steering wheel is inserted in an architecture of intelligent sensors, able to monitor the psychophysical state of the driver, in order to avoid accidents due to sleep attacks and microsleeps. All the indications will come from the steering wheel, where the hands and the finger actuate a great part of the car control. Main goal of the research is to define the right parameters for driver's psycho-physical status monitoring during simulated tests. The heart of this paper is the application of multivariate statistics methods for evaluating the correlations between the physiological parameters acquired (EEG, galvanic skin response or resistance, peripheral temperature and heart rate variability).

Keywords: biorobotics, microsleep, physiological parameters, safety in automotive, statistics

1 INTRODUCTION

PSYCAR project, funded by European Union (EU) in a Regional plan, starting from Lombardy Italian Region and Austrian Region, is one of the projects aiming to the determination of the correct psycho-physical parameters to be monitored in the driver and car system to increase safety. The methodology presented in this paper is innovative for the field of automotive safety, because all the driver's physiological parameters are acquired using sensors on the steering wheel and on the safety belt, which are continuously in contact with the driver's body. The driver does not have to do anything in particular or, in any mode, different from what he is used to do when entering and driving his/her vehicle.

Contact author: C. Zocchi[1], A. Rovetta[2], F. Fanfulla[3]

[1]E-mail chiara.zocchi@polimi.it

[2]E-mail alberto.rovetta@polimi.it

[3]E-mail ffanfulla@fsm.it

Drivers' fatigue has been implicated as one of the causal factor in many accidents because of the marked decline in the drivers' abilities of perception, recognition and vehicle control abilities while sleepy [1-5]. Driving under the influences of drowsiness will cause: 1) longer reaction time, which may lead to higher risk of crash, particularly at high speeds; 2) vigilance reduction including non-responses or delaying responding where performance on attention-demanding tasks declines with drowsiness; 3) deficits in information processing, which may reduce the accuracy and correctness in decision-making. Many factors can cause drowsiness or fatigue in driving including lack of sleep, long driving hours, use of sedating medications, consumption of alcohol and some driving patterns such as driving at midnight, early morning, midafternoon hours, and especially in a monotonous driving environment [6]. Accurate and non intrusive real-time monitoring of driver's drowsiness would be highly desirable, particularly if this measure could be further used to predict changes in driver's performance capacity.
Two major categories of methods have been proposed to detect drowsiness in the past few years: one focuses on detecting physical changes during drowsiness by image

processing techniques, such as average of eye-closure speed, percentage of eye-closure over time, eye tracking as quantization of drowsiness level and driver's head movements. These image-processing based methods use optical sensors or video cameras to detect eye-activity changes in drowsiness and can achieve a satisfactory recognition rate (i.e. Mercedes-Benz studies [7]). The other methods, followed in the PSYCAR project, are about the measure of driver's physiological changes, such as Heart-Rate Variability (HRV), Galvanic Skin Response (GSR), peripheral Temperature (THE) and electroencephalogram (EEG), as a means of detecting the human cognitive states [8-11].

2 SIMULATOR SYSTEM

A simulator system has been developed at the Robotics Lab. of the Politecnico of Milan. The system consists of 1) a computer games steering wheel (Logitech Momo) with pedals and brake, 2) a simulated highway projected in front of the driver, giving him the impression of actually driving, 3) the driving cabin simulator mounted on a 6-DOF dynamic Stewart motion platform (developed at Keplero University of Linz) and 4) the EEG measurement system (Figure. 1). On the right hand, GSR, HRV and THE sensors are placed in order to measure these driver's parameters and to reduce movement artefacts.

Figure 1 Simulator System.

2.1 GSR, THE AND HRV SENSORS

According to previous study [12], GSR was measured using 30mm² non polarizable Ag/AgCl electrodes placed on the median and the ring finger of the right hand with adhesive tape. Typical GSR values fell in the range [150; 300] kΩ. For the HRV measure a photoplethysmographic sensor was placed on the forefinger (Figure 2). From the HRV measured, the R-R form and the beats per minutes (BTS) are calculated.

Figure 2 GSR and HRV placement on the right hand.

2.2 EEG RECORDING

EEG recording (Embla S7000 and Somnologica Software – Embla - Broomfield, CO - USA) was performed using standard procedures and scored manually in a 30-seconds epoch according to Rechtschaffen and Kales' criteria [13]. The equipment provided simultaneous measurements of EEG_s (C_3-A_2; C_4-A_1; O_1-A_2; O_2-A_1), EOG_s, submental EMG, EKG, airflow by nasal cannula, thoracic and abdominal respirogram by means of a plethysmographic method (X-trace, Embla - Broomfield, CO - USA), SaO_2 by means of a pulse-oximeter.

Microsleeps (MS) were scored as follows [14]: a period of at least 3s with a ϑ (4–7 Hz) rhythm replacing a α rhythm or appearing on a background of desynchronized EEG on all four EEG channels, and without eye-blinking artefacts. Slow eye movements were accepted [15]. The presence of α rhythm was considered as wakefulness, and thus excluded microsleep. No maximal length was defined for microsleep, so that it could evolve into established sleep if it lasted long enough.

All the recordings were separately analyzed by two expert technicians individually and independently, and finally reviewed by the physician.

2.3 TEST PROTOCOL

All subjects executed one or more 30min driving simulation. Before starting the data acquisition, a psychological questionnaire about general sleep/wake habits is completed, on which also date, time and environmental conditions are written. The car at the start of every simulation session is always positioned at the same point of the virtual highway. Each subject, before driving for the first time is also trained to use the simulator and to always follow the same pre-defined route for 5min. At the same time all sensors are calibrated.

After these initial procedures, the driver starts the simulation and the data acquisition is also initialized. During the procedure and in pre-defined times, that the subject does not know, an obstacle appears on the screen and the driver has to brake immediately. In this way, his/her reaction time is measured and stored among all the other parameters acquired (these data will be used in next studies). This response time along with the data from the polysomnography signals [16, 17] will determine driver attention level. The simulations are always made in dark and noiseless conditions in order for the person to have much more possibilities to fall asleep.

2.4 SUBJECTS

25 subjects (22 men and 3 woman; age range, 24 to 47; mean age 35[±5] years), with not particular pathologies, were studied during the execution of one or more 30min driving simulation.

These healthy subjects had no clinical evidence of snoring or sleep apnoeas and no complaint of excessive daytime sleepiness (EDS). They were recruited between students of the Robotics Course (Politecnico of Milan) and the medical team of the Sleep Room (Fondazione Maugeri of Montescano (PV)). Informed consent and a preliminary psychological questionnaire were obtained from all subjects, and the study was also approved by the hospital ethics committee. For the statistical study subjects were divided into 2 groups: one containing subjects who had MS during the driving simulation and the other group the subjects without MS appearance. MS appearance was determined from the EEG.

3 MULTIVARIATE STATISTICS

The purpose of the statistical analysis is to find a relation between all the measured parameters and the driver's attention and vigilance decrease. The index of the driver's attention is measured by studying the EEG signals and microsleeps. In addition to these, another very important parameter that determines driver attention is the reaction time to the appearing obstacles (study not reported in this paper).

The stored data are statistically analyzed using MATLAB (version 7, revision 14): the observed phenomena are not linear and so a standard linear analysis is not adequate. So multivariate analysis is used in order to identify categories of input variable related to a certain controllable output index. Different analysis methods are used to determine all the necessary statistical parameters: the first analysis is based on simple mean value and standard deviation for each signal acquired and for each group. In addition, covariance and cross-correlation matrixes are calculated to determine a possible correlation of one acquired parameter to another, but also to correlate all the acquired parameters with the driver's safety index, derived from the polysomnographical data. Furthermore, a cluster analysis is made, following the hierarchical and the K-means methods, in order to investigate grouping in the data.

Studying the results of all the above statistical multivariate analysis methods, the upgrade of the already existing fuzzy logic controller may be possible in further works.

3.1 MEAN AND STANDARD DEVIATION

The simulator system proposed and discussed in this paper is used in a daily basis in order to acquire enough data to adequately support the statistical analysis. Some preliminary observations can already be done. By observing the data acquired during simulations made with persons that slept during the night before as usual, some interesting facts on the GSR parameter can be noticed [18]: the more difficult the driving conditions, the lower the GSR values. The GSR is inversely proportional to the perspiration and so this result means that the driver skin's perspiration is higher when the driving conditions are difficult (curved circuit, fast car speed).

This also means that the driver is more vigilant when the simulation conditions are difficult, because of the fact that the skin's perspiration is inversely proportional to the person's relaxation. Examined from another point of view, the lower the GSR value, and the more vigilant the driver is.

However considering subjects divided into MS/no MS groups (13/12), GSR and HRV (also RR and BTS) seem to not vary very much as shown in Table I, II and Figure 3, 4. The boxplots have lines at the lower quartile, median, and upper quartile values. The whiskers are lines extending from each end of the boxes to show the extent of the rest of the data. Outliers are data with values beyond the ends of the whiskers.

TABLE I - Mean and SD of GSR values

GSR	mean $[\Omega \, x10^5]$	standard deviation $[\Omega \, x10^5]$
MS	2,31	0,85
No MS	2,33	0,49

TABLE II - Mean and SD of HRV values

HRV	Mean [ms]	standard deviation [ms]
MS	1,48	0,24
No MS	1,47	0,17

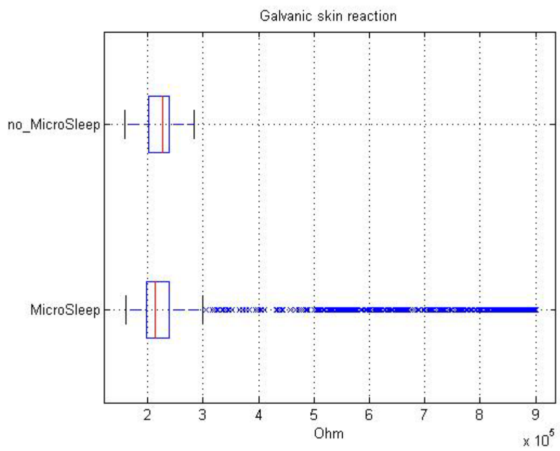

Figure 3 GSR boxplots.

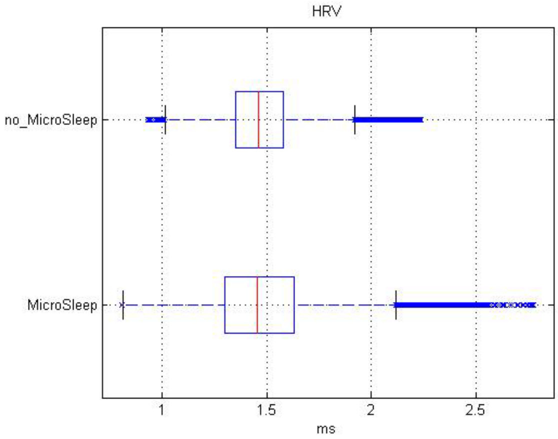

Figure 4 HRV boxplots.

An important observation is that the mean value of the driver's THE is generally higher when he/she has MS during the simulation (Table III, Figure. 5): the lower THE indicates that no MS subjects are more vigilant and reactive, due maybe also a greater vasoconstriction.

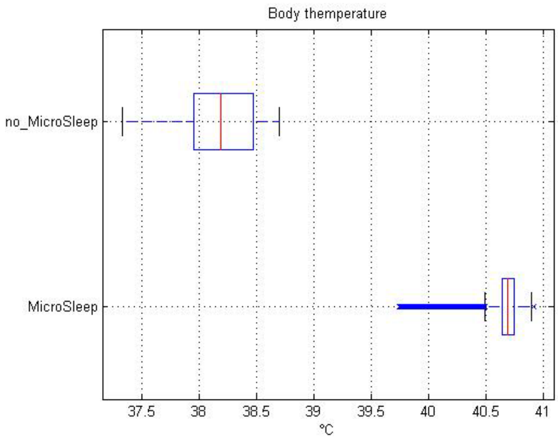

Figure 5 THE boxplots.

TABLE III - Mean and SD of THE values

THE	Mean [°C]	standard deviation [°C]
MS	40,66	0,16
No MS	38,15	0,34

The previous analysis is not good enough to understand the correlations between the variables acquired during the simulations.

3.2 CORRELATION BETWEEN PARAMETERS

The hypostasis about the parameters correlation brings to the Multivariate Analysis. In easy situations, in which data are about one parameter for each person of the champion chest, mean and variance give simple information on the gravity centre and the dispersion of the observed values [19]. When there are 2 parameters, supplementary information is given by the covariance or the correlation coefficient that measures the parameters dependence. There are also complex situations, like this case, in which more than 2 parameters have to be considered for each subject: it's difficult find the dependences between parameters and plot data. The covariance matrix of the variables $X_{(1)}, \dots, X_{(P)}$ is the pxp matrix with the variance of the single variables on the diagonal and the covariance between the variables $X_{(i)}$ and $X_{(j)}$ for $i \neq j$. In the same way the correlation matrix (Table 4) has the correlation coefficient between the variables $X_{(i)}$ and $X_{(j)}$ for $i \neq j$ outside the diagonal. If the unit of one variable changes, its weight in the final results will be modified: in order to avoid the scale effects, it's better to analyse data normalised (centred and reduced). In particular if x_i is the mean of the i variable and σ_i^2 is the variance, then the new variable is (1):

$$y_{hi} = \frac{x_{hi} - \overline{x_i}}{\sigma_i} \tag{1}$$

The correlation matrixes for each group are here reported (Table 4 and 5):

Table IV - Correlation matrix for the MS group.

	BTS	GSR	HRV	RR	THE
BTS	1	-0,20	-0,00	-0,27	0,40
GSR	-0,20	1	-0,01	0,66	-0,80
HRV	-0,00	-0,01	1	0,00	-0,00
RR	-0,27	0,66	0,00	1	-0,62
THE	0,40	-0,80	-0,00	-0,62	1

Table V - Correlation matrix for the no MS group

	BTS	GSR	HRV	RR	THE
BTS	1	-0,13	0,00	-0,14	-0,67
GSR	-0,13	1	-0,00	0,48	0,01
HRV	0,00	-0,01	1	-0,00	-0,00
RR	-0,14	0,48	-0,00	1	-0,06
THE	-0,67	0,01	-0,00	-0,06	1

From tables IV and V we can notice that there is a high negative correlation between GSR and THE (about 80%) for the no MS group: this indicates a strong inverse relationship between these parameters. BTS and THE are directly correlated in the MS group (about 40%), while are inversely correlated in the other (about 67%). This information will be very useful for the fuzzy logic controller activation. The GSR and RR are positive correlated for each group. Besides HRV seems not to be correlated with other parameters.
Using this information with the others from previous studies [18], the rules for an upgrade of the already existent fuzzy logic controller can be written.

3.3 PRINCIPAL COMPONENTS ANALYSIS (PCA)

PCA was then used in order to reduce data complexity: the data projection is good when the dispersion of the points, is the greatest [20] that is when the variance of the points belonging to the real champion chest is the greatest. From the observation of the variance explained, it's assumed that more than 90% of information belongs to the III principal components and so, for further analysis, only 3 components are considered. In this way the redundancy are eliminated and the complexity is reduced.
Two different clustering methods, Hierarchical and K-Means methods are then applied to data from PCA, in order to find grouping in all subjects data related to MS appearance.

3.4 HIERARCHICAL CLUSTERING

Hierarchical clustering is a way to investigate grouping in the subjects' data, simultaneously over a variety of scales, by creating a cluster tree (Figure 6) that is not a single set of clusters, but rather a multi-level hierarchy, where clusters at one level are joined as clusters at the next higher level. This allows deciding what level or scale of clustering is most appropriate in the application.
In order to have a better tree, the distances between the links are calculated minimizing the distance typology "correlation". It's possible to verify it using the Cophenet index: the better the approximation, the greater the index is: in this case c=0,9646. The Hierarchical method found two clusters where subjects are divided according to the MS appearance with about 67% of goodness.

3.5 K-MEANS CLUSTERING

K-means clustering can best be described as a partitioning method. That is the function k-means partitions the observations in the data into K mutually exclusive clusters and returns an indices vector, indicating to which of the k clusters it has assigned each observation. Unlike the hierarchical clustering method, k-means does not create a tree structure to describe the groupings in the data, but rather creates a single level of clusters. Another difference is that K-means clustering uses the actual observations of objects or individuals in the data and not just their proximities. These differences often mean that k-means is more suitable for clustering large amounts of data. k-means treats each observation in the data as an object having a location in space and it finds a partition in which objects within each cluster are as close to each other as possible, and as far from objects in other clusters as possible. Each cluster in the partition is defined by its member objects and by its centroid, or center, the point to which the sum of distances from all objects in that cluster is minimized (Figure 7). k-means computes cluster centroids differently for each distance measure, to minimize the sum with respect to the measure specified.
From Figure 7 we can immediately observe that in 1 cluster there are only 3 subjects. Maybe this result is due to the small champion chest considered in this study and so the results of the Hierarchical clustering are the only considerate in further analysis.

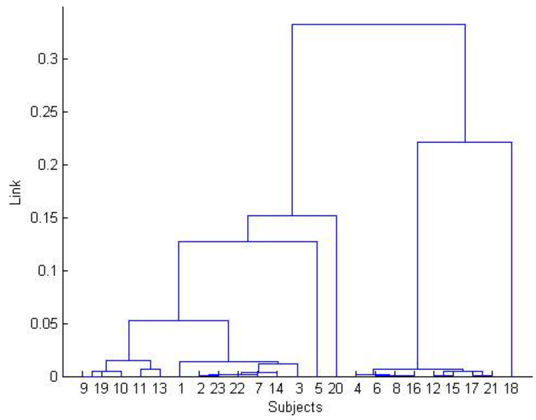

Figure 6 The numbers along the horizontal axis represent the subjects in the original data set. The links between objects are represented as upside down U-shaped lines: the height of the U indicates the distance between the objects.

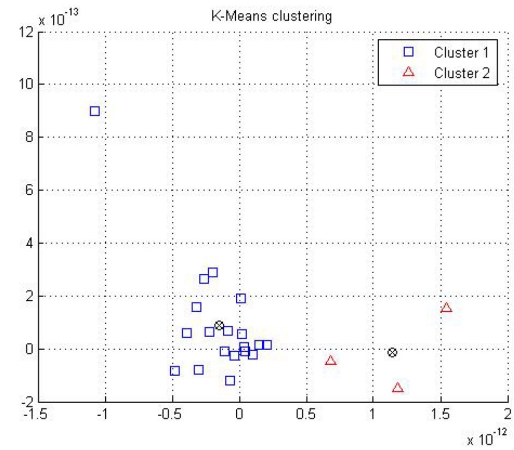

Figure 7 K-Means clustering

3.6 HIERARCHICAL CLASSIFICATION RESULTS

Classification results can be summarized in the confusion matrix. In this matrix the rows represent the real classes, i.e. classes with data of the training set, while the columns are the classes assigned to the objects after the application of the classification technique (i. e. hierarchical clustering, see Table VI). So the numbers outside the diagonal are objects that, as well they belong to a class, are erroneously assigned to another.

Table VI - Confusion matrix

FITTING			
CLASS	MS'	No MS'	tot
M	6	3	9
n	8	6	14
Tot	14	9	23

The parameter that simply summarizes the result of a classification is the error rate, ER% [20] defined as (2):

$$ER\% = 1 - \frac{\sum_g c_{gg}}{n} 100 \qquad (2)$$

where c_{gg} are the elements on the confusion matrix diagonal.

The sensibility of a class is the percent ratio between the objects assigned to that class c_{gg} and the total number of objects belonging to the same class n_g (3):

$$Sn_g = \frac{c_{gg}}{n_g} \cdot 100 \qquad (3)$$

The sensibility defines the ability of a class of representing the objects of that class. The specificity of a class is the percent ratio between the object of the considered class assigned to the class g' and the total objects assigned to that class $n_{g'}$ (4):

$$Sp_g = \frac{c_{gg}}{n_{g'}} \cdot 100 \qquad (4)$$

It defines the ability of a class to isolate objects of that class from the other classes, (i.e. the degree of purity). Another index of diversity is the Gini's one, defined like this (5):

$$G.I. = \sum_{k \neq k'} p_k \cdot p_{k'} \qquad (5)$$

where p_k is the probability of the k event and the summation runs on the products between couple of different events. This index gives the impurity quantity of a group.

All these parameters are collected for evaluating the fitting goodness (Table VII):

Table VII Parameters for the classification

Gini index$_{real}$	ER$_{fitt}$	Sn$_{fitt}$	Sp$_{fitt}$	Gini index$_{fitt}$
23,82%	66,67%	47,83%	42,86%	90,70%

The Sn_{fitt} indicates a better class representation than the specificity Sp_{fitt}. The Gini's index related to the initial value, gives the following decrease of impurity.

These parameters show that the Hierarchical method can be used as a classifier in our work with about a 40% of goodness.

4 CONCLUSION

The already developed simulation system along with the well defined protocol also presented earlier in this paper is being used to acquire data for the statistical analysis and the fuzzy controller set-up. The final results of the research will be presented after the validation of the system.

The methodology discussed and proposed is innovative for the field of safety in automotive, because it aims to acquire and use the information derived from a set of non wearable sensor in contact with he driver. Nevertheless, the experience acquired by these simulation procedures will be used to set up the final simulator system.

Further studies will be about the spectral EEG and HRV analysis, the reaction times and the circadian rhythms influence.

REFERENCES

[1] Stoohs R.A., Guilleminault C., Itoi A. and Dement W.C., Traffic Accidents in Commercial Long-Haul Truck Drivers: The Influence of Sleep-Disordered Breathing and Obesity. *Sleep*, Vol. 17, 7, pp. 619-623.

[2] Moller H.J., Simulator Performance, Microsleep Episodes, and Subjective Sleepiness: Normative Data using Convergent Methodologies to Assess Driver Drowsiness. *Journal of psychosomatic research*, Vol. 61, 3, pp. 335, 2006.

[3] Philip P., Simple reaction time, duration of driving and sleep deprivation in young versus old automobile drivers. *Journal of sleep research,* pp. 8-9, 1999.

[4] Folkard S., Black times: Temporal determinants of transport safety. *Accident analysis and prevention*, Vol. 29, pp. 417,1997.

[5] Philip P., Objective measurement of sleepiness in summer vacation long-distance drivers. *Electroencephalography and clinical neurophysiology,* Vol. 102, pp. 383, 1997.

[6] Lenne M.G., *Time of day variations in driving performance*. Oxford, 1997.

[7] http://www.omniauto.it/magazine/articolo/2219/mercedes_contro_il_colpo_di_sonno.html

[8] Vuckovic A., Radivojevic V., Chen A.C.N. and Popovic D., Automatic recognition of alertness and drowsiness from EEG by an artificial neural network. *Med. Eng. Phys.*, Vol. 24, pp. 349–360, Jun. 2002.

[9] Roberts S., Rezek I., Everson R., Stone H., Wilson S. and Alford C., Automated assessment of vigilance using committees of radial basis function analyzers. *Inst. Elect. Eng. Science Measure. Technol.*, Vol. 147, pp. 333–338, nov. 2000.

[10] Khalifa K.B., Bedoui M.H., Raytchev R. and Dogui M., A portable device for alertness detection, in *Proc. 1st Ann. Int. IEEE-EMBS Special Topic Conf. Microtechnologies in Medicine and Biology*, pp. 584–586, Oct. 2000.

[11] Wilson B.J., and Bracewell T.D., Alertness monitor using neural networks for EEG analysis. *Proc. IEEE Signal Processing Society Workshop on Neural Networks for Signal Processing X*, Vol. 2, pp. 814–820, Dec. 2000.

[12] Rada H., Dittmar A., Delhomme G. and al. Bioelectric and microcirculation coutaneus sensors for the study of vigilance and emotional response during tasks and tests. *Biosensors and Bioelectronics*, Vol.. 10, pp. 7-15, 1995.

[13] Rechtschaffen A. and Kales A., A manual of standardized terminology, techniques and scoring system for sleep stages in human adults. *U.S. Government Printing Office*, Washington. DC, 1968.

[14] Priest B., Brichard C., Aubert G., Liistro G. and Rodenstein D.O., Microsleep during a Simplified Maintenance of Wakefulness Test. A Validation Study of the OSLER Test. *Am J Respir Crit Care Med*, Vol. 163, pp. 1619–1625, 2001.

[15] Harrison Y. and Horne J.A., Occurrence of “microsleeps” during daytime sleep onset in normal subjects. *Electroencephalogr Clin Neurophysiol*, Vol. 98, pp. 411–416, 1996.

[16] Laboratory of Robotics, Politecnico di Milano, under European Union Commission for Science Workshop, Detection and Multimodal Analysis of Brain Weak Signals to Study Brain Function and Disease. *European Union Workshop*, Milan, 28-29 November 1997.

[17] Pinelli P., Baroni L., Zara D. and Battaglia S., Impairment of Delay Verbal Reactions in Dementia. *Advances in Occupational Medicine and Rehabilitation*, Vol. 4, pp. 87-93, Pavia 1998.

[18] Zocchi C., Rovetta A., Giusti A. and al., Feasibility analysis on a car control system by psychic-phisical parameters. *JoMaC* (to be published).

[19] Baldi P., *Appunti di Metodi Matematici e Statistici*, Clueb 1996.

[20] Forina M., Drava G. and Boggia R., Validation procedures in near-infrared spectrometry. *Analitica Chimica Acta*, 1994.

ISSN 1590-8844
International Journal of Mechanics and Control, Vol. 07, No. 02, 2006

DESIGN AND CHARACTERIZATION OF A FOUR CIRCULAR-ARC CAM PROFILE

Chiara Lanni, Marco Ceccarelli, Cristina Tavolieri

DiMSAT, University of Cassino, Italy

ABSTRACT

In this paper we have proposed a kinematic analysis for four circular-arc cams with profile design purposes. In particular, an algebraic formulation has been used as a function of geometrical parameters and cam profile characteristics. Numerical examples have been reported to prove the soundness of the deduced algorithm and to investigate on practical feasibility of the obtained design. Displacement, velocity and acceleration diagrams have been deduced for a synthesized cam profile by using equivalent slider-crank mechanisms in order to propose also a fairly simple procedure for testing cam profiles through a low-cost test-bed.

Keywords: mechanical transmission, cams, mechanism analysis, experimental tests

1 INTRODUCTION

Cam-follower systems are largely employed as mechanical transmissions because they are compact, well working and resistant devices. Cams are one of the first choice of many designers for motion control where high precision, repeatability, and long life are required. A cam is specially shaped piece of metal or other material which is used to transmit a desired motion to another mechanical element by direct surface contact. Usually, a cam mechanism is composed by three basic parts, such as: a cam which is the driving member; a follower which is the transmitting member; and a fixed frame, [1]. Cam mechanisms can be very cheap and simple. They have few moving parts and can be built even with very small size, as reported for example in [2-9]. In particular, cam mechanisms are widely used also in timing mechanisms, clocks, instrument of mechanical music, automatons, music boxes, lever locks, payload machines, climbing protection systems, [3-9]. In addition, all automotive engine depend on cams for their proper valve function.

Contact author: Chiara Lanni

LARM: Laboratory of Robotics and Mechatronics
DiMSAT - University of Cassino
Via di Biasio 43, 03043 Cassino (Fr), Italy
E-mail: lanni@unicas.it

Therefore, cams are used extensively in vehicles and machinery of all types [1, 2] such as screw machines, spring, winders, assembly machines, textile machinery, cutting and forming presses, printing press, internal combustion machine, fast manufacturing equipment and mechanical calculators, [2, 10-16].

In general, the main design phase for a cam transmission consists in defining a suitable cam profile that can provide the prescribed displacement diagram of the follower. The traditional approach to design cam profiles is based on a limited set of functions for a parabolic, harmonic, cycloidal, trapezoidal, polynomial profiles, [2, 10, 15-18] and their combinations [16]. Usually the profiles are obtained by graphical and/or analytical methods as in [19-22] or by software methods as in [1, 23, 24].

In this paper we have addressed attention to specific cam profiles, which are called circular-arc cams, [1, 2, 12, 13]. These profiles are composed of a collection of circular-arcs that smoothly connect the base circle with the maximum rise circle. The use of circular-arc profiles cannot provide a cam with any prescribed displacement diagram but can provide a cam that reaches the prescribed lift. The main disadvantage of circular-arc profiles is that sudden changes can occur in the acceleration of the follower at the points where arcs of different radii are joined, [2]. Nevertheless, recently new attention has been addressed to circular-arc cams by using descriptive viewpoint [25], and for design purposes, [19, 26, 27, 29, 30], since they may show interesting characteristics for practical application.

Circular-arc cams can be easily machined and can be used in low-speed applications [13]. They remain attractive because of easy of accurate manufacture and checking. Also, the use of circular arcs avoid the problem of negative radius which is happen frequently in polynomial design; in terms of curvature considerations, the radius at every point on the profile is well known, [1, 2, 11, 12, 15, 16]. In addition, circular-arc cams could be used for micro-mechanisms and nano-mechanisms since very small manufacturing can be properly obtained by using elementary geometry, [3-9].

However, a limited number of circular-arcs are usually advisable so that design, construction and operation of those cam transmissions can be not very complicate and they can become an interesting compromise for simplicity and economic characteristics that are the basic advantages of circular-arc cams [12].

At LARM: Laboratory of Robotics and Mechatronics in Cassino a specific line of research, even with teaching purposes as outlined by master thesis, [31-33], has been devoted to the study of circular-arc cams with the aim to develop modern computer-oriented algorithms both for analysis and synthesis purposes. Thus, starting from two circular-arc cams a formulation has been deduced from a suitable geometrical model and by using the concept of equivalent mechanisms for high pairs, [28, 34]. Successively, an extension has been proposed for the case of three circular-arc cams, [29, 35, 36]. A preliminary experimentally results of using four circular-arc cams have been reported in [38]. From the numerical analysis viewpoint it has been possible also to advise a design for a suitable low-cost easy-operation test-bed for cams. It has been useful not only to experimentally check the numerical results of proposed formulation but also to investigate more on the kinematic and dynamic behavior of cam transmissions, [39-46]. This activity concerning to: formulating a kinematic design problem for cam profiles in computer-oriented algorithms; deriving an experimental procedure for fairly simple identification of curvature in cam profiles, [47].

In this paper, we have focused on four circular-arc cams by taking into considerations on geometrical design parameters. In particular, an analytical formulation has been proposed for four circular-arc cams by using a formulation of two circular-arc cams as a first attempt of a generalization to cam profiles with high number of circular arcs. Consequently, the circular-arc cams can be used to design approximate polynomial cams when a suitable large number of circular arcs are designed in the cam profile.

In addition, slider-crank equivalent mechanisms have been considered for an easy computation of displacement, velocity and acceleration of the follower during operation, since the change of curvature at joining points between two consecutive arcs gives a sudden change of acceleration that has been recognized as a peculiar characteristics, [2,16]. However, the kinematic analysis has been useful to develop an experimental procedure that easily check the cam profiles.

An experimental test-bed has been built at Laboratory of Robotics and Mechatronics in Cassino in order to validate the numerical results and characterize the cam profile experimentally.

2 TWO CIRCULAR-ARC CAMS

In Fig.1 schemes are reported for two circular-arc cam profile, Fig.1a) and its characteristic loci, Fig.1b).

Referring to the scheme of Fig. 1a), a cam profile can be seen as composed by: a rise segment, a dwell arc, a return segment, an action angle, and a base circle. In particular, the rise segment is a portion of the cam profile, which is related to the rise angle α_r, where the motion of the follower is away of the cam center. The dwell arc is related to the dwell angle α_d, during which the follower is at the maximum rise named as lift h. The return segment is a return portion with angle α_{r*}, in which the motion of the follower is directed to the cam center, [4]. The action angle $\alpha_a=\alpha_r+\alpha_d+\alpha_{r*}$ is the total angle for the motion of the follower with respect to the cam center O. The base circle with radius ρ_0 is the smallest circle centered on the cam rotation axis; and ρ is the radius of the roller follower. Usually, a cam profile shows a symmetrical design with $\alpha_r=\alpha_{r*}$, as shown in Fig.1a).

In addition, referring to Fig.1b) with respect to the reference frame OXY, the profile of a cam is defined by: the base circle Γ_0 with radius ρ_0, which is centred in point C_0=O; the first circle Γ_1 with radius ρ_1, which is centred in point C_1; the second circle Γ_2 with radius ρ_2, which is centred in point C_2; the third circle Γ_3 with radius (ρ_0+h), which is centred in point C_3.

Referring to Figs.1a) and b), characteristic points of cam profile can be identified as point A (x_A; y_A), which is the point joining Γ_0 with Γ_1; B (x_B; y_B), which is the point joining Γ_1 with Γ_2; C (x_C; y_C), which is the point joining Γ_2 with Γ_3. x, y are the Cartesian co-ordinates of a general point with respect to reference OXY; the co-ordinates of a specific point are indicated with subscript letter of the point.

Design conditions on characteristic loci can be expressed by using circles Γ_i (i= 1, 2, 3).

In a previous papers [34, 40] an analytical description has been presented for the case of design parameters α_r, α_d, α_{r*}, h, ρ_0, ρ_2 and co-ordinates of center point C_2, and profile points A and C are given, it is possible to determine the co-ordinates of points C_1, C_2 and B. In particular, when α_a is assumed to be equal to 180 deg., the co-ordinate x_A is equal to zero since also x_1 is equal to zero. A suitable system of algebraic equations can be deuced in order to obtain the co-ordinates of points C_1, C_2 and B by means of the following conditions:

- the first circle Γ_1 passing across points A and B can be written as

$$\left(x_B - x_1\right)^2 + \left(y_B - y_1\right)^2 = \left(x_A - x_1\right)^2 + \left(y_A - y_1\right)^2 \qquad (1)$$

- the second circle Γ_2 passing across points B and C can be expressed as

$$\left(x_B - x_2\right)^2 + \left(y_B - y_2\right)^2 = \left(x_C - x_2\right)^2 + \left(y_C - y_2\right)^2 \qquad (2)$$

- coincident tangents to Γ_1 and Γ_2 at the point B can be described as

$$\frac{x_2 - x_1}{y_2 - y_1} = \frac{x_B - x_2}{y_B - y_2} = \frac{x_B - x_1}{y_B - y_1} \qquad (3)$$

When the condition x_1=x_A=0 is assumed, Eqs. (1) to (3) can be grouped as

$$\begin{gathered} x_B^2 + y_B^2 - 2y_1y_B - y_A^2 + 2y_1y_A = 0 \\ x_B^2 + y_B^2 - 2x_2x_B - 2y_2y_B - x_C^2 - y_C^2 + 2x_2x_C + 2y_2y_C = 0 \\ x_2y_B - x_2y_1 + x_By_1 - x_By_2 = 0 \end{gathered} \qquad (4)$$

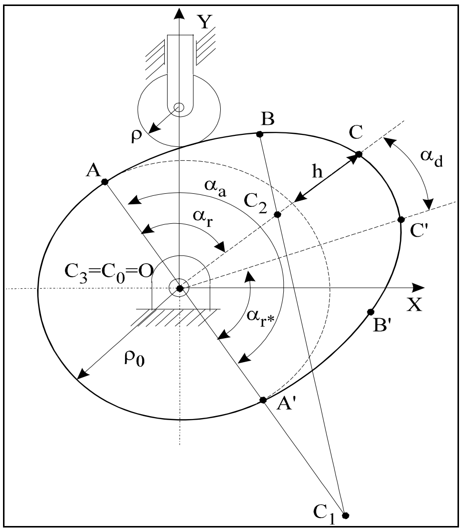

a)

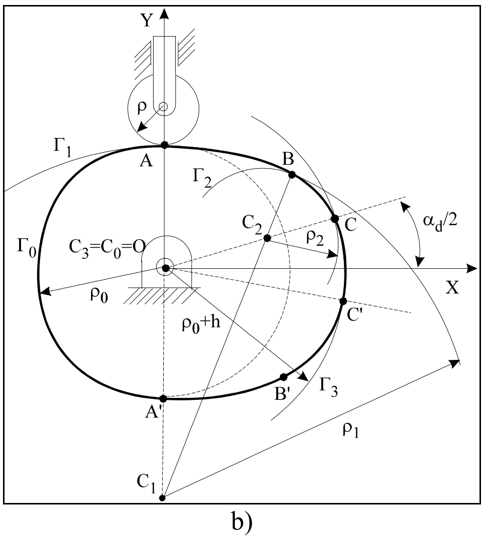

b)

Figure 1: Kinematic schemes for two circular-arc cams with roller-followers: a) profile; b) characteristic loci.

Thus, the co-ordinates of the significative points of two circular-arc cam C_1, C_2 and B are obtained by solving Eqs.(4) for the rise angle α_r. It is worth to noting that only one solution of Eq.(4) is significative from mechanical design viewpoint.

3 A DESIGN OF FOUR CIRCULAR-ARC CAMS

Figure 2) shows a scheme of four circular-arc cam profiles under examination in this paper. Four circular-arc cams has been designed by combining sequentially two designs of two circular-arc rise profile. In fact, if one considers the reference frame OXY, the profile of the cam is defined by the base circle with radius ρ_0, which is centred in point C_0=O; the first circle which is centred in point C_1; the second circle which is centred in point C_2; the third circle which is centred in point C_3; the fourth circle which is centred in point C_4; the fifth circle with radius (ρ_0+h) which is centred in point O.

Characteristic points of four circular-arc cam profile can be identified as: point A (x_A; y_A), which is the point joining the base circle with the first one; B (x_B; y_B), which is the point joining the first circle with the second one; C (x_C; y_C), which is the point joining second circle with the third one; D (x_D; y_D), which is the point joining third circle with the fourth one; E (x_E; y_E), which is the point joining fourth circle with the fifth one.

Simplicity and reliability of the proposed procedure for design two circular-arc cams can be useful to deduce the design profile of four circular-arc cams.

The procedure applied for four circular-arcs can be summarized by considering the schemes reported in Fig.3:

- define the design parameters α_r, α_d, α_{r*}, h, ρ_0;
- subdivide the rise angle in two parts equal to $\alpha_r/2$ respectively;
- assign the radius ρ_2 for the second circle Γ_2;

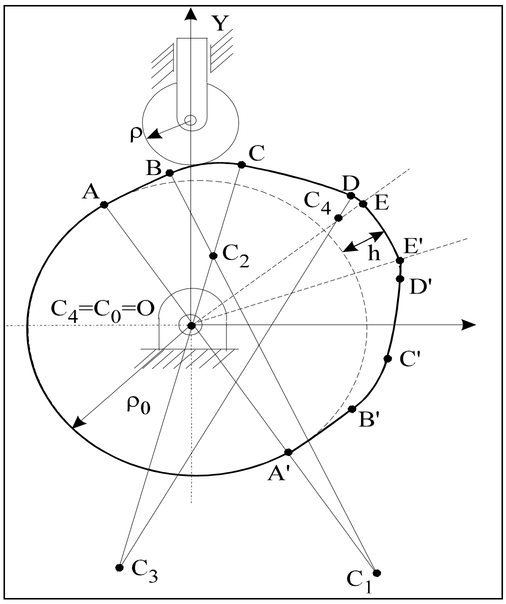

Figure 2: A scheme of four circular-arc cam profile.

ISSN 1590-8844
International Journal of Mechanics and Control, Vol. 07, No. 02, 2006

- assign the radius ρ_4 for the fourth circle Γ_4;
- apply the algorithm for two circular-arc in the first middle portion AC of the rise angle Fig.3a);
- determine the value of the co-ordinates of points C_1, C_2 and B;
- apply the algorithm for two circular-arc in the second middle portion CE of the rise angle Fig.3b);
- determine the value of the co-ordinates of points C_3, C_4 and D.

By considering the scheme of Fig.3a) to obtain the coordinate of points C_1, C_2 and B is necessary to solve Eqs.(4).
In addition to complete the design of four circular-arc it is necessary to apply the same abovementioned procedure from points C to E, as shown in Fig.3b).
Referring to Fig.3b), when the numeric values of the parameters $\alpha_r/2$, α_d, α_{r*}, h, ρ_0, ρ_4 and profile points C and E are given, it is possible to determine the co-ordinates of points C_3, C_4 and D.
A suitable system of algebraic equations can be deduced by means of the following conditions:

- the third circle passing across points C and D can be written as

$$(x_C - x_3)^2 + (y_C - y_3)^2 = (x_D - x_3)^2 + (y_D - y_3)^2 \tag{5}$$

- the fourth circle passing across points D and E can be expressed as

$$(x_D - x_4)^2 + (y_D - y_4)^2 = (x_E - x_4)^2 + (y_E - y_4)^2 \tag{6}$$

- coincident tangents to second and third circles at the point C can be described as

$$\frac{x_C - x_2}{y_C - y_2} = \frac{x_C - x_3}{y_C - y_3} \tag{7}$$

- coincident tangents to third and fourth circles at the point D can be described as

$$\frac{x_D - x_4}{y_D - y_4} = \frac{x_D - x_3}{y_D - y_3} \tag{8}$$

Thus, the co-ordinates of the significative points C_3, C_4 and D are obtained by solving Eqs.(5) to (8) for the second part, CE of the rise angle α_r. Since, only one solution is significative from of mechanical design viewpoint.

4 NUMERICAL EXAMPLES

Equations (4) to (8) can be solved by using Maple software [48]. Numerical examples have been computed to prove the soundness and efficiency of the proposed design algorithm. In particular, referring to the scheme shown in Fig.2, numeric values for design parameters are assumed as h=12 mm; ρ=40 mm; α_r=65 deg.; α_d=50 deg.; α_{r*}=65 deg.; and co-ordinates of points A=(0, ρ) mm, C=(24.71, 38.79) mm and E=(47.13, 21.98) mm.
Data and design results of the enclosed numerical examples have been grouped in Tables I and II.
Figures 4 and 5 show design shape of the cam profile, with the data reported in Tables I and II.
In particular, Fig.4a) shows the Example 1 reported in Tables I and II. One can note that, when the roller follower moves along AB and CD arcs the cam profile is concave; when the roller follower moves along BC and DE arcs the cam profile is convex.

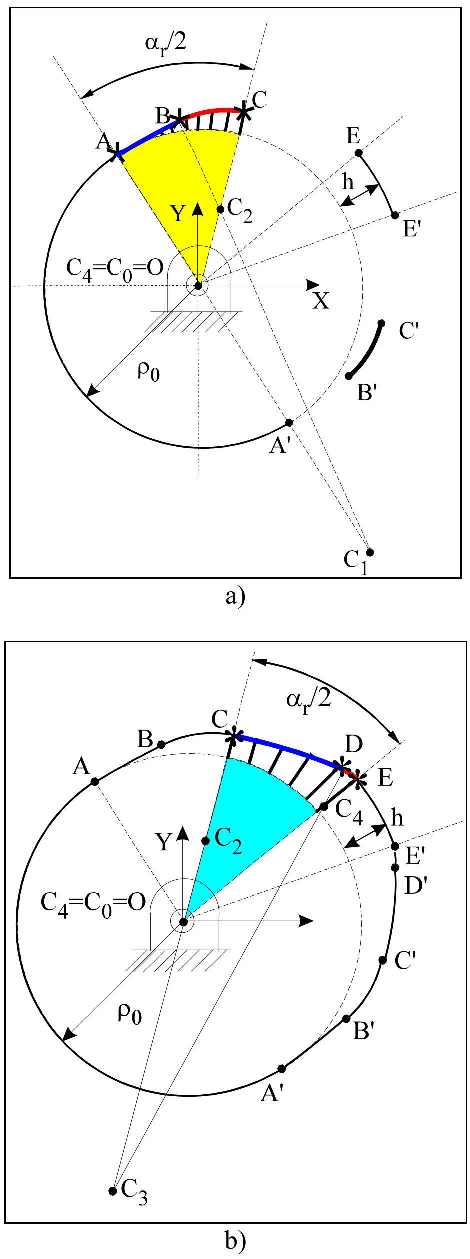

Figure 3: Kinematic schemes for four circular-arc cams with roller-followers: a) first middle portion AC of α_r; a) second middle portion CE of α_r.

Figure 4b) shows the Example 2 reported in Tables I and II. One can note that, when the roller follower moves along AE arc the profile of the cam is convex.

ISSN 1590-8844
International Journal of Mechanics and Control, Vol. 07, No. 02, 2006

Figure 5 shows the Example 3 reported in Tables I and II. One can note that, when the roller follower moves along AB arc the profile of the cam is concave; when the roller follower moves along BE arc the profile of the cam is convex.
The proposed three design cases differ for the type of curvature. It depends by the numerical values of the design parameters ρ_2 and ρ_4.
It is worthing to note that, the curvature of the function and its reciprocal radius of curvature has great significance during the design profiles. In fact, cam contours may have portions, which are concave, convex or flat. Infinitesimally short flats of infinite radius occur at all inflection points on the cam surface where it changes from concave to convex or vice versa. Consequently, a problem occurs when:

- the radius of roller follower is too large to follow the locally smaller negative (or concave) local radius on the cam;
- the radius of roller follower is larger than the smallest positive (or convex) local radius on the cam curve. This problem is well known as undercutting:
- in transition points from concave to convex and vice versa the sign of radii of curvature changes like vector.

Consequently there is a direct dependence between acceleration of a follower and a curvature of cam, and between dynamic loads in mechanism and machine. For these reasons there is a practical necessity in determining more detailed dependency and quantitative estimation of acceleration value, process dynamics in dependence of cam profile, geometric and kinematic parameters of cam and mechanism as a whole.

Table I - Design data for numerical examples in Figs.4 and 5.

Data Example	ρ_2 [mm]	ρ_4 [mm]	x_{C_2}, y_{C_2} [mm, mm]	x_{C_4}, y_{C_4} [mm, mm]
1	22	17	12.89, 20.24	31.72, 14.80
2	5	12	22.03, 34.58	36.25, 16.90
3	18	13	15.04, 23.61	35.35, 16.48

Table II - Design results for numerical examples in Figs.4 and 5.

Results Examples	x_B, y_B [mm, mm]	x_{C_1}, y_{C_1} [mm, mm]	x_D, y_D [mm, mm]	x_{C_3}, y_{C_3} [mm, mm]
1	5.47, 40.95	0, 56.22	40.05, 29.61	-198.86, -312.16
2	22.22, 39.58	0, -541.60	42.95, 26.86	-451.32, -708.43
3	41.20, 11.22	0, 92.88	42.44, 27.37	-1077.75, -1691.73

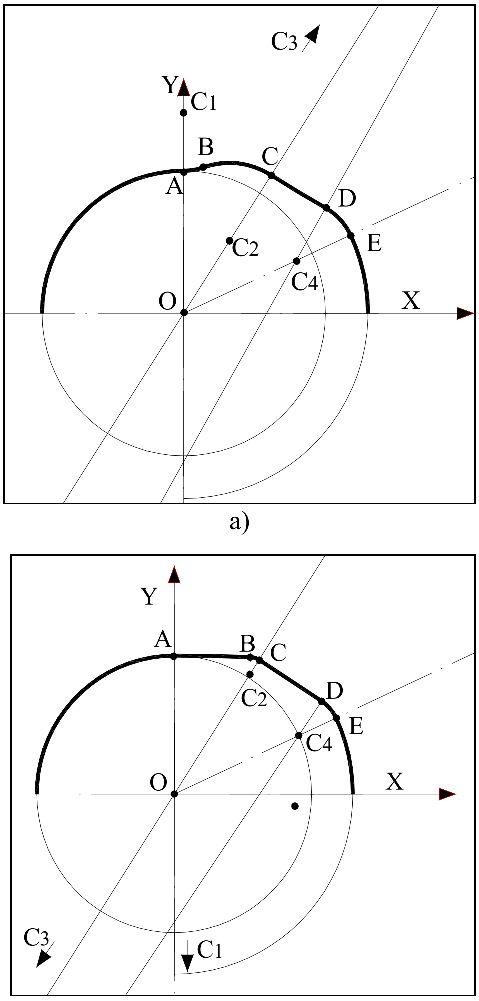

b)

Figure 4 Graphical representation of a practical feasible solution with data in Tables 1 and 2:
a) Example 1; b) Example 2.

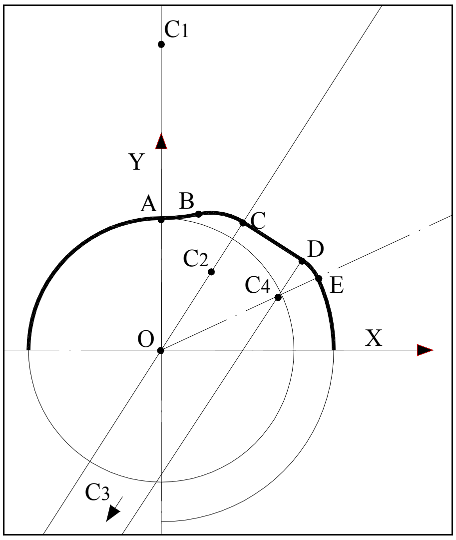

Figure 5 Graphical representation of a practical feasible solution for Example 3 in Tables 1 and 2.

5 NUMERICAL SIMULATIONS OF KINEMATIC PROPERTIES

An equivalent mechanism can be defined as one, which provides motion identical to that of a given member on the original mechanism. From a kinematic viewpoint, the cam mechanism consists of two shaped members that are connected by a fixed third body called fixed frame. Either shaped member may be the cam with the other the follower. At any instant, these shaped bodies may be replaced by an equivalent mechanism that is represented by a slider-crank. At any instant a new point of contact and a new equivalent mechanism can be considered, since, the equivalent mechanism changes during the rotation of cam. The equivalent mechanism method has two advantages: it permits the analysis of cams and followers of any form moving in any manner; it provides a concept of the relative movement of the members. The method is applicable to any cam shape since the profile can be considered as composed of a series of small circular arcs, [2, 18].

By using an equivalent slider-crank mechanism method a kinematic analysis of four circular-arc cam for the case of Example 1, reported in Fig.4a) can be carried out in order to characterize the displacement, velocity and acceleration of a reference point M on the follower, as shown in Fig.6.

Star points are the points corresponding to those points on the cam profile and they describe the location of the reference point M along the follower path.

In particular, Fig.6a) shows a slider-crank equivalent mechanism for the first arc AB. The crank of the first equivalent slider-crank mechanism corresponds to segment OC_1 whereas the coupler corresponds to segment C_1M when point M is coincident with the roller follower center.

Figure 6b) shows a slider-crank equivalent mechanism for the second arc BC. The crank of the second equivalent slider-crank mechanism corresponds to segment OC_2 whereas the coupler corresponds to segment C_2M when point M is coincident with the roller follower center.

Figure 6c) shows a slider-crank equivalent mechanism for the third arc CD. The crank of the third equivalent slider-crank mechanism corresponds to segment OC_3 whereas the coupler corresponds to segment C_3M when point M is coincident with the roller follower center.

Figure 6d) shows a slider-crank equivalent mechanism for the fourth arc DE. The crank of the fourth equivalent slider-crank mechanism corresponds to segment OC_4 whereas the coupler corresponds to segment C_4M when point M is coincident with the roller follower center.

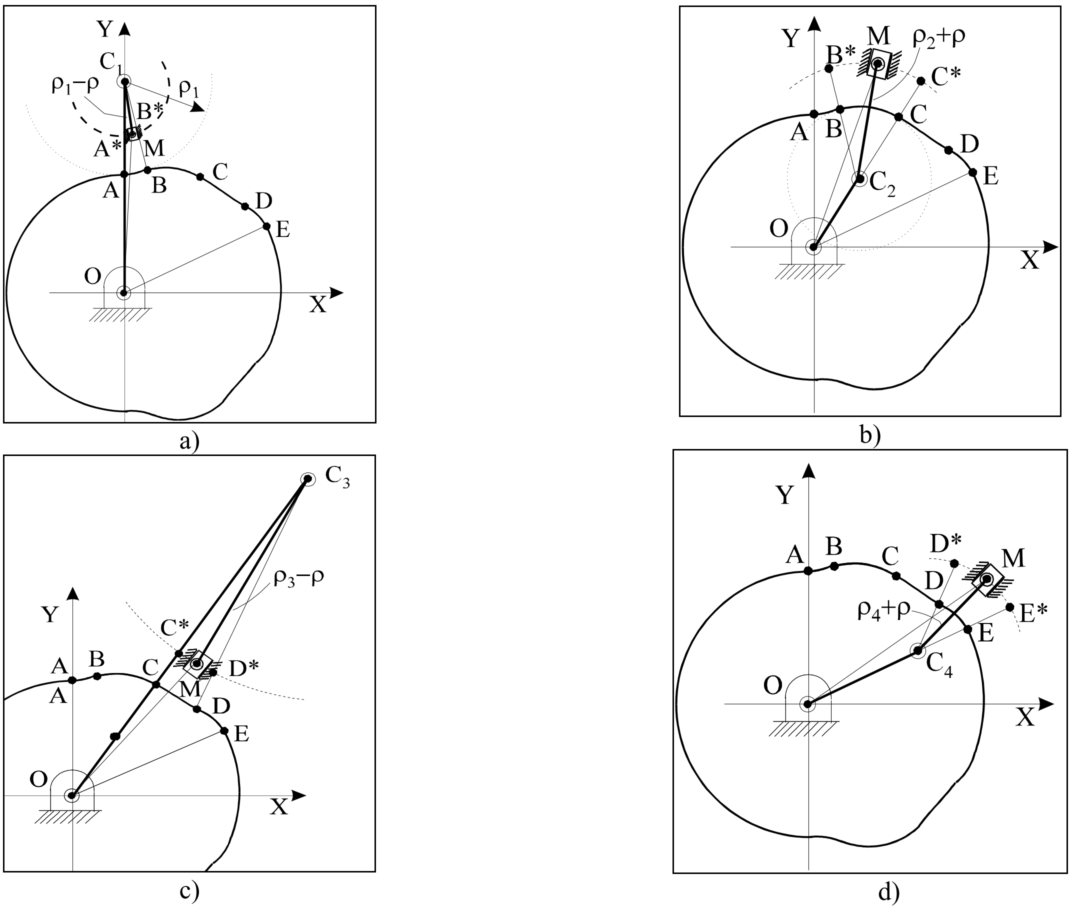

Figure 6 Slider-crank equivalent mechanisms for four circular-arc cams of the illustrative example in Fig.4a): a) at the first arc AB; b) at the second arc BC; c) at the third arc CD; b) at the fourth arc DE.

Figure 7 shows numerical results of the kinematic analysis for the feasible case of Fig.4a), by using the equivalent mechanisms of Figs.6, when an input constant velocity of 1 rad/s is assumed.
It is worthing to note that at corresponding points A, B and so on of the cam profile, the values of the acceleration are indicated by A_a, B_a, etc. and the values of the velocity are indicated by A_v, B_v, etc. Particularly, at point A the acceleration value is indicated by A_a and the velocity value is A_v. Figure 7a) represents the displacement diagram in which one can note the continuity of the curve. It worth nothing that the curvature of the cam is concave during AB and CD arcs and convex during BC and DE arcs, respectively. Figure 7b) represent the velocity diagram in which one can note the discontinuity when the radii suddenly change. Figure 7c) shows the acceleration diagram in which one can note that there are jumps in the acceleration values at the points joining the circular arcs.
The acceleration is equal to zero from E to E' since the roller is assumed to run the circular dwell path at constant velocity. In the acceleration diagram, values B_a and B_{a1} are introduced to identify the characteristic jump at the point B joining two circular arcs of the cam profile. Similarly points C_1, D_1, and E_1 are introduced.

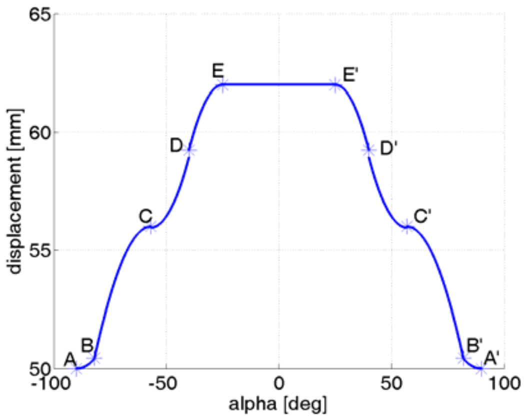

a)

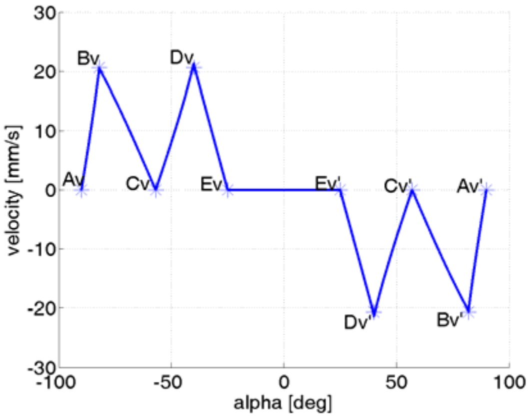

b)

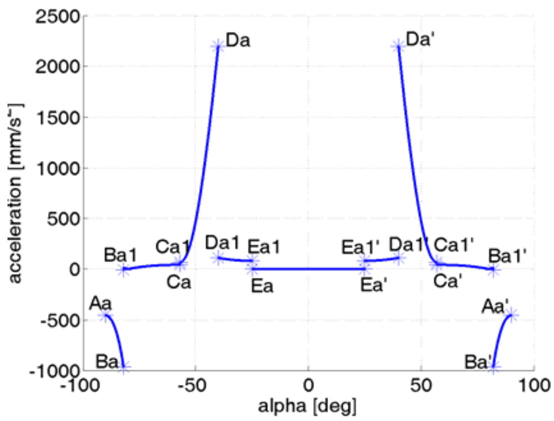

c)

Figure 7 Results of numerical simulations of point M for the four circular-arc designs of Example 1 in Fig.4a): a) displacement; b) velocity; c) acceleration.

6 EXPERIMENTAL TESTS

The geometric model and use of equivalent slider-crank mechanisms have suggested also a mechanical design of a low-cost easy-operation test-bed for circular-arc cams as outlined in [29, 34, 35].
A scheme of a measuring system that has been set up at the LARM: Laboratory of Robotics and Mechatronics, in Cassino, is shown in Fig.8. The test-bed and built prototype of four circular-arc cam are shown in Fig.9a) and b), respectively.
The built test-bed for circular-arc cams is composed by commercial measuring sensors and equipment. Thus, it has been thought convenient to use Lab View software [49] with NI 6024E Acquisition Card [50] in order to work with suitable virtual instruments, which manage commercial sensors. Referring to Figs. 8 and 9, one accelerometer S_1 [51], has been installed on the free extremity of the follower to monitor the acceleration of the follower motion. In addition, dynamic properties can be experimentally evaluated by using a dynamic torsion meter S_2 [52], which has been installed on the actuator shaft of the motor. A signal conditioner and amplifier U_2 has been used in order to provide suitable power supply to S_2 and to reduce the noise in the measured signal. One encoder S_3 [53] and one tachometer S_4, [54] have been installed also on the camshaft. The encoder gives the possibility to monitor the angle of the camshaft, whereas the tachometer is used to monitor the angular velocity of the camshaft. A signal conditioner and amplifier U_1 has been used in order to provide suitable power supply to S_3 and S_4 to reduce the noise in the measured signal.
Three different power supply sources A_1, A_2 and A_3 have been used in order to provide different input voltages for the sensors and motor M.
Thus, an experimental test can be easily performed by considering different velocity of rotation for shaft on which a cam has been previously installed. Illustrative results is shown in Figs.10 to 12.

ISSN 1590-8844
International Journal of Mechanics and Control, Vol. 07, No. 02, 2006

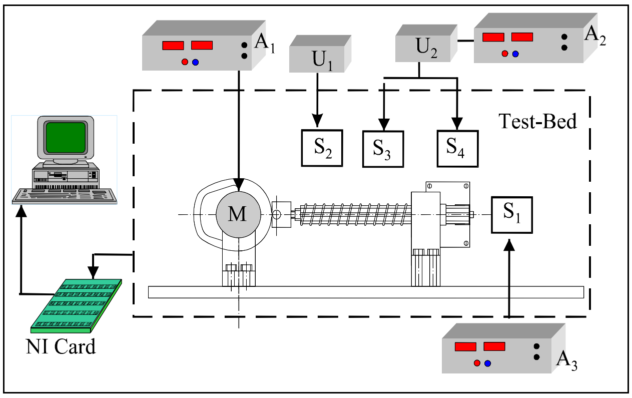

Figure 8 A general scheme for a low-cost easy-operated test-bed for circular-arc cams at LARM in Cassino.

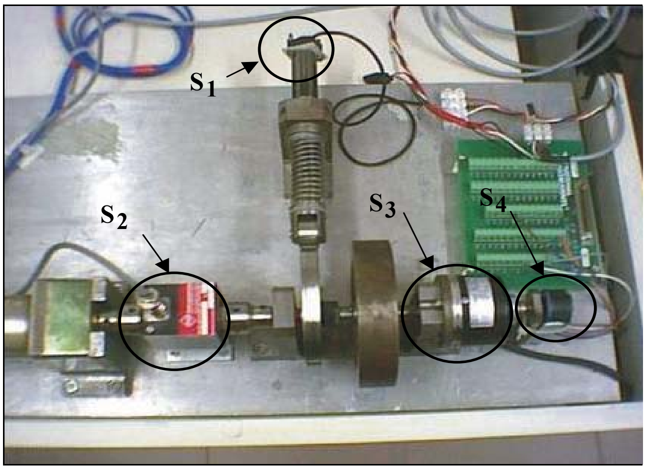

a)

b)

Figure 9 The built test-bed for circular-arc cams at LARM: a) a view; b) a tested four circular-arc cam prototype.

Figure 10 shows the experimentally measured actuator torque and horizontal acceleration for a full rotation of 360 deg. of the cam when the shaft is rotated continuously at a quasi-constant velocity of 66 rpm for several turns. The plot of Fig.10b) can be compared with the plot of Fig.7c).
The diagrams of measured accelerations are characterized by eighteen significant points, as sketched in Fig.11, by comparing them to the fourteen points reported in Fig.7c).
In addition, A is the point at which the value of the acceleration starts decreasing at A_a value because a change of curvature from base to first circle is presented for the rising of the profile. From A to B the acceleration decreases to the minimum value B_a. Then it increases to points C at value C_a because there is a change of curvature from first to second circle passing through point B_1 at value B_{1a}.
From C to C_1 the value of the corresponding acceleration C_a and C_{1a} decrease very small. From C_1 to D the acceleration decreases suddenly from the values C_{1a} to D_a, due to a further sudden change of curvature from second to third circles. From D_a to E_{1a}, passing though D_{1a}, the acceleration value increases again because there is a sudden change of curvature from third to fourth circles. From points E_1 to E the value of the acceleration E_{1a} to E_a decreases again. From E to E' the value of the acceleration E_a to E_a' is approximately constant in a very short time. The acceleration values E_{1a}' seems to be coincident with point E_a' because the jump is so near that is not experimentally observable. The acceleration plot should be symmetric with respect the middle point between EE' but it is not because when the follower moves along AB arc, the follower experiences some opposite action since it is necessary a larger force and a smaller acceleration is measured.
Along B'A' the acceleration is different than that one in the rise arc AB because the spring pushes back the follower. If one compares the acceleration plot of Fig.7c) with the diagram acceleration of Fig.10b), referring to the scheme of Fig.11, one can note that the acceleration values at points A, A', B and B', B_1, B_1' C, C_1, D', E and E' are quite similar but the negative values of the measured accelerations at points D and C' are quite different with respect the values that are obtained by the numeric simulation. The values at points E and E' are quite similar to those obtained in the numerical results. The differences among the case of Figs.7c), 10b) and 11 depend by the value of the actuator and output torque. For the numerical simulation of Fig.7c) the actuation torque and output torque are assumed as constant.
During the experimental measurements regarding with Fig.10b) the output and actuation torques are not constant due to the asymmetry of the mechanical design of a cam. However, even if the experimental measurements are carried out by using a suitable fly wheel, the value of the actuator torque cannot be achieved as constant, although the value of the output torque can be considered approximately constant. It is worth noting that the differences between the numerical and experimental results of Figs.7 and 10 are mainly due to the effect of spring force, inertia and friction.
In fact, the contribution of these forces has not been taken into account in the simulation, whose results are reported in Fig.7. Nevertheless, the effect of these forces is usually not negligible in real conditions. In addition, in transition points from concave to convex and vice versa there is a point or portion with radius of curvature equal to zero. As a consequence acceleration of the follower increase abruptly and impact load appears.

ISSN 1590-8844
International Journal of Mechanics and Control, Vol. 07, No. 02, 2006

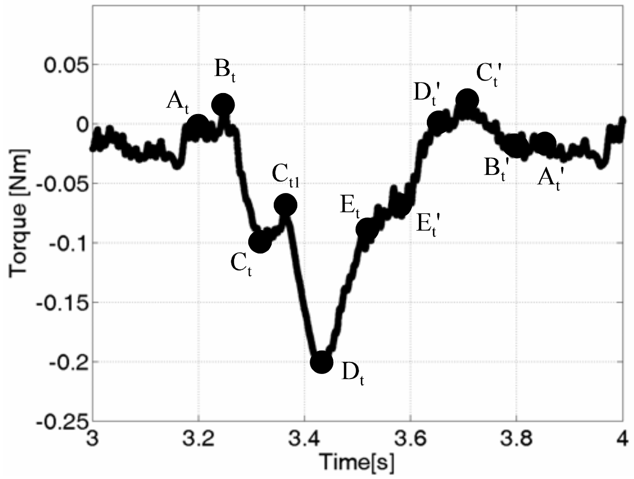

a)

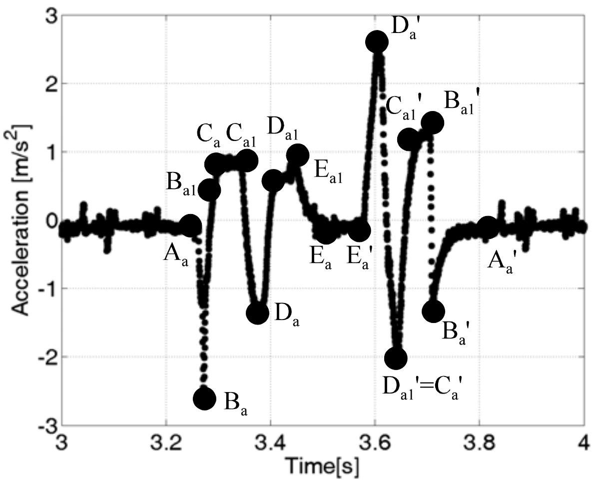

b)

Figure 10 Experimental results of a full rotation for the three circular-arc cam design by using the test-bed of Fig.7 when the shaft velocity is 66 rpm: a) torque plot; b) acceleration plot.

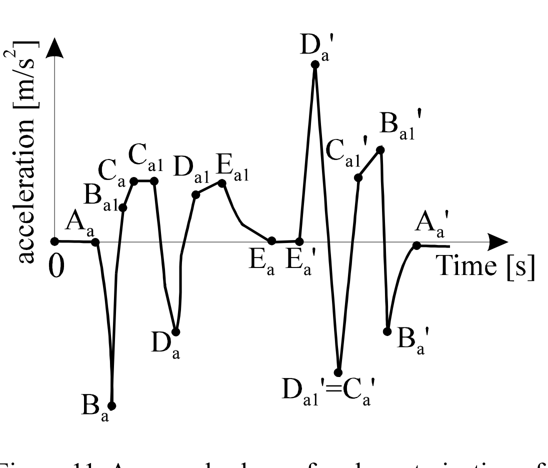

Figure 11 A general scheme for characterization of acceleration diagram of Fig.7c) by using results from the test-bed of Fig.10.

Similarly, Fig. 12 shows the experimentally measured actuator torque and horizontal acceleration for a full rotation of 360 deg. of the cam when the shaft is rotated continuously at a quasi-constant velocity of 110 rpm for several turns.

In particular, Figs. 12 show that inertial forces and higher velocity produce larger noise and vibration. The acceleration measured during the dwell is not constant but has a linear increment from points A_a' to A_a, because the input velocity is not constant during the real behaviour of the system, although flywheel has been installed. In conclusion, the experimental evaluation of the acceleration diagram by using the proposed test-bed and procedure can be used to verify not only the kinematic characteristics of a cam, but mainly the cam profile itself, since both the diagram and its typical maximum and minimum values are representative of the geometry of the cam profile and its manufactured quality.

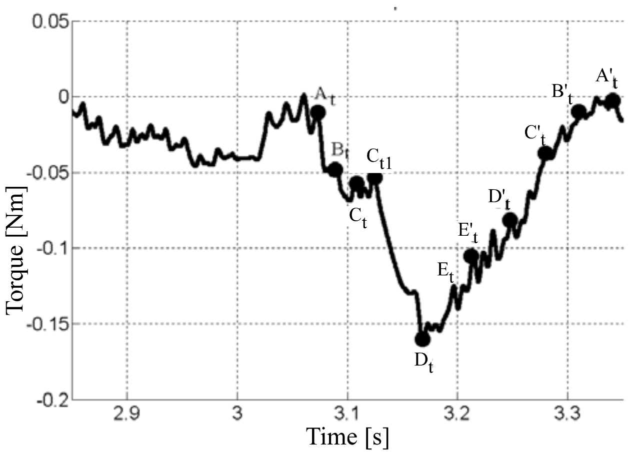

a)

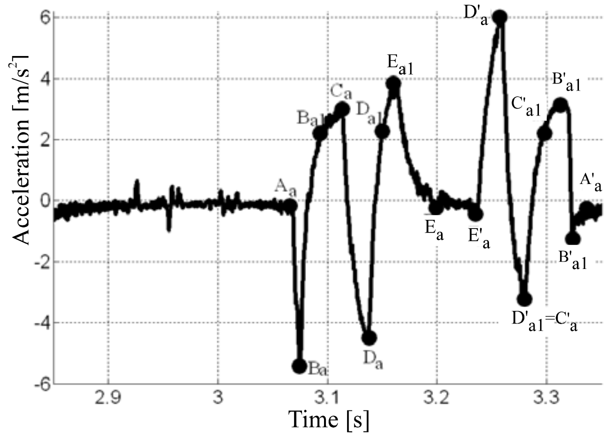

b)

Figure 12 Experimental results of a full rotation for the three circular-arc cam design by using the test-bed of Fig.7 when the shaft velocity is 110 rpm: a) torque plot; b) acceleration plot.

7 CONCLUSIONS

In this paper we have proposed an analytical formulation, which describes the basic design characteristics of four circular-arc cams. A design algorithm has been deduced from the formulation, which has permitted to solve design problems with suitable numerical efficiency. Numerical examples have been reported in the paper to show and discuss the design solutions and engineering feasibility of four circular-arc cams. By using an equivalent slider-crank mechanism, a kinematic analysis has been carried out to characterize the displacement, velocity and acceleration of a reference point on the follower. Experimental tests have permitted to characterize the operation and practical feasibility of the proposed cam profile. The experimental results show that the sudden change of curvature radius directly affects the acceleration response. The system behaviour shows a worsening when velocity increases and therefore cam profiles with circular arcs are proved to be of practical interests for certain ranges of speed operation only.

REFERENCES

[1] Norton R.L., *Cam design and manufacturing handbook*. Industrial press, New York, 2002.

[2] Scotto Lavina G., *Applications of mechanics applied to machinery*. Ed. Sistema, Roma, 1971, (in Italian).

[3] Horological Journal, webpage http://www.bhi.co.uk/hj/May%20News.pdf, 2005.

[4] Tempomatic, webpage http://www.tempomatic.it/imers_jv100.htm, 2005.

[5] Automates-ancients, webpage http://www.automates-anciens.com/version_italienne/colonna_titoli/colonna_titoli_italiano.htm, 2005.

[6] Musicameccanica, webpage www.musicameccanica.it/ musiche.htm, 2005.

[7] Acmgguides, webpage http://www.acmgguides.com, 2006.

[8] Sportraing, webpage http://www.sportraining.net/forzamezzi-utilizzati.htm, 2005.

[9] Sercas, webpage http://www.sercas.it/c1_mi.htm, 2005.

[10] Angeles J. and Lopez-Cajun C.S., *Optimization of cam mechanisms.* Kluwer Academic Publishers, Dordrecht, 1991.

[11] Norton R., *Chapter 7: Cam and cams follower. Modern kinematic: developments in the last forty years*. Ed. Erdman G.A., A Wiley-Interscience Publication, New York, 1993.

[12] Magnani P.L. and Ruggieri G. *Mechanisms for automatic machinery*. UTET, Torino, 1986, (In Italian).

[13] Chironis N.P., *Mechanisms and mechanical devices sourcebook*. McGraw-Hill, New York, 1991.

[14] Colombo Filippetti, webpage http://mycf.cofil.it/, 2006.

[15] Chen F.Y, *Mechanics and design of cam mechanisms*, Pergamon Press, New York, 1982.

[16] Rothbart H.A., *Cams design, dynamics and accuracy*. John Wiley & Sons, New York, 1956.

[17] Tesar D., Matthew G.K., *The dynamic synthesis, analysis, and design of modelled cam systems*, D.C. Heath and Company, Lexington, Mass., 1976.

[18] Uicker J.J. Jr., Pennock G.R. and Shigley J.E., *Theory of machine and mechanisms*. McGraw-Hill, New York, 2003.

[19] Doughty S., Four circle cam design. *SAE Technical,* paper n.932381, 1993.

[20] Zhang Y. and Shin J.-H., A computational approach to profile generation of planar cam mechanisms. *Journal of Mechanical design*, Technical briefs, Vol.126, No.1, pp.183-188, 2004.

[21] Biswas A., Stevens M. and Kinzel G.L., A comparison of approximate methods for the analytical determination of profiles for disk cams with roller followers. *Mechanism and Machine Theory*, Vol. 39, pp.645-656, 2004.

[22] Antonescu O., Antonescu P. and Martineac A., Unitary method for kinematic synthesis of mechanisms with rotary disc-cam. *The Ninth IFToMM International Symposium on Theory of Machines and Mechanisms, SYROM 2005,* Bucharest, Vol.1, pp. 1-6, 2005.

[23] McGarva J. R., Concept and improvement of cam mechanisms using CAD. *IX. IFToMM Congress*, Milan, pp.735-738, 1995.

[24] Aziz R., Development of an integrated system for cam design and manufacture with graphical user interface. *Proceedings of the 1996 ASME Design Engineering Technical Conference and Computers in Engineering Conference*, Irvine, paper n.96-DETC-MECH-1017, 1996.

[25] Krasnikov V.F., Dynamics of cam mechanisms with cams countered by segments of circles. *Proceedings of International Conference on Mechanical Transmissions and Mechanisms*, Tianjin, pp.237-238, 1997.

[26] Lovasz E.-C., Modler K.-H. and Perju D., Use of coupled circular-arc profiles as driving profiles. *The National Romenia Symposium with International Attendance Prasic'02*, Brasov, 2002, (in German).

[27] Modler K.-H., Perju D. and Lovasz E.C., The use of circular profiles in mechanism technology. *VIII-th International Symposium for Mechanisms Theorie and Practice SYROM 01*, Bucaresti, 2001, (in German).

[28] Lanni C., Ceccarelli M. and Carvhalo J.C.M., An analytical design for two circular-arc cams. *Proceeding of 4th Iberoamerican Congress on Mechanical Engineering*, Santiago de Chile, Vol. 2, 1999.

[29] Lanni C., Ceccarelli M. and Greco G., Numerical and experimental analysis of three circular-arc radial

cams. *Revista Mecanisme si Manipuletoare, ARTOMM-IFToMM*, Vol. 3, No. 1, pp.43-48, 2004.
[30] Oderfeld J. and Pogorzelski A. On designing plane cam mechanisms. *Proceedings the Eight World Congress on the Theory of Machines and Mechanisms*, Prague, Vol. 3, pp. 703-705, 1991.
[31] Bianchi A., Design and construction of a test-bed for cams with polycentric arc-profiles. *Master Thesis*, LARM, University of Cassino, Cassino, 2002. (In Italian).
[32] Greco G., Analysis and experiments of three circular-arc cams. *Master Thesis*, LARM, University of Cassino, Cassino, 2002, (In Italian).
[33] Fabrizi A., Numerical and experimental validation for a test-bed polycentric radial cams. *Master Thesis*, LARM, University of Cassino, Cassino, 2004, (In Italian).
[34] Lanni C., Ceccarelli M. and Figliolini G., An analytical formulation for two circular-arc cams. *CSME Transactions on Mechanical Engineering*, Vol.25, No.1, pp.29-49, 2001.
[35] Lanni C., Ceccarelli M. and Figliolini G., An analytical design for three circular-arc cams. *Mechanism and Machine Theory*, Vol. 37, pp.915-924, 2002.
[36] Lanni C., Ceccarelli M. and Greco G., An experimental characterization of cam profiles with three circular-arcs. *International Journal Gearing and Transmissions*, No.2, pp.49-60, 2004.
[37] Lanni C., Carbone G., Ceccarelli M. and Ottaviano E., Numerical and experimental analyses of radial cams with circular-arc profiles. *Proc. IMechE Part C: Journal of Mechanical Engineering Science*, Vol. 220 No.C1, pp.111–126, 2006.
[38] Tavolieri C., Ceccarelli M. and Lanni C., An experimental analysis for four circular-arc cams. *12th National Conference on Machine and Mechanism, NaCoMM*, IIT Guwahati, pp.53-59, 2005.
[39] Carbone G., Lanni C., Ceccarelli M. and Lopez-Cajùn C., Dynamic effects of curvature change in the profile of two-circular-arc cams. *Proceedings of V Iberoamerican Congress of Mechanical Engineering*, Merida, pp.1247-1252, 2001.
[40] Lanni C., Carbone G., Ceccarelli M. and Ottaviano E. Numerical and experimental analysis of radial cams with circular arc profiles. In *International Symposium on Multibody Systems and Mechatronics MUSME2005*, Uberlandia, paper 34-MUSME05, pp.391-405, 2005.
[41] Lanni C., Carbone G., Ottaviano E. and Ceccarelli M. Modelling of cam transmissions. *Proceedings of First International Congress design and Modelling of Mechanical Systems, CMSM'2005,* Paper n. CMSM05LANNI, 2005.
[42] Lanni C., Bianchi A., Carbone G. and Ceccarelli M., Numerical and experimental performance analysis of cam profile in two-circular-arc cams. *IFToMM2004, Proceedings of the 11th World Congress in Mechanism and Machine Science*, pp.1060-1064, 2004.
[43] Lanni C., Ottaviano E., Ceccarelli M. and López Cajún C., Análisis y validación experimental de levas policéntricas con seguidores radiales y excéntricos., *7º Congreso Iberoamericano de Ingenieria Mecanica*, México D.F., paper n. 50 Analysis and Experimental, 2005.
[44] Carbone G., Lanni C., Lopez-Cajùn C. and Ceccarelli M., Numerical and experimental simulation of dynamic operations of cams. *Multibody Dynamics 2005, ECCOMAS Thematic Conference,* J.M. Goicolea, J.Cuadrado, J.C.García Orden (eds.), Madrid, CD Proceedings, paper n.MB023, 2005.
[45] Carbone G., Lanni C., Ceccarelli M., Incerti G. and Tiboni M., A characterization of cam transmissions through an identification of lumped parameters. *Proceedings of IDETC/CIE 2006, ASME 2006, Mechanisms & Robotics Conference*, Philadelphia, paper n. DETC2006-99218, 2006.
[46] Lanni C., Ceccarelli M. and Lopez-Cajun C., An experimental validation of three circular-arc cams with offset followers. *Mechanics Based Design of Structures and Machines,* Vol. 34, No. 3, (in print), 2006.
[47] Ceccarelli M., Carbone G., Lanni C. and Ottaviano E., A fairly simple method to identify the curvature of a cam profile. *ASME International Design Engineering Technical Conferences IDETC'04*, Salt Lake City, paper DETC2004-57387, 2004.
[48] Hardy D.W. and Walker C.L., *Doing mathematics with scientific workplace*. Brooks/Cole Publishing Company, Pacific Grove, 1995.
[49] National Instruments, *LabVIEW for Windows: data acquisition VI reference manual*. 1993.
[50] National Instruments, *DAQ: 6023E/6024E/6025E Users Manual*. 2000.
[51] Kistler Instruments, *Operating instruction capacitive accelerometer type 8305A2*. 2002.
[52] FGP Instr., *Dynamic torsion meter mod. CD 1050, user's manual.* 1995.
[53] Baumer Electric, *Incremental encoder mod. BHG 06.25W5000-B2-5*. 2001.
[54] Hewlett Packard, *Incremental encoder mod. HEDS-5701 G00*. 2001.

ISSN 1590-8844
International Journal of Mechanics and Control, Vol. 07, No. 02, 2006

EXPERIMENTAL TESTS AND RHEOLOGICAL MODEL FOR THE DEVELOPMENT OF A TRACTOR SEMI-ACTIVE SUSPENSION CONTROL

Federico Cheli Alfredo Cigada Nicola Ragno Emanuele Zappa

Politecnico di Milano

ABSTRACT

The aim of this study is to develop a numerical model of an agricultural vehicle front axle hydraulic suspension system. This model provides the analysis of the comfort (vertical dynamics) for the full vehicle, allowing the performance evaluation of a semi-active suspension control.

The suspension is characterized by friction phenomena, non-linear viscous damping (pointed out by experimental tests): the description of its behaviour through a simple spring-damper model is then unreliable.

A more complex model, able to correctly describe the suspension behaviour, with particular reference to hysteresis and friction, is then required. This kind of models are known as "rheological models". The rheological model developed in this study is based on the experience of the authors in the field of rubber dynamic response simulation; although not completely new, the proposed model is however innovative for the study of the vehicle suspension devices. The model is characterised by the following main characteristics:

- it is determined by five parameters: everyone of the parameters can be identified through experimental tests and has a well defined physical meaning;
- it is generally valid: it is suitable not only for the application described in this paper, but it can reproduce the actual behaviour of systems characterized by non-linear viscous damping and friction;
- it can be implemented in the simulations of semi-active control systems;
- the dynamic behaviour of the agricultural vehicle suspension can be accurately reproduced by the proposed model.

Keywords: rheological model, semi-active control tractor suspension

INTRODUCTION

In order to increase productivity, tractors have been equipped with automatic driving systems, useful when the machine takes up with activities involving continuous and coordinated control sequences.

These technical improvements, necessary to decrease the working time, have to take into account the physical stress induced to the operator. In order to decrease the working time significantly, the driver exposure to stress must be limited, so that physical fatigue is also reduced.

Contact author: Emanuele Zappa

Politecnico di Milano
Via La Masa 34, 20158 Milano, Italy

In the driver's cabin the operator is exposed to thermal, acoustical and mechanical stresses.

The reduction of the vertical vibrations – object of this paper – has always been achieved through a spring-suspended seat.

Only in the latest years studies in this field have become more incisive and particular suspensions, which are mainly located in the fore carriage, have been studied.

However, this device, not only has to reduce the vehicle vibrations, but it also has to maintain the correct vehicle trim (Figure 1), regardless to the implement carried.

As shown in Figure 1, the implement dimensions can be comparable to the vehicle ones, the suspension system must therefore be tuning for the carried load changes. For this reason, the system can not be based on the common spring (elastic element) and damper (damping element), but it needs a controlled hydraulic device.

ISSN 1590-8844
International Journal of Mechanics and Control, Vol. 07, No. 02, 2006

In this way, a twofold advantage is obtained:

- the hydraulic suspension system can offer stiffness higher than the spring-based one, being characterised by lower dimensions;
- the vehicle trim can be modified and the suspension can be enabled or disabled, according to the working conditions.

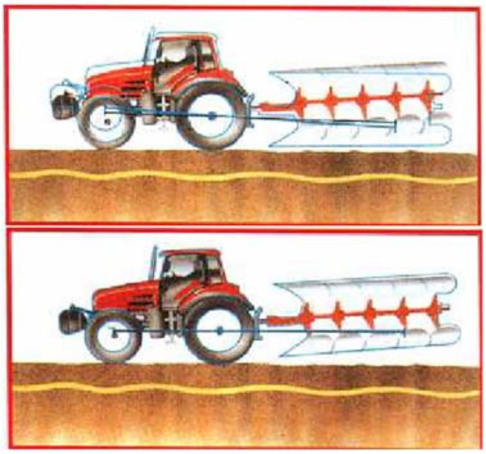

Figure 1 Regulation of the vehicle trim through hydraulic suspension

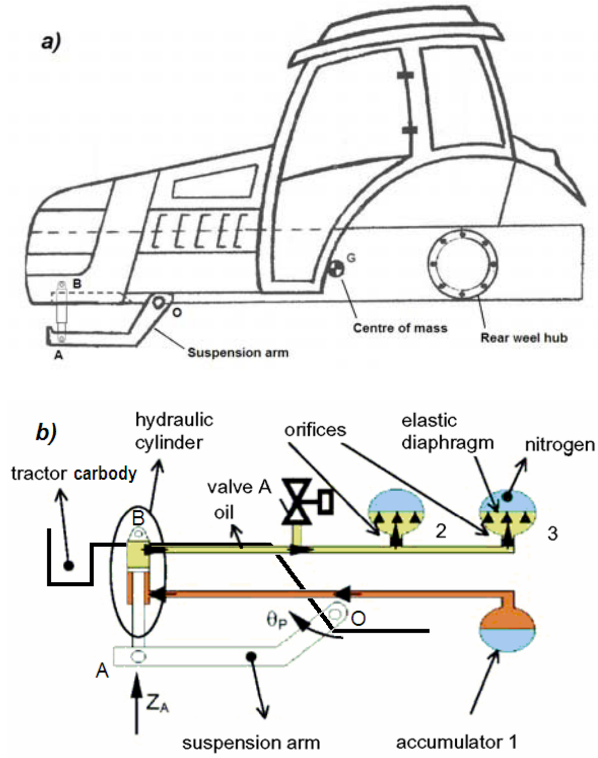

Figure 2 Tractor scheme (a) and hydraulic model for the front suspension (b)

The suspension will be enabled in case of driving on asphalt or dirt roads or during some farm activities, such as seeding. It will be disabled in case of trailing conditions of the machine, such as plowing.

In Figure 2 the hydraulic suspension model is illustrated. Each hydraulic cylinder (only one cylinder can be represented due to the lateral view) is joined to two separate circuits; a pipe connects the lower connector of each hydraulic cylinder to the accumulator number 1, while a second pipe connects the upper connectors to accumulators number 2 and 3 when valve A is closed and to a reservoir when valve A is opened. The fluid flowing into the hydraulic circuit is oil under pressure.

The dynamic behaviour of the vehicle equipped by a passive suspension system can be optimised through the application of a semi-active control using a strategy, based on the possibility of varying the damping parameter r in the simplest case, or stiffness k and damping r values in more sophisticated applications [1]. This type of control can be done by tuning some devices which determine the value of the two parameters. In the case of the suspension system proposed in this paper, the damping value is changed by varying the diameter of the orifice in the accumulator (2 and 3) inlet (Figure 3).

The variation of relative "pin-orifice" displacement (Figure 3) causes different oil flow sections and thus, different values of damping r. They range from the lowest one, obtained when the pin is at the maximum distance from the orifice, to the highest one, obtained when the pin is at the minimum distance from the orifice.

On the other hand, the stiffness k value can be modified, for instance, by temporarily excluding one or both the two accumulators 2 and 3: in this case the system would only work with two possible stiffness values k.

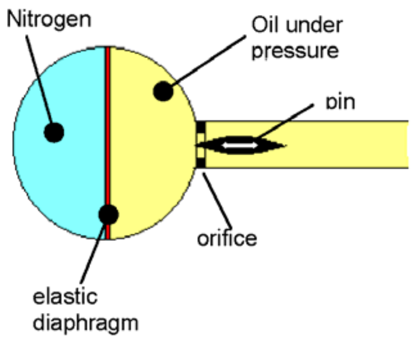

Figure 3 Nitrogen shock absorber: accumulator and pin used for camping variation

Semi-active control techniques do not require high engine power consumption, as they operate modifying one or more parameters of the system and not directly applying forces, as active controls do by replacing passive elements, such as the spring-damper in a suspension system, with active ones.

In case of a tractor the suspension system power is so high that the use of active control systems becomes very expensive in terms of energy dissipation.

The paper is organised in three fundamental steps: the first part describes the study of the suspension system kinematic analysis, useful for planning the second step: the experimental tests. Starting from experimental data, a rheological model of the suspension system is introduced and validated in the third part.

1 THE KINEMATIC ANALYSIS OF THE SUSPENSION

The suspension kinematic behaviour, represented in Figure 4, is analysed before describing and interpreting results obtained from experimental studies. Note that in the model of Figure 4 the spring connecting points A and B represent the stiffness effect due to the accumulators shown in Figure 2. The plots of Figure 5 help in understanding some facts related to kinematics: vertical reduced stiffness (evaluated at points A and C using the model of Figure 4) are shown as a function of the arm vertical relative displacement.
Kinematic analysis of the suspension points out two fundamental aspects:

- due to its geometrical characteristics the motion of the suspension arm extremity (point A in Figure 4) can be reproduced considering the vertical displacement only;
- suspension geometry does not introduce kinematic non-linearity, therefore, every non-linearity pointed out by the analysis of experimental tests cannot be attributed to the system kinematics.

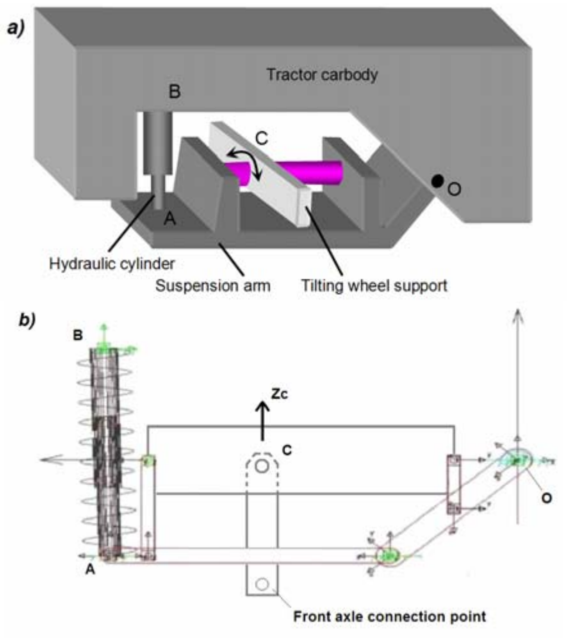

Figure 4 Scheme of the front suspension (a) and kinematic model (b)

In Figure 4 the term z_C represents the vertical displacement of the front wheel hub; one of the test bench pistons used to simulate the displacement of the tractor front wheels is fixed at point C. During the tests, described in chapter 2, point C is moved with harmonic displacement laws, with varying amplitude and frequency values.

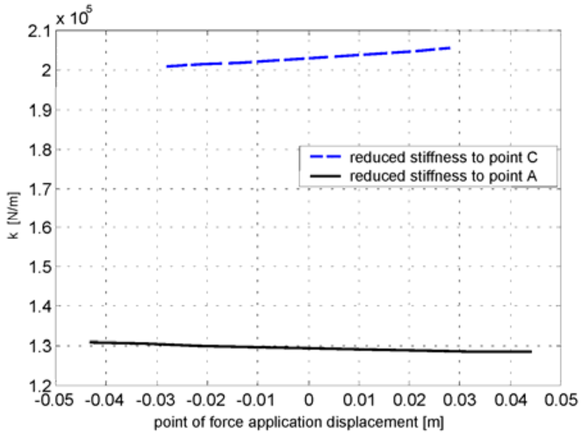

Figure 5 The reduced stiffness of the suspension

2 THE EXPERIMENTAL MEASUREMENTS

Experimental tests have been developed to deeply understand the system suspension behaviour under different quasi-static and dynamic operating condition. The experimental data are used to develop the rheological model of the suspension system described in the paper and to identify its characterizing parameters (cap. 3).
The described tests are the following:

- quasi-static tests;
- constrained carbody dynamic tests;
- free carbody dynamic tests.

The first and second test sets will be used to tune the rheological model parameters, while the latter will be used for the complete model validation.
The full vehicle (without wheels) is supported by three hydraulic actuators which also generate forces (Figure 6). The actuators are connected to two rear wheel hubs and to the mid point of the front axle.
Each actuator is equipped with an LVDT displacement transducer, used for both closed-loop displacement control and measurement of the impressed displacement.
Two Brüel & Kjær ICP accelerometers are also used for the dynamic free car test; the accelerometers are mounted at points A and B of Figure 4, in order to measure the vertical acceleration of these points; by means of the measured acceleration time histories the transfer function of the suspension will be obtained.
During the tests the tractor can be subjected to:

- a vertical translation: all three actuators are driven in-phase with the same displacement;
- a pitch rotation: the rear actuators are driven in-phase, while the front one moves with a 180° phase shift;
- a roll rotation: the two rear actuators are driven with 180° relative phase, while the front one is blocked.

Thus, a generic stress imposed on each of these three actuators produces a combination of the three mentioned motion types.

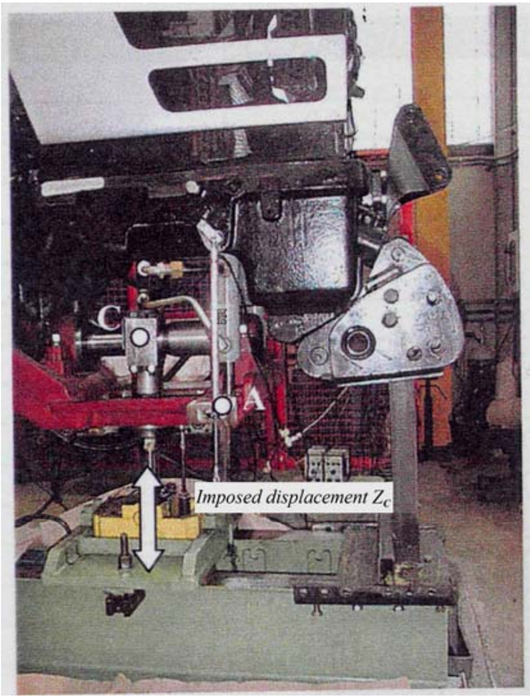

Figure 6 The experimental test bench

2.1 QUASI-STATIC TEST

In this type of test points B and O in Figure 4 are fixed, while the test bench piston causes (in C) a very slowly varying displacement time history z_c.

2.1.1 Test description

In the quasi-static tests, the tractor carbody motion is inhibited as follows:

- rear actuators are blocked;
- the front car extremity is stiffly constrained to the test bench through a fixing tool.

The goal of the tests is to determine the value of static stiffness and the rheological numerical model, as it will be later described.

The quasi-static test consists of compressing and rebounding the pistons once, moving the front actuator “very slowly” with a triangular wave, defining the amplitude in order to cover the full piston span.

2.1.2 Test results

From this test (see Figure 7) the following results can be acquired:

- the value of static stiffness *k,* obtained by calculating the average slope of the hysteresis cycle;
- the height of the hysteresis cycle ΔF;
- the distance necessary to pass from the value of maximum force in the lowest cycle branch to the maximum force in the higher cycle branch (x_2). This value indicates how sharp-cornered the cycle is.

These measured values will be used in the subsequent phase, consisting in the identification of the numerical rheological model parameters.

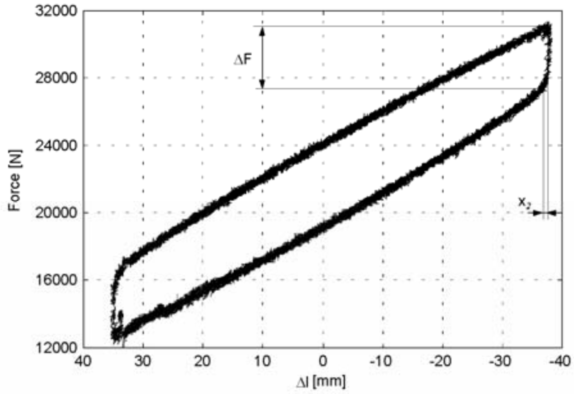

Figure 7 Constrained vehicle test: quasi-static test

2.2 CONSTRAINED CARBODY TEST

As performed in the quasi-static test, points B and O in Figure 4 are kept fixed, while the test bench piston causes (in C) displacement z_c to the suspension arm.

2.2.1 Test description

This kind of test is defined “constrained carbody test”, since the supporting tractor structure (*car*) is blocked on test bench. This test set is carried out with the same carbody suspension system used in constrained car case; it is then possible to stress only the suspension arm displacing the front actuator. In these tests an harmonic motion is imposed to the front actuator with variable amplitude and frequency.

Note that Δl is defined as: $\Delta l = Z_C - Z_{C\,mean}$, where $Z_{C\,mean}$ is the mean value of the possible vertical positions of point C (Figure 4).

2.2.2 Test results

This test enables to obtain hysteresis cycles diagrams (force *F* vs displacement Δl), produced for each compression and extension cycle. Hysteresis cycles have been defined for each test frequency and each value of imposed Δl. The obtained results have been interpreted as follows:

- from 0.5 to 2 Hz (Figure 8): the cycle shape at low compression velocity and piston extension points out energy dissipation mainly due to frictional phenomena. Furthermore, this dissipation form persists, by increasing the motion frequency. Indeed, starting from the of coulomb hysteresis cycle configuration, the cycle will be subject to extension, due to viscous damping;
- from 2.5 to 7.5 Hz (see Figure 9) a variation in cycle shape and slope is observed: as frequency grows the shape tends to become elliptical and thus, viscous forms of energy dissipation become active. Furthermore, the decrease in cycle inclination- which indicates a decrease of the equivalent stiffness- is also observed.

This set of experimental results shows that the tested dissipation system is subject to behaviour modifications due to frequency variation (i.e., since the oscillation amplitude is kept constant, due to the change of working velocity). A typical behaviour of a coulomb spring-damper system changes into the typical one of a shock absorber (viscous damping). This is shownin Figure 10a and Figure 10b. The diagrams show the dependence of the equivalent stiffness *k* and equivalent damping *r* reduced to point C (Figure 4); different tests were carried out at frequency *freq* ranging between 0.5 and 5 Hz, with amplitudes of ±20 mm and ±40 mm.

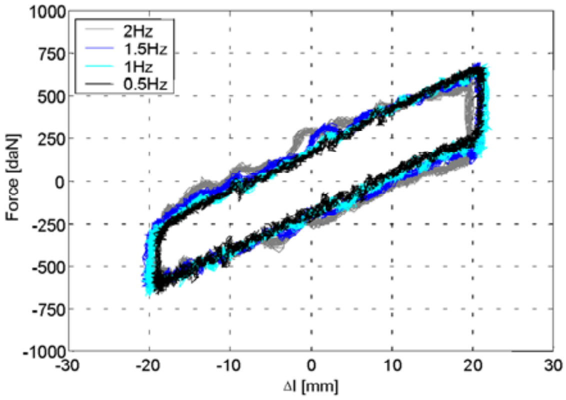

Figure 8 Constrained vehicle test: suspension hysteresis cycle at "low frequency"

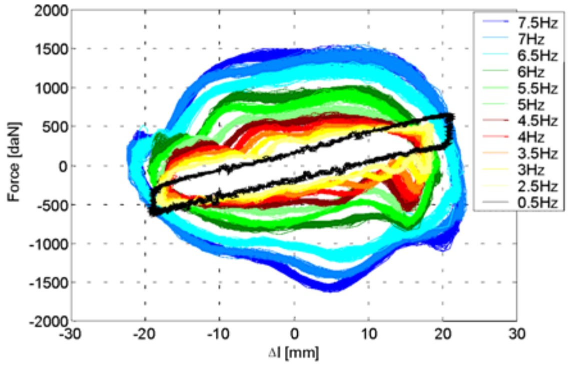

Figure 9 Constrained vehicle test: suspension hysteresis cycle at "high frequency"

Parameters *k* and *r* are strictly frequency dependent, while the dependence on amplitude is evident in the damping graph and is smaller in the stiffness one. It can be noted how the *k* value decreases as frequency increases, while, at the same rate, *r* tends asymptotically to a constant value. This confirms what stated in the first part of the paragraph concerning the behaviour to which the dissipative system is subject in case of increasing working velocity: the spring-damper system with certain stiffness and damping changes into a shock absorber with very low stiffness and a constant damping value (the behaviour tends to be merely viscous). Indeed, the sloped and parallelogram shaped hysteresis cycles become more ellipsis-like and their main axis directions get closer to the Cartesian axis as frequency increases (Figure 9).

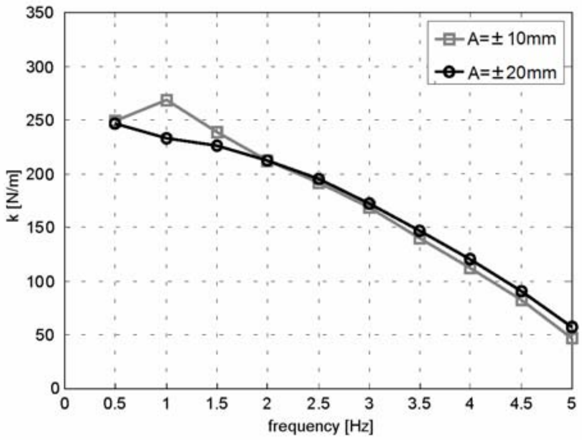

Figure 10.a Constrained vehicle test: equivalent suspension stiffness as a function of frequency and amplitude

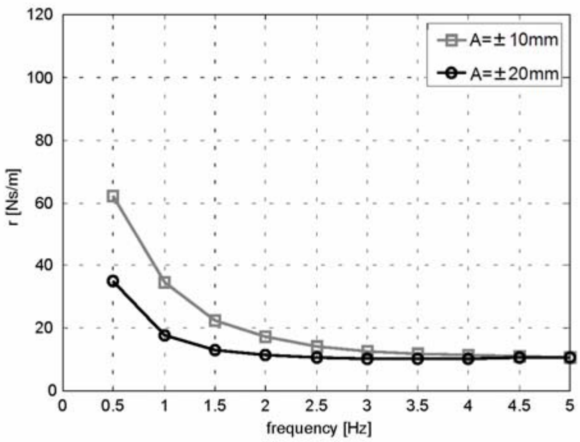

Figure 10.b Constrained vehicle test: equivalent suspension damping as a function of frequency and amplitude

2.3 FREE VEHICLE TEST

In this case point B and O in Figure 4 are free to pivot on the vehicle rear axle, while the test bench piston causes (in C) triangular shaped or harmonic displacement time histories z_c with variable frequency and amplitude.

2.3.1 Test description

Free vehicle tests differ from the constrained carbody ones only because the fixing tool is removed and thus, the tractor is free. During this type of tests only the tractor front axle is moved, while the rear actuators are blocked. Therefore, this configuration makes the tractor free to pivot around the rear axle. This test simulates the passage of the tractor front wheels over an harmonic or triangular terrain profile (since this is the shape of the wave given to the actuator), note that the filtering effect due to tyres is not considered because wheels are not mounted. The aim of the test is to define an experimental transfer function between the acceleration $acc_{carbody}$ of point B (Figure 4) and the $acc_{front\ axle}$ of point A, in order to evaluate its efficiency (position and height of

resonance peak) and to compare the results of following numerical suspension model.
The use of a transfer function for the analysis of a non linear system is not theoretically correct, but this function however can visualise some system characteristics, such as the natural frequency. Moreover the amplitude of the suspension system oscillation are not very large: the nonlinearities are then reasonable too.
In Figure 11 a transfer function estimation obtained with experimental tests is shown; the displacement imposed to point C is harmonic (one test at each frequency between 0.5 and 5 Hz, with 0.5 Hz steps) with amplitude of ±15 mm.

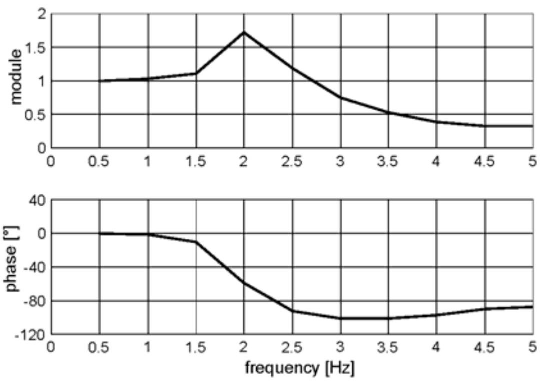

Figure 11 Experimental free vehicle test: transfer function $acc_{carbody}/acc_{axle}$

2.3.3 Test results
In Figure 11 the transfer function peak, representing the natural frequency of the system, is close to 2 Hz. At the resonance peak the dynamic amplification is moderate (about 1.7) due to the damping.

3 THE SUSPENSION MODEL

The model arises from the need of reproducing the behaviour of the vehicle, with particular attention to the suspension system, in order to predict the performances of a semi-active control system and to allow tuning of the controller parameters. A simple mass-spring-damper model is not suitable to completely model the system: in fact stiffness k and damping r are functions of frequency, as demonstrated through the experimental results shown in paragraph 2.
Figure 12 points out the characterizing elements of this model. The fundamental equation used for the development of the rheology model is (see [2] and [3]):

$$m_p \cdot \ddot{z}_A + F_{viscous}(\dot{x},\beta) + F_{el}(x,k) + F_{friction}(x, x_2, F_{a_{max}}, x_{b,} F_{a_b}) = R \quad (1)$$

where:

- R is the force imposed to the front suspension axle reduced to point A (Figure 4)
- Z_A is the vertical displacement of the point A
- m_p is the front suspension axle mass reduced to point A
- $F_{el}(x,k) = -k \cdot x$ is the equivalent elastic force
- $F_{friction} = F_{friction}(x, x_2, \Delta F, x_{b,} F_{a_b})$ is the friction force.
- $F_{viscous} = F_{viscous}(\dot{x},\beta) = -r|\dot{x}|^{\beta} \cdot sign(\dot{x})$ is the viscous equivalent force.

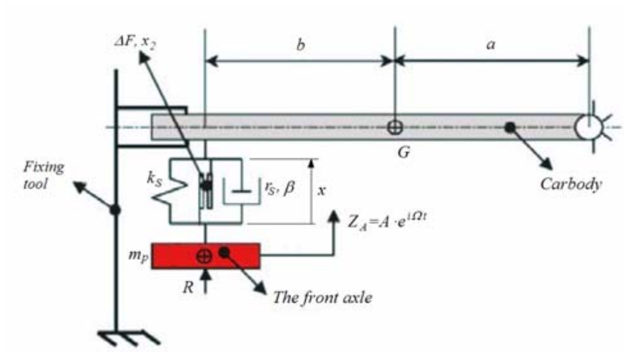

Figure 12 Non linear mass-spring-frictional pad-damper model (Configuration of constrained car test)

Each force component will be described in the next paragraph; the parameters used in the force expressions can be identified starting from the experimental tests.

3.1 THE FRICTION FORCE MODEL

Friction force is characterized by significant hysteresis, that is, the force applied by the system at a certain time t_1 not only depends on the system state at time t_1 but also from the system state assumed in the close past (Figure 13). This force is a non linear function of the relative carbody-axle position x [4] and it also depends upon two parameters: x_2 and ΔF.

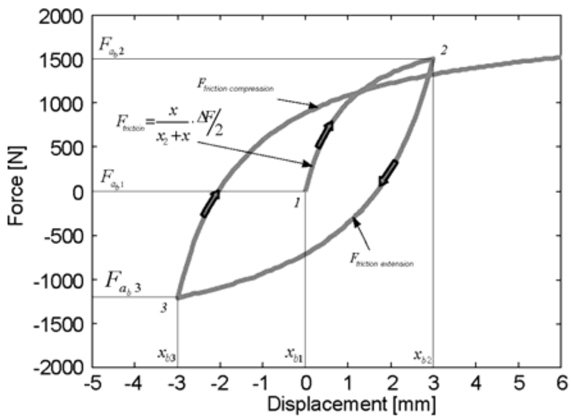

Figure 13 Hysteresis cycle only due to friction force

In literature ([4]) curves which describe compression and extension phases of an hysteresis cycle are:

- compression:

$$F_{friction} = F_{a_b i} + \left[\frac{x - x_{bi}}{x_2 \cdot \left(1 - \frac{F_{a_b i}}{\Delta F/2} \right) \cdot \left(x - x_{bi} \right)} \right] \cdot \left(\frac{\Delta F}{2} - F_{a_b i} \right) \quad (2)$$

- extension:

$$F_{friction} = F_{a_b i} + \left[\frac{x - x_{bi}}{x_2 \cdot \left(1 + \frac{F_{a_b i}}{\Delta F/2} \right) \cdot \left(x - x_{bi} \right)} \right] \cdot \left(\frac{\Delta F}{2} + F_{a_b i} \right) \quad (3)$$

where:

- x is the value of the current suspension position (it is a variable in the numerical integration), in case of fixed carbody x=-Z_A (Figure 12);
- x_{bi} = ($x_{brake\ point}$) is the last value of variable x achieved before feed reverse, that is, before the transition from compression to extension (or vice versa). It is a variable in the numerical integration. Its variation occurs only in case of feed reverse, otherwise it is constant and equal to the last achieved value (x_{bi}=x_{b2} during extension and x_{bi}=x_{b3} during compression, see Figure 13);
- F_{abi}= ($F_{friction\ break\ point}$) is the last value achieved by friction force $F_{friction}$ before feed reverse. It is a variable in the numerical integration; its variation only occurs in case of feed reverse, otherwise it is constant and equal to the last achieved value (F_{abi}=F_{ab2} during extension and F_{abi}=xF_{ab3} during compression);
- ΔF is the force gap due to the friction hysteresis cycle (see Figure 7). It is a constant. Its value is measured only by the hysteresis cycle obtained in the quasi-static test;
- x_2 is the displacement required to pass from the minimum value of friction force to the maximum (see Figure 7). This parameter shows how much sharp-cornered is the friction hysteresis cycle. It is a constant. Its value is extracted by the hysteresis cycle obtained in the quasi-static test.

3.2 THE ELASTIC FORCE

Elastic force represents the classic stiffness term, it is then considered linear with the relative carbody-axle displacement through the coefficient k. (F_{el}= - $k\,x$). The k coefficient is a constant and is equal to the value obtained in the quasi-static test (Figure 7).

3.3 THE VISCOUS FORCE

In the mass-spring-damper models ([5]) energy dissipation produces the elliptical shape of the cycle in "force vs displacement" diagram. The cycle area is reciprocally proportional to damping coefficient r.
Viscous force acquires its typical expression:

$$F_r = -r\,\dot{x} \quad (4)$$

that is, viscous force is proportional to velocity. In mass-spring-non linear damper the viscous force is proportional to velocity through a constant coefficient r, but this proportionality is not linear, because the velocity is raised to a power β:

$$F_{viscous} = -r \cdot \left|\dot{x}\right|^{\beta} \cdot sign(\dot{x}) \quad (5)$$

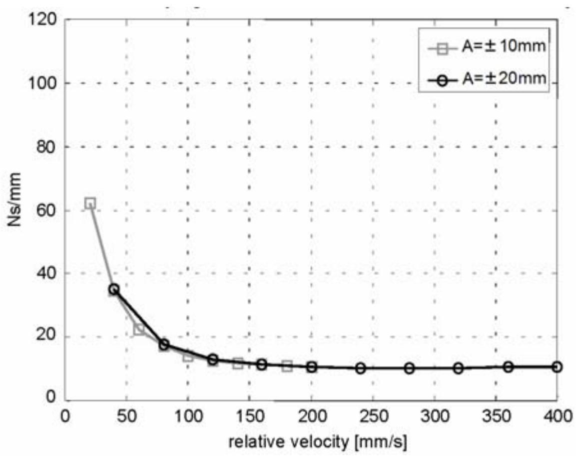

Figure 14 Constrained vehicle test: equivalent suspension damping as a function of relative velocity $\dot{x}$ (see also Figure 10)

The expression of viscous force given in **Errore. L'origine riferimento non è stata trovata.**) is useful for taking into account localised and distributed flow resistance; the value of β was obtained by fitting the experimental data (**Errore. L'origine riferimento non è stata trovata.**) with the suspension numerical model, setting the r value equal to the asymptotic value to which it tends in diagram (*high relative velocity r*) in **Errore. L'origine riferimento non è stata trovata.**.

4 RESULTS OF THE RHEOLOGICAL MODEL

The parameters of the model proposed in chapter 3 were identified through the experimental tests shown in chapter 2.
The following diagrams show the comparison between some constrained vehicle experimental tests and the simulation of the same situation obtained with the rheological model.

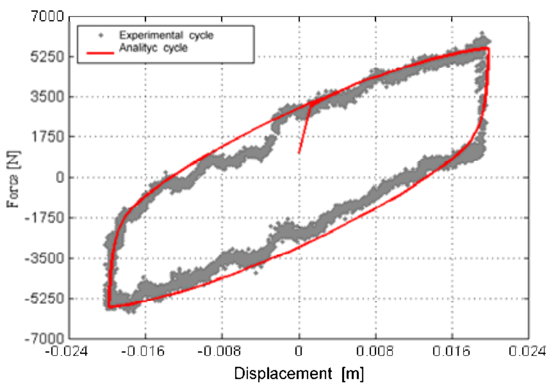

Figure 14 Constrained vehicle test hysteresis cycle: comparison between experimental and numerical results at 2 Hz, 40 mm stroke

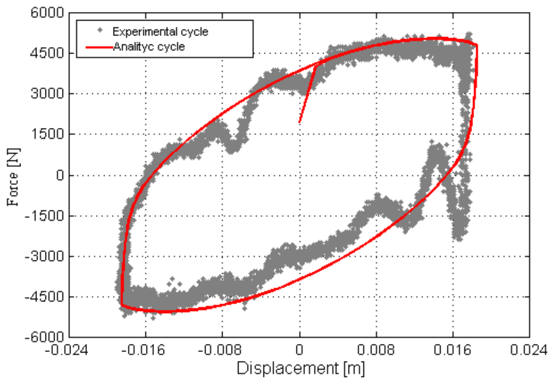

Figure 15 Constrained vehicle test hysteresis cycle: comparison between experimental and numerical results at 3 Hz, 40 mm stroke

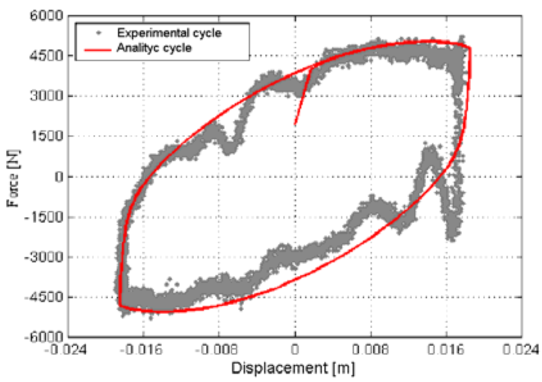

Figure 16 Constrained vehicle test hysteresis cycle: comparison between experimental and numerical results at 4.5 Hz, 40 mm stroke

Diagrams of Figures 15, 16, 17 and 18 compare the analytic force hysteresis cycles generated by the constrained vehicle test to the corresponding experimental ones. The experimental cycle shapes are well approximated by numerical simulation, even if at higher frequencies (4.5 and 7.5 Hz) localized oscillations are shown in experimental data: this phenomenon was investigated and was find to be due to some vibration introduced by the test bench control.

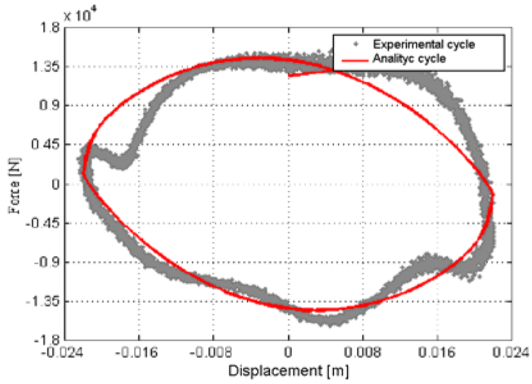

Figure 17 Constrained vehicle test hysteresis cycle: comparison between experimental and numerical results at 7.5 Hz, 40 mm stroke

In Figure 18 the comparison between experimental and numerical free vehicle test is shown in terms of transfer function between the car and the front axle vertical acceleration. The experimental data were already shown in Figure 11, while the numerical data come from the model described in chapter 3.
As can be seen the model correctly reproduces the suspension dynamics and can then be used, in the next chapter, to develop the model of the full vehicle.

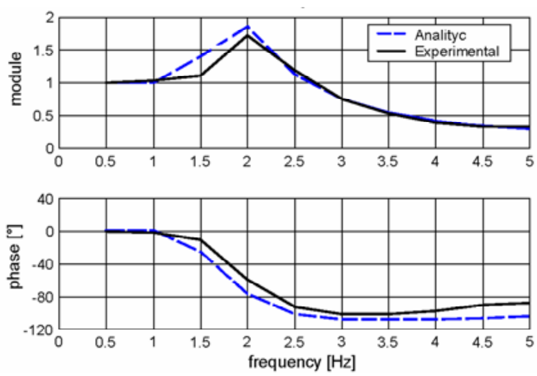

Figure 18 Comparison between experimental and numerical free vehicle test: transfer function $acc_{carbody}/acc_{axle}$ (the complete non linear model described in paragraph 3 was used)

5 FULL VEHICLE MODEL

The full vehicle was modelled using the multibody software for dynamic simulation "Adams View"; this software tool allows for the definition of force models in Fortran language: the front axle suspension behaviour was introduced with the rheological model developed in this paper.
The AdamsView implemented model is illustrated in Figure 19 and was used to simulate obstacle passing test.
Here tyres are represented by linear elastic and damping elements and their values k_P and r_P are equal to the radial ones [6]. The aim is to simulate the comfort of a vehicle running on a straight line at constant speed and crossing an obstacle.

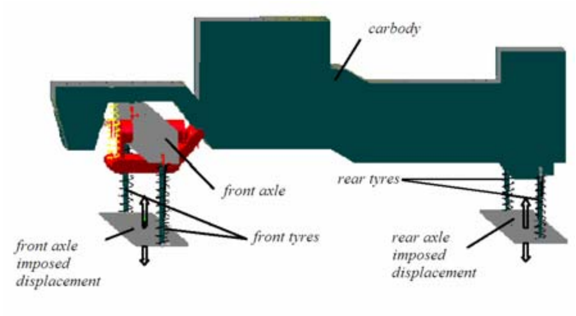

Figure 19 Tractor multibody model of full vehicle for dynamic simulation

5.1 PASSIVE SUSPENSION

The obstacle shape used in the simulation is the "bump", which is commonly used in car dynamic studies. The same bump shape equation:

$$y_v(x_v) = A \cdot e^{\frac{1}{2}\left(\frac{x_v}{c}\right)^2} \tag{5}$$

was used for both front and rear axles, with a difference in bump application time depending on vehicle speed.
In (5) c is a parameter proportional to the obstacle width (in this case c = 0.4 m) and the amplitude A is 0.1m.

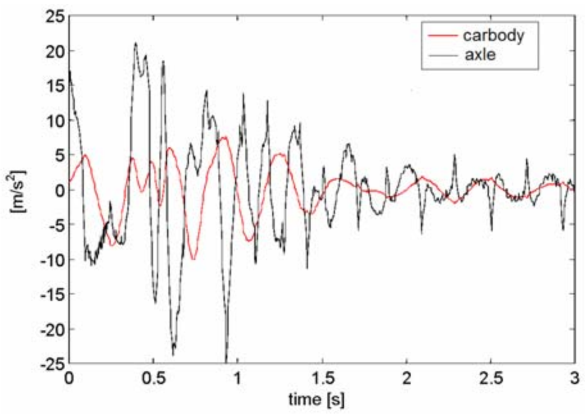

Figure 20 Numerical simulation: bump obstacle at 40 km/h time history of the carbody and the axle acceleration

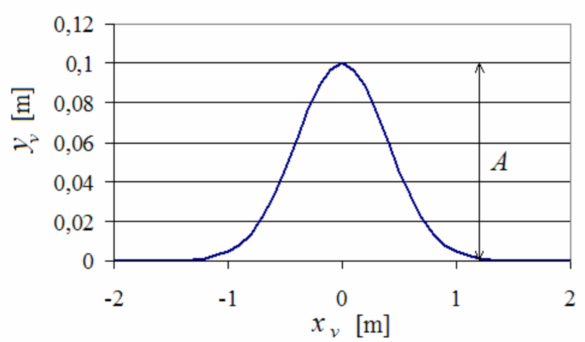

Figure 21 The "bump" obstacle profile

The y_v time histories have been applied as front axle and rear axle imposed displacements (see Figure 19). The results shown in Figure 23 were obtained simulating a 40 km/h obstacle pass-by.
Figure 22 describes the displacements (vertical translations) of car centre of gravity (z_{car}), point A (z_{axle}) and the relative car-axle displacement which corresponds to the one between points A and B (Figure 4).
Figure 23 shows a resonance frequency of about 2.5 Hz in the car and of about 6 Hz in the axle.

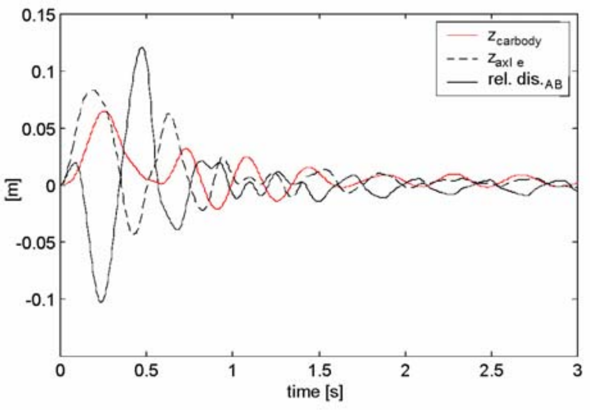

Figure 22 Numerical simulation: bump obstacle at 40 km/h, carbody and front axle vertical displacement time histories, plotted together with relative displacement between points A and B of Figure 4 (front suspension elongation)

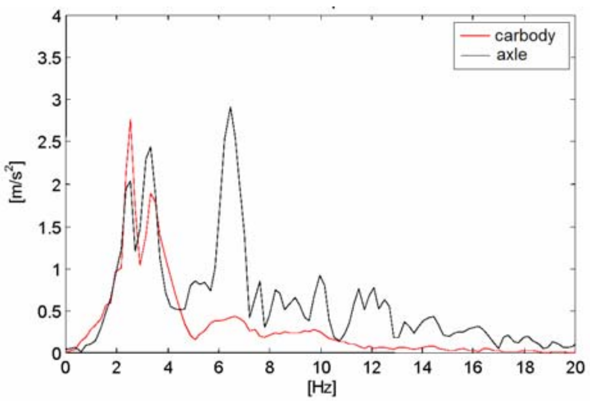

Figure 23 Numrical simulation: bump at 40 km/h, carbody and axle vertical acceleration spectra

5.2 SEMI ACTIVE SUSPENSION

The semi-active control system is expected to be the best control strategy in terms of absorbed power reduction, production cost and loss of reliability. This conclusion is based on literature results mentioned in [7] and [8]. The strategy aims to vary the stiffness and damping parameters of the system, while the vehicle is running, in order to reduce vibrations and shocks as much as possible. The front suspension rheological model receive stiffness and damping parameters as an input and allow to simulate the vehicle

dynamics behaviour as a function of these two values. In this way a number of control strategies can be numerically tested, without the need of building any physic control device. Experimental tests will be done on the numerically optimized control solution only, allowing to get cost and time reduction.
In order to transfer the numerical control strategy on the physical vehicle, it is however important to associate stiffness and damping parameters to a mechanical configuration of the control system (such as the position of the pin shown in Figure 3).
Although the goal of this paper is not the control strategy but the development and the validation of the suspension model, an example of semi-active control is shown here as an example of the model application.
A possible (very simple) control strategy provides that *k* and *r* can vary. In this application *k* and *r* do not vary continuously, but they can only assume two values each. *k* varies when one or both actuators 2 and 3 are working (Figure 2), while the variation of *r* depends on the oil flowing through the orifices. The variation is generated by controlling the opening and closing of two solenoid valves. This reduces engine power absorption to the minimum and grants maximum reliability to the system. In case the two solenoid valves fail, the suspension system becomes passive, but it keeps on working, even if not optimally.
A different and more accurate damping regulation strategy was implemented in a Simulink model: in this control strategy the damping coefficient can be varied continuously between a maximum and minimum value, by moving the pin in the orifice (Figure 3).
The implemented control is a PID type and the attempt to minimise the pitch angle variations: one of the most important parameters affecting comfort.
The simulation results showed in the following are about the obstacle passing tests.
In Figure 24 and Figure 25 results obtained with the proposed semi-active control are compared with those produced with the passive suspension system simulation.

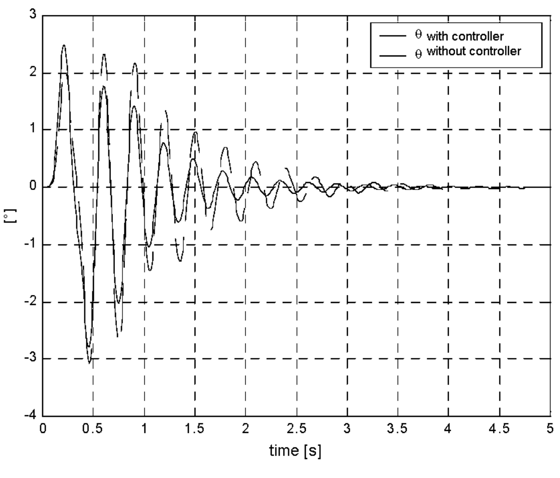

Figure 24 Pitch oscillation due to bump at 40 km/h: comparison passive and semi – active suspension

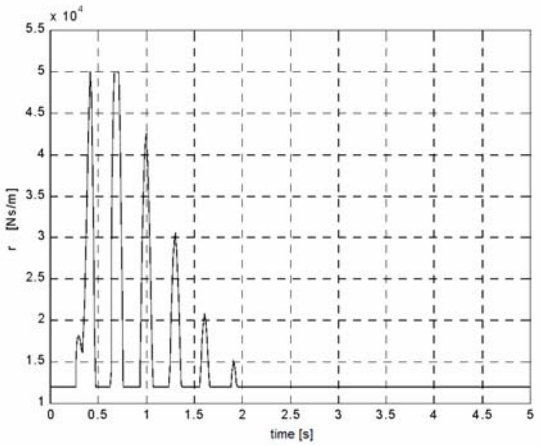

Figure 25 Damping values generated by the controller

CONCLUSIONS

This paper describes a rheological model for a tractor front suspension characterised by:

- 5 constant parameters (stiffness and damping coefficients are also included);
- each parameter was experimentally measured and identified and has its own physical meaning.

The frictional model parameters are:

- *k*: is constant and measured in the quasi-static test. It is dependent on accumulator pressure and volume. It was experimentally measured;
- ΔF: is constant and measured in the quasi-static test;
- x_2: is constant and measured in the quasi-static test;
- β: is constant, depends on the hydraulic pipe diameter. Its value is determined through the simulation of constrained car test;
- *r*: is constant, depends on the orifice diameters located before the accumulator inlet. The *r* value increases when diameter decrease; the magnitude is computed through the constrained car test.

Therefore, the classic spring-damper model becomes a particular case of the rheological model, by eliminating the friction force and considering $\beta = 1$.
The suspension model has been implemented in the vehicle comfort model and it can be used for the simulation of semi-active control.
The integration was possible because the proposed rheology model is not a “black box”, but each of its parameters is still linked to the physics of real system.

The proposed model can vary:

- the shape of hysteresis cycle due to friction,
- the non-linear dependency of viscous force.

Because of these reasons it is also suitable for describing the behaviour of systems different from the proposed one such as rubber elements, where coulomb frictions, non-linear elastic and viscous forces are present.

REFERENCES

[1] Schalk Els P. and Van Niekerk J.L., Dynamic Modelling of an Off – Road Vehicle for the Design of a Semi – Active, Hydropneumatic Spring – Damper System. *Vehicle System Dynamics Supplement*, 33, pp. 566-577, 1999.

[2] Warner B., An Analytical and Experimental Investigation of Friction and Gas Spring Characteristics of Racing Car Suspension Dampers. *SAE Transactions*, *Journal of Commercial Vehicles*, Section 2, 1996.

[3] Garibaldi L. and Onah H.N., *Viscoelastic material damping technology*, Becchis Osiride, 1996.

[4] Berg M., *A model for rubber spring in the dynamic analysis of rail vehicles*. Division of Railway Technology, Department of Vehicle Engeneering, Kungl Tecniska Hogskolan, Stockholm, Sweden.

[5] Diana G. and Cheli F., *Dinamica e vibrazione dei sistemi*, UTET Libreria, 1993.

[6] Brassart F.P. and Wright M.E., A Machine to Study Vertical Tire Stiffness and Damping Coefficient. *SAE Transactions*, *Journal of Commercial Vehicles*, Section 2, 1993.

[7] Wilkinson and Crolla, Investigations into Alternative Suspensions for Commercial Vehicles. *SAE Transactions*, *Journal of Commercial Vehicles*, Section 2, 1993.

[8] Von Glasner E.C., Gohring E., Povel R. and Schutzner P., Analysis of Intelligent Systems for Commercial Vehicles, *SAE Transactions*, *Journal of Commercial Vehicles*, Section 2, 1993.

ACKNOWLEDGMENTS

The authors thanks SAME S.p.A for the support in the research and Eng. Contessini for the contribution to the experimental tests.

ISSN 1590-8844
International Journal of Mechanics and Control, Vol. 07, No. 02, 2006

TEMPLATE FOR PREPARING PAPERS FOR PUBLISHING IN INTERNATIONAL JOURNAL OF MECHANICS AND CONTROL

Author1* Author2**

* affiliation Author1

** affiliation Author2

ABSTRACT

This is a brief guide to prepare papers in a better style for publishing in International Journal of Mechanics and Control (JoMaC). It gives details of the preferred style in a template format to ease paper presentation. The abstract must be able to indicate the principal authors' contribution to the argument containing the chosen method and the obtained results. (max 200 words)

Keywords: keywords list (max 5 words)

1 TITLE OF SECTION (E.G. INTRODUCTION)

This sample article is to show you how to prepare papers in a standard style for publishing in International Journal of Mechanics and Control.
It offers you a template for paper layout, and describes points you should notice before you submit your papers.

2 PREPARATION OF PAPERS

2.1 SUBMISSION OF PAPERS

The papers should be submitted in the form of an electronic document, either in Microsoft Word format (Word'97 version or earlier).
In addition to the electronic version a hardcopy of the complete paper including diagrams with annotations must be supplied. The final format of the papers will be A4 page size with a two column layout. The text will be Times New Roman font size 10.

Contact author: author1[1], author2[2]

[1]Address of author1.

[2]Address of author2 if different from author1's address.

2.2 DETAILS OF PAPER LAYOUT

2.2.1 Style of Writing

The language is English and with UK/European spelling. The papers should be written in the third person. Related work conducted elsewhere may be criticised but not the individuals conducting the work. The paper should be comprehensible both to specialists in the appropriate field and to those with a general understanding of the subject.
Company names or advertising, direct or indirect, is not permitted and product names will only be included at the discretion of the editor. Abbreviations should be spelt out in full the first time they appear and their abbreviated form included in brackets immediately after. Words used in a special context should appear in inverted single quotation mark the first time they appear. Papers are accepted also on the basis that they may be edited for style and language.

2.2.2 Paper length

Paper length is free, but should normally not exceed 10000 words and twenty illustrations.

2.2.3 Diagrams and figures

Figures and Tables will either be entered in one column or two columns and should be 80 mm or 160 mm wide respectively. A minimum line width of 1 point is required at actual size. Captions and annotations should be in 10 point with the first letter only capitalised *at actual size* (see Figure 1 and Table VII).

ISSN 1590-8844
International Journal of Mechanics and Control, Vol. 07, No. 02, 2006

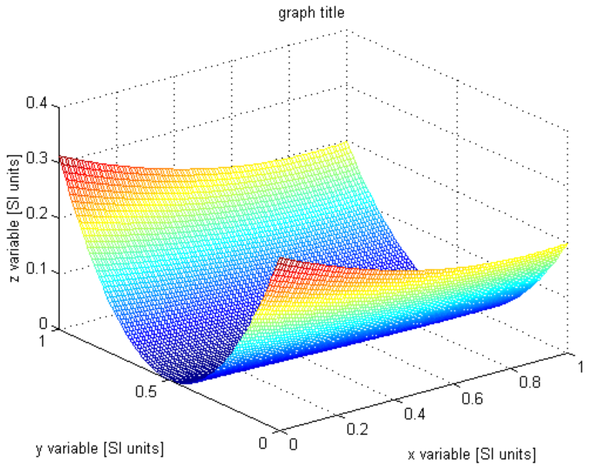

Figure 1 Simple chart.

Table VII - Experimental values

Robot Arm Velocity (rad/s)	Motor Torque (Nm)
0.123	10.123
1.456	20.234
2.789	30.345
3.012	40.456

2.2.4 Photographs and illustrations

Authors could wish to publish in full colour photographs and illustrations. Photographs and illustrations should be included in the electronic document and a copy of their original sent. Illustrations in full colour …

2.2.5 Equations

Each equation should occur on a new line with uniform spacing from adjacent text as indicated in this template. The equations, where they are referred to in the text, should be numbered sequentially and their identifier enclosed in parenthesis, right justified. The symbols, where referred to in the text, should be italicised.

- point 1
    - point 2
        - point 3

1. numbered point 1
    2. numbered point 2
        3. numbered point 3

$$W(d) = G(A_0, \sigma, d) = \frac{1}{T}\int_0^{+\infty} A_0 \cdot e^{-\frac{d^2}{2\sigma^2}} dt \qquad (1)$$

3 COPYRIGHT

Authors will be asked to sign a copyright transfer form prior to JoMaC publishing of their paper. Reproduction of any part of the publication is not allowed elsewhere without permission from JoMaC whose prior publication must be cited. The understanding is that they have been neither previously published nor submitted concurrently to any other publisher.

4 PEER REVIEW

Papers for publication in JoMaC will first undergo review by anonymous, impartial specialists in the appropriate field. Based on the comments of the referees the Editor will decide on acceptance, revision or rejection. The authors will be provided with copies of the reviewers' remarks to aid in revision and improvement where appropriate.

5 REFERENCES (DESCRIPTION)

The papers in the reference list must be cited in the text. In the text the citation should appear in square brackets [ ], as in, for example, "the red fox has been shown to jump the black cat [3] but not when...". In the Reference list the font should be Times New Roman with 10 point size. Author's first names should be terminated by a 'full stop'. The reference number should be enclosed in brackets.
The book titles should be in *italics*, followed by a 'full stop'. Proceedings or journal titles should be in *italics.* For instance:

REFERENCES (EXAMPLE)

[1] Smith J., Jones A.B. and Brown J., *The title of the book*. 1st edition, Publisher, 2001.

[2] Smith J., Jones A.B. and Brown J., The title of the paper. *Proc. of Conference Name*, where it took place, Vol. 1, paper number, pp. 1-11, 2001.

[3] Smith J., Jones A.B. and Brown J., The title of the paper. *Journal Name*, Vol. 1, No. 1, pp. 1-11, 2001.

[4] Smith J., Jones A.B. and Brown J., *Patent title*, U.S. Patent number, 2001.

International Journal of Mechanics and Control – JoMaC
Published by Levrotto&Bella

TRANSFER OF COPYRIGHT AGREEMENT

NOTE: Authors/copyright holders are asked to complete this form signing section A, B or C and mail it to the editor office with the manuscript or as soon afterwards as possible.	*Editor's office address:* Andrea Manuello Bertetto Elvio Bonisoli *Dept. of Mechanics* *Technical University-Politecnico di Torino* ***C.so Duca degli Abruzzi, 24. 10129 Torino – Italy*** e_mail: jomac@polito.it fax n.: +39.011.564.6999

The article title:

By:____

To be Published in ***International Journal of Mechanics and Control JoMaC***
Official legal Turin court registration Number 5320 (5 May 2000) - reg. Tribunale di Torino N. 5390 del 5 maggio 2000

A Copyright to the above article is hereby transferred to the JoMaC, effective upon acceptance for publication. However the following rights are reserved by the author(s)/copyright holder(s):
1. All proprietary rights other than copyright, such as patent rights;
2. The right to use, free or charge, all or part of this article in future works of their own, such as books and lectures;
3. The right to reproduce the article for their own purposes provided the copies are not offered for sale.
To be signed below by all authors or, if signed by only one author on behalf of all co-authors, the statement A2 below must be signed.

A1. All authors:

SIGNATURE__________________________________DATE____________ SIGNATURE__________________________________DATE____________

PRINTED NAME____ PRINTED NAME____

SIGNATURE__________________________________DATE____________ SIGNATURE__________________________________DATE____________

PRINTED NAME____ PRINTED NAME____

A2. One author on behalf of all co-authors:
"I represent and warrant that I am authorised to execute this transfer of copyright on behalf of all the authors of the article referred to above"

PRINTED NAME____

SIGNATURE____________________________________ TITLE____________________________________ DATE________________

B. The above article was written as part of duties as an employee or otherwise as a work made for hire. As an authorised representative of the employer or other proprietor. I hereby transfer copyright to the above article to Editel-Pozzo Gros Monti effective upon publication. However, the following rights are reserved:
1. All proprietary rights other than copyright, such as patent rights;
2. The right to use, free or charge, all or part of this article in future works of their own, such as books and lectures;
3. The right to reproduce the article for their own purposes provided the copies are not offered for sale.

PRINTED NAME____

SIGNATURE____________________________________ TITLE____________________________________ DATE________________

C. I certify that the above article has been written in the course of employment by the United States Government so that no copyright exists, or by the United Kingdom Government (Crown Copyright), thus there is no transfer of copyright.

PRINTED NAME____

SIGNATURE____________________________________ TITLE____________________________________ DATE________________

CONTENTS

next number scheduled titles:

MEMS Inertial Guidance Systems for Low Cost Vehicles
P. Maggiore, M. Velardocchia

Nonlinear Elastic Characteristic of Magnetic Suspensions through Hilbert Transform
E. Bonisoli

Design Parameters Sensitivity Analysis of a New Diesel Locomotive
P. Belforte, F. Cheli, A. Collina, L. Prone, G. Tomasini

A Stress Evaluation Strategy for Designing Squat Structures
C. Rosso

Design of Advanced Robotic Systems for Assembly Automation
M. Callegari, A. Gabrielli, M. C. Palpacelli, M. Principi